MARIA S. MERIAN – Berichte

Hydrothermal Systems Along Knipovich Ridge

Cruise No. MSM109

6 July – 3 August 2022
Tromsø (Norway) – Reykjavik (Iceland)
Knipovich Venting

Bohrmann G, Büttner H, Coulibaly O, dos Santos Ferreira C, Hüttich D, Knutsen SM, Kleint J, Malnati J, Marschall L, More PS, Renzelmann H, Serje Gutierrez A, Rehage R, Renken J, Reuter C, Schade T, Schröder M, Smrzka D, Spiesecke U, Streuff K, Tibebu A

Gerhard Bohrmann
University of Bremen, MARUM

2022

Table of Contents

1 Cruise Summary

1.1 Summary in English

R/V MARIA S. MERIAN cruise MSM109 surveyed the Knipovich and Molløy Ridges for hydrothermal vents previously unknown from these ultra-slow spreading ridges. Especially from the 500-km-long Knipovich Ridge, no locations were available where hydrothermal fluids are emitting from the seafloor into the hydrosphere, despite some exploration attempts by various groups of scientists. Investigations were carried out in four regions: 1) at the southern Knipovich Ridge, 2) in a young submarine volcanic area north of the Logachev Seamount, 3) at the Axial Volcanic ridge (AVR) at 77°27'N, which we called the Brøgger Ridge, and 4) on the Molløy Ridge. A total of 16 CTD stations were run, of which 6 stations were performed as Tow-yo CTD profiles. We measured 2829 nm with the hull-mounted Multi-beam and PARASOUND. High resolution multi-beam and backscatter data were generated during 8 AUV dives. The AUV dive data from MARUM Seal and the AUV data provided by the Norwegian Petroleum Directorate formed the basis for 13 ROV-QUEST dives. Clear evidence of hydrothermalism was found in two of the four areas. In the young volcanic area north of the Logachev seamount, hydrothermal precipitates were found and sampled at two locations. In area no. 3, east of the Brøgger Ridge, numerous active and inactive vents were found and sampled at a water depth of approx. 3,200 m, on the eastern edge of the graben. In addition to a black smoker, which expelled 316°C hot fluids, other hydrothermal vents of up to 4°C were also sampled. By mapping with the ROV QUEST, we were able to identify a hydrothermal field about 1 km long and 200 m wide for the Knipovich Ridge, which we named Jøtul hydrothermal field. Methane concentrations are unusually high, up to 4.9 µmol/L in the water and up to 18.8 mmol/L in the hydrothermal fluid.

1.2 Zusammenfassung

Die Expedition mit FS MARIA S. MERIAN MSM109 untersuchte den Knipovich und Molløy Rücken nach hydrothermalen Quellen, die bisher von diesen ultra-langsam spreizenden Rücken unbekannt waren. Besonders vom 500 km langen Knipovich Rücken lagen trotz Explorationsversuchen verschiedener Wissenschaftlergruppen, keine Lokationen vor, an denen hydrothermale Fluide aus dem Untergrund in die Hydrosphäre emittieren. Untersuchungen wurden in vier Regionen durchgeführt: 1) Am südlichen Knipovich Rücken, 2) in einem jungen submarinen Vulkangebiet nördlich des Logachev Seamounts, 3) am Axialen Vulkanischen Rücken (AVR) bei 77°27‘N, den wir Brøgger Rücken nannten und 4) auf dem Molløy Rücken. Insgesamt wurden 16 CTD-Stationen gefahren, wovon 6 Stationen als Tow-yo-CTD-Profile gefahren wurden. Mit dem bordeigenen Multibeam und PARASOUND haben wir 2829 nm vermessen. Hochauflösende Multibeam- und Backscatter-Daten wurden während 8 AUV-Tauchgängen generiert. Die AUV-Tauchdaten von MARUM Seal und die bereitgestellten AUV-Daten des Norwegian Petroleum Directorates bildeten die Grundlage für 13 ROV QUEST-Tauchgänge. In zwei der 4 Gebiete konnten eindeutige Belege für Hydrothermalismus gefunden werden. In dem jungen Vulkangebiet nördlich des Logachev Seamounts wurden an zwei Stellen hydrothermale Präzipitate gefunden und beprobt. Im Gebiet Nr. 3 östlich des Brøgger Rückens wurden in 3200 m Wassertiefe am östlichen Grabenrand zahlreiche, unterschiedlich aktive und inaktive Vents gefunden und beprobt. Neben einem Black Smoker, der 316°C heiße Fluide ausstieß, wurden auch

andere hydrothermale Fluidaustritte bis zu 4°C beprobt. Durch die Kartierung mit dem ROV QUEST konnten wir erstmals für den Knipovich Rücken ein hydrothermales Feld von ca. 1 km Länge und 200 m Breite ausweisen, das wir mit dem Namen Jøtul Hydrothermalfeld bezeichneten. Die Methankonzentrationen sind mit bis zu 4,9 µmol/L im Wasser und bis zu 18,8 mmol/L in den hydrothermalen Flüssigkeiten ungewöhnlich hoch.

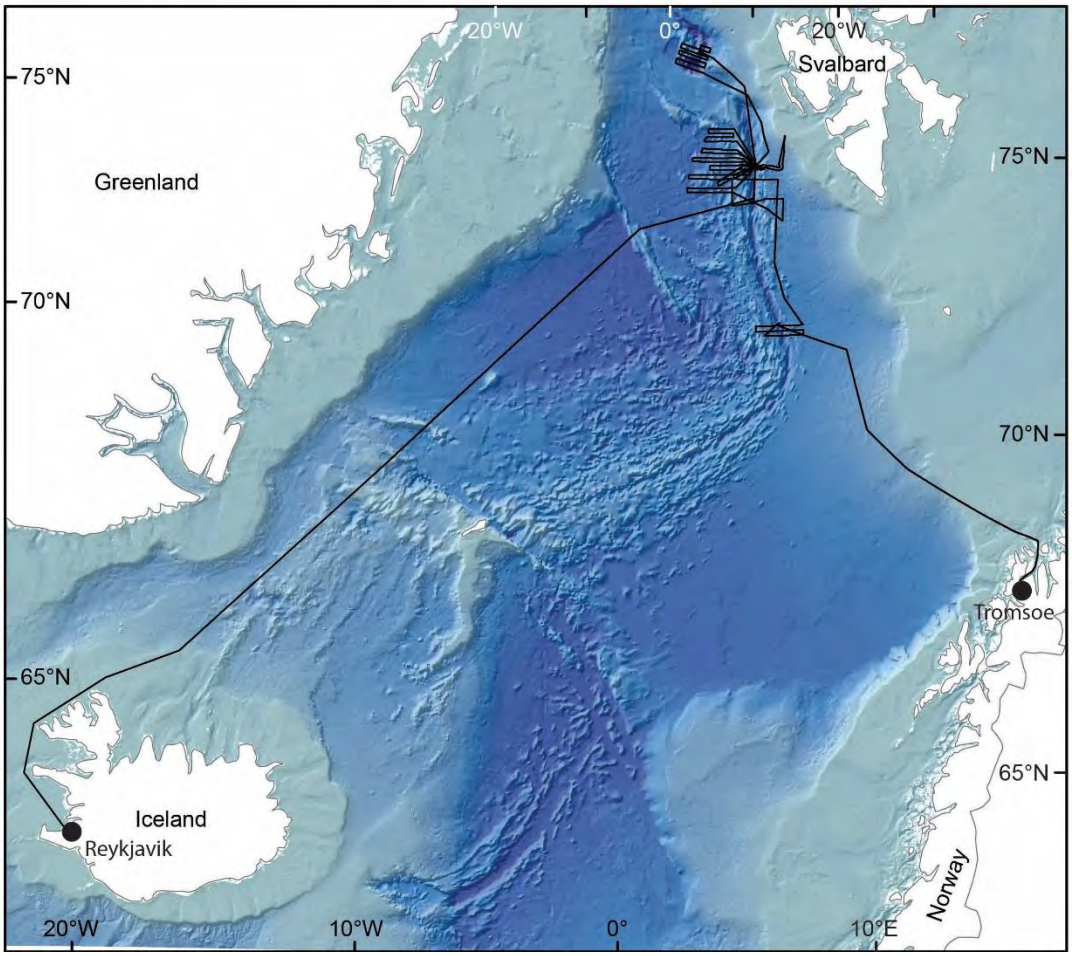

Fig. 1.2.1 Ship track of R/V MARIA S. MERIAN cruise MSM109 from Tromsø to Reykjavik.

2 Participants

2.1 Principal Investigators

Name	Institution
Bohrmann, Gerhard, Prof.	MARUM, GeoB
Römer, Miriam, Dr.	MARUM
Streuff, Katharina, Dr.	GeoB
Smrzka, Daniel, Dr.	GeoB

2.2 Scientific Party

Name	Discipline	Institution
Bohrmann, Gerhard, Prof.	ROV dives / Chief Scientist	MARUM, GeoB
Streuff, Katharina, Dr.	MBES, PARASOUND, ROV	GeoB
Smrzka, Daniel, Dr.	MAPRs, ROV	GeoB
dos Santos Ferreira, Christian	MBES, PARASOUND	MARUM, GeoB
Marschall, Lara	MBES, PARASOUND	MARUM, GeoB
Malnati, Janice	ICOS, GC, CTD	GeoB
Kleint, Jan, Dr.	ISMS, KIPS	MARUM, GeoB
Renzelmann, Henri	CTD	MARUM, GeoB
Knutsen, Stig Morten	ROV dives	NPD
Serje Gutiérrez, Angelly	MBES, PARASOUND, ROV dives	MARUM, GeoB
Coulibaly, Ousmane	AUV, ROV	MARUM
Spiesecke, Ulli	AUV	MARUM
More, Pooja Sanjay	AUV	MARUM
Renken, Jens	AUV	MARUM
Büttner, Hauke	ROV	MARUM
Reuter, Christian	ROV	MARUM
Hüttich, Daniel	ROV	MARUM
Rehage, Ralf	ROV	MARUM
Schade, Tobias	ROV	MARUM
Schröder, Marcel	ROV	MARUM
Tibebu, Abraham	ROV	MARUM

Fig. 2.1 Scientific crew onboard R/V MARIA S. MERIAN during MSM109.

2.3 Participating Institutions

MARUM Center for Marine Environmental Sciences, University of Bremen, Leobener Straße 8, D-28359 Bremen, Germany, http://www.marum.de

GeoB Fachbereich Geowissenschaften der Universität Bremen, Klagenfurter Straße 2-4, D-28359 Bremen, Germany, https://www.geo.uni-bremen.de

NPD Norwegian Petroleum Directorate, Professor Olav Hanssens vei 10, 4021 Stavanger, Norway, https://www.npd.no/en/

Briese Briese Schiffahrts GmbH & Co KG, Abteilung Forschungsschifffahrt, Hafenstr. 12, D-26789 Leer, Germany, https://briese-research.de/

Crew Members from Briese Shipping Operator

Name	Discipline
Maass, Bjoern	Master
Peters, Ralf	Chief Mate
Schilling, Sandra	1st Officer
Bruns, Bastian	2nd Officer
Ogrodnik, Thomas	Chief Engineer
Schwieger, Philipp	2nd Engineer
Rottkemper, Oliver	Electrician
Maggiulli, Michael	System Operator
Herrmann, Jens	Electronics
Vredenborg, Enno	Bosun
Balezos, Georgios	Ship's mechanic
Peschkes, Peter	Ship's mechanic
Grunert, Holger	Ship's mechanic
Wolff, Andreas	Ship's mechanic
Masannek, Paul	Ship's mechanic
Schrapel, Andreas	Ship's mechanic
Preuss, Georg	Ship's mechanic
Seidel, Iris	Stewardess
Brehm, Matthias	1st Cook
Sauer, Jürgen	Motorman
Meyfarth, Torsten	Fitter
Peschel, Jens	Ship's mechanic
Jawadi, Nilufar	Ship's doctor

3 Research Program

3.1 Description of the Work Area

The proposed study sites, Knipovich Ridge and Molløy Ridge, are two of several segments of the of the Mid-Atlantic Ridge north of the Arctic circle (66°N), which are considered as the Arctic

Mid-Ocean Ridge (AMOR; Pedersen et al., 2010a). The AMOR consists of the Kolbeinsey, the Mohns, the Knipovich, and the Molløy Ridges, the Lena Trough, and the Gakkel Ridge (Fig. 3.1). The Knipovich Ridge is situated asymmetrically between Svalbard and NE Greenland, and extends from 73°30'N to 78°40'N. It is bordered by the Molløy Fracture Zone in the north and the Greenland-Senja Fracture Zone at the Mohns-Knipovich Ridge Bend in the South. With a spreading rate of <1.5 cm/yr it is one of the slowest and most obliquely spreading mid-ocean ridges on the planet (Fig. 3.1). Magnetic and gravimetric surveys along the ultraslow-spreading Gakkel Ridge and Mohns Ridge (Crane and Solheim, 1995) showed ongoing sustained and continuous seafloor spreading. Investigations in the past, that were predominantly performed by international scientists, have shown that Knipovich Ridge is characterized by a rather complex structure (Okino et al., 2002; Chamov et al., 2010, Curewitz et al., 2010, Zarayskaya, 2017).

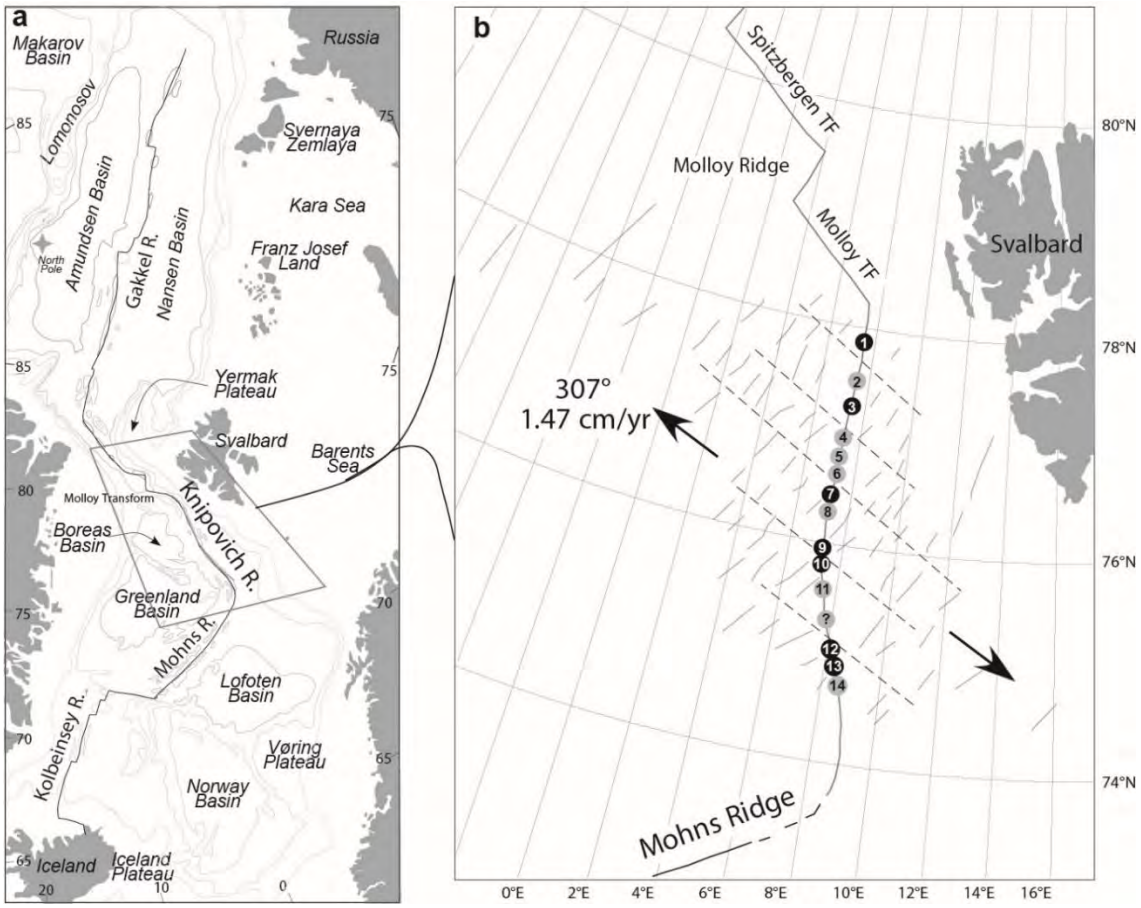

Fig. 3.1a Locations of Arctic Mid-Ocean Ridges, continental land masses, and Knipovich Ridge north of Mohns Ridge. Contour lines of the ocean basin depths in 1,000 m intervals**.**

Fig. 3.1b Segmentation of Knipovich Ridge and tentative magnetic lineations. The numbered circles indicate centers of spreading segments. Gray circles correspond to weaker segments (from Curewitz et al., 2010).

A bathymetry grid originating from seafloor mapping and other comprehensive investigations was collected during four Russian cruises with R/V AKADEMIK NIKOLAI STRAKHOV (2006, 2007 and 2009). Based on the morphology and specifically on the morpho-structural segmentation, major tectonic elements of Knipovich Ridge have been classified. These investigations revealed that the formation of this active plate boundary was accompanied by the alteration of geodynamic

settings with the predominance of strike-slip and normal faults. These processes still compete in the formation of the ridge's rift zone (Okino et al., 2002).

The Knipovich Ridge is uninterrupted by transform faults even though the available bathymetric and gravity data have been interpreted to indicate the presence of seven magmatic strong (1st or 2nd order?) and seven magmatic weak (2nd or 3rd order?) segments (Fig. 3.2, after Okino et al., 2002). Four of the magmatic robust segments fall at the intersection between the rift valley and linear chains of off-axis seamounts. This segmentation scheme correlates well with the identified magnetic anomaly pattern and locations of proposed discontinuities.

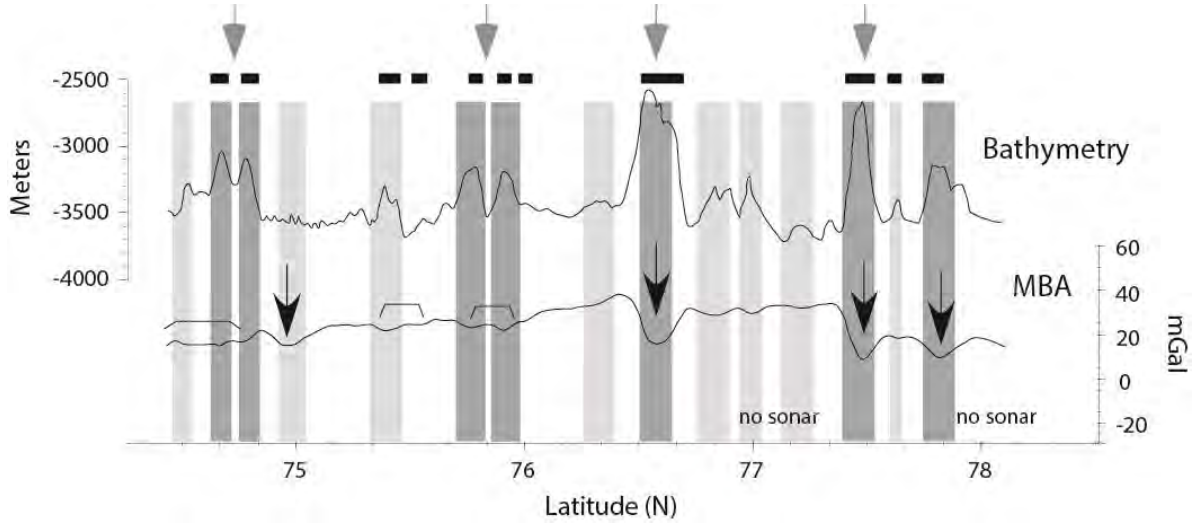

Fig. 3.2 Top: Along-axis bathymetric profile with identified spreading segments. Dark gray vertical bars indicate robust segments anchoring off-axis seamount chains (gray downward pointing arrows); light gray vertical bars indicate smaller, weaker segments; black boxes mark seafloor dominated by hummocky lava flows and pillow ridges identified in sonar records. Bottom: Corresponding mantle Bouguer anomaly (MBA) profile shows minima (black arrows and brackets) beneath identified segment centers (from Curewitz et al., 2010).

The rift zone of Knipovich Ridge is generally formed in a transtension environment. Differences in the spreading formation in its northern and southern parts resulted in differences in morphological structures. The northern part has a well-defined rift valley with a V-shaped cross profile and two magmatic segments as uplifts perpendicular to the spreading. The latter are separated by short rhombic strike-slip basins with reduced volcanic manifestations. The strike-slip basins occupy most part of the rift, and volcanic build-ups seem to be absent. By contrast, the southern area has a shallower rift valley with a U-shaped cross profile and one perpendicular spreading uplift formed within a large extension basin. This area represents a stress accommodation zone with chaotic relief of low-amplitude faults. Moreover, spreading along the magmatic segment south of 76°N is characterized by brittle tectonic spreading. As supported by physical modeling (Dubinin et al., 2013), the northern part of Knipovich Ridge shows up as an alteration of shears and orthogonal pull-apart structures with topographic heights correlating to increased volcanic activity. On one hand, those findings are consistent with the observation that the crust beneath the ridge is cold, favoring brittle behavior, and thin in the magmatic segments (Jokat et al., 2012). On the other hand, the alteration fits to the postulation of spreading cells (second order segments as described in Carbotte et al., 2016). Focusing of the melt possibly caused

by the presence of spreading cells was firstly shown by Okino et al. (2002) and revised by Jokat et al. (2012). First evidences of these mechanisms were reported by Schlindwein et al. (2013), who showed a seismic gap beneath a cluster of axial volcanic cones.

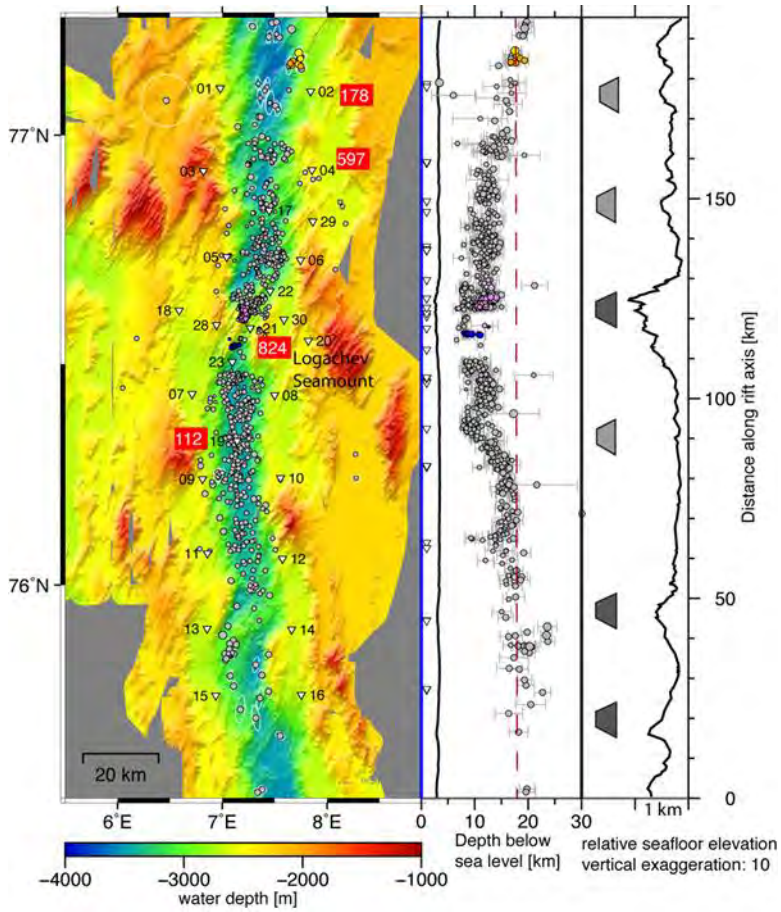

Fig. 3.3 Left: Map of Knipovich Ridge showing the epicenters of the 1,000 best recorded earthquakes out of 15,000 events detected by the KNIPAS network (Schlindwein et al. 2017). Triangles mark seismometer locations. Colored events are part of seismic swarms. Numbers in red boxes indicate short duration events. Middle: Hypocenter locations indicate maximum depth of faulting, corresponding to an isotherm of about 600°-800°C, red dashed reference line highlights shallowing of Hypocenters towards Logachev Seamount. Right: Exaggerated rift axis relief and segmentation from Curewitz et al. (2010).

From 2016 to 2017 the passive seismic network KNIPAS (Schlindwein et al., 2017) recorded earthquakes between 75.7°N and 77.1°N along Knipovich Ridge to study its active spreading processes and refine ridge segmentation based on seismicity (Fig. 3.3). Different depth levels of the brittle-ductile boundary are obvious, as well as areas without brittle deformation in the crust. The maximum depth of faulting clearly decreases towards Logachev Seamount in the center of a 1st or 2nd order segment. The volcano is underlain by a prominent seismic gap and showed seismic swarm activity in March and June 2017. The seismicity pattern is very similar to the Segment-8 volcano on the ultraslow spreading Southwest Indian ridge (Schmid et al. 2017), that hosts a melt body in the seismic gap feeding ongoing intrusion activity. Logachev Seamount may therefore be considered magmatically active, and heat to drive hydrothermalism can be expected.

Further signs of hydrothermalism stem from the observation of short duration events. Such events have mostly been associated with fluid release in sediments (Franek et al. 2017, Batsi et al. 2019). Across the network, 4 stations show significant numbers of such events. Apart from stations 21 and 19 associated with magmatism in the rift valley, stations 02 and 04 at the intersection of subordinate magmatic rift structures with the rift flank show frequent short duration events, partly following the deeply seated seismic swarms near station 02.

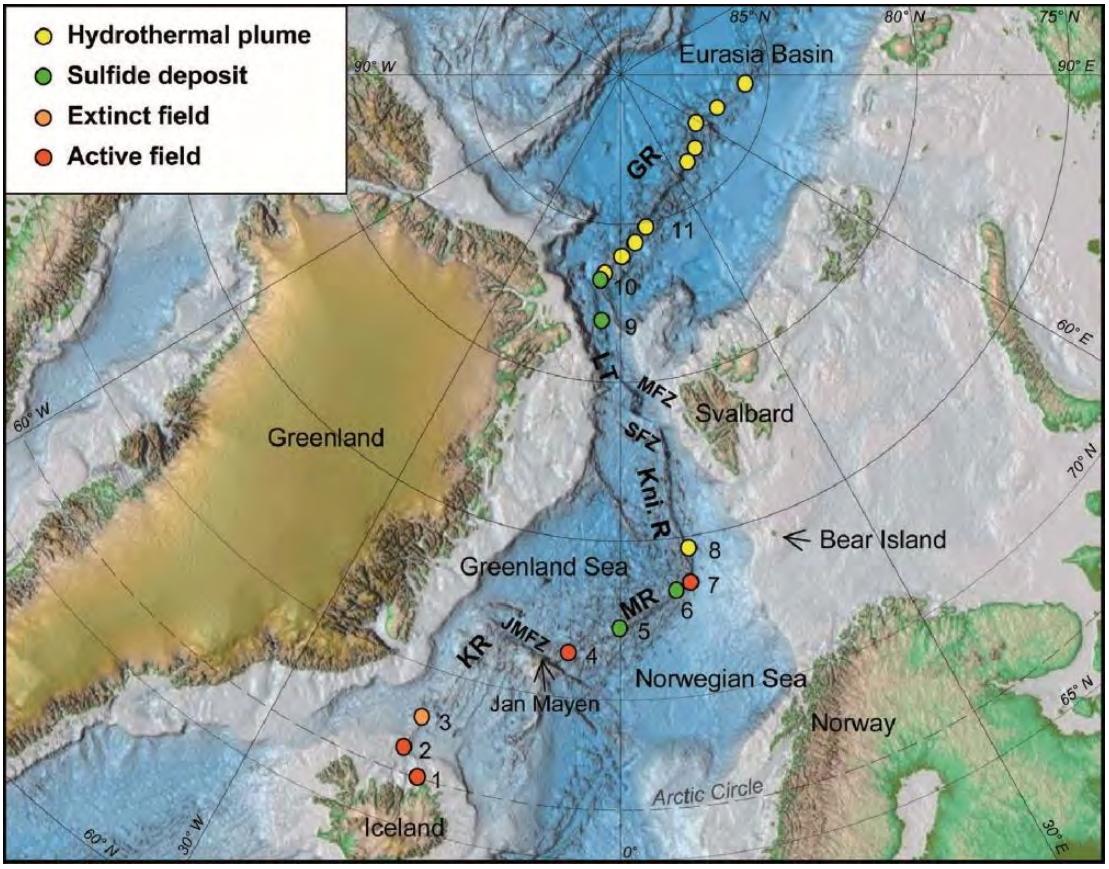

Fig. 3.4 **A**rctic Mid-Ocean Ridges (AMORs) showing locations of active and extinct hydrothermal vent fields. Grimsey (1), Kolbeinsey (2), Squid Forest extinct field (3), Jan Mayen, Soria Moria, and Troll Wall (4), Copper Hill (5), Mohn's Treasure (6), Loki's Castle (7), hydrothermal plume (8), sulfide deposits (9), sulfide deposits (10), hydrothermal plume (11) from Pedersen et al., 2010a). GR-Gakkel Ridge, LT-Lena Trough; MFZ-Molløy Fracture Zone; SFZ-Spitsbergen Fracture Zone; Kni. R-Knipovich Ridge; MR-Mohns Ridge; JMFZ-Jan Mayen Fracture Zone; KR-Kolbeinsey Ridge.

As summarized by Vogt (1986), Knipovich Ridge terminates at its northern end against both, the continental margin of Svalbard and the Molløy Fracture Zone (Fig. 3.1). The 120-km-long Molløy Fracture Zone, striking 300°, intersects with the north-trending Molløy Ridge in the middle of the Fram Strait. In the area of the intersection, the Molløy Deep or Molløy Hole, which represents the deepest water depth of 5,669 m in the northern North Atlantic according to Klenke and Schenke (2002), has formed. The Molløy Ridge itself shows complex topography with a series of elevations, whereas the location of the spreading axis is not well defined. Rock samples dredged along the Molløy Ridge are all peridotites (Snow et al., 2001) indicating that mantle material is outcropping at the ridge. It terminates 60 km to the north against the Spitsbergen Fracture Zone adjacent to the Svalbard continental margin (Crane et al., 1982). At this intersection a fairly deep

depression defined by the 4,000m-isobaths called the Hayes Deep (Thiede et al., 1990) has formed as well. The 308° striking Spitsbergen Fracture Zone reveals an offset of 145 km to the northwest, where the Lena Trough is representing the spreading zone of the northward following Gakkel Ridge.

Until recently, Arctic mid-ocean ridges and their hydrothermal systems were some of the least explored elements of the global ridge system. In contrast, there is considerable scientific interest in these systems, e.g., because of their ultraslow spreading rates, the high density of mantle-derived peridotites, their proximity to continental margins, and voluminous accumulations of organic-rich sediments with high hydrocarbon generation potential on parts of the ridges. Systematic exploration of the spreading ridges north of Iceland (i.e., AMOR) during the past 25 years documented a large number of active and inactive venting sites. Locations of approximately 20 active and extinct vent areas have been either identified during seafloor observations, or inferred from physicochemical anomalies of the seawater that are caused by hydrothermal plumes and from dredge sampling of hydrothermal precipitates (Fig. 3.4).

Decreasing spreading rates and decreasing influence of the Icelandic hot spot toward the north along the AMOR result in a south-north change from shallow and magmatically-robust to a deep and magmatically-starved ridge system (Pedersen et al., 2010a). This contrast gives rise to a large variability in the geology of the ridges and in the formation and geochemistry of associated hydrothermal vent fields. The known vent sites at the southern part of AMOR are either low-temperature or white smoker fields. At the deep, northern parts of AMOR, large black smoker vent fields have been located. Physicochemical anomalies of the seawater and sulfide deposits at the seabed suggest that black smoker-type venting is common. Several of these venting sites may be peridotide-hosted. The hydrothermal activity at parts of the AMOR is 2 to 3 times higher than that expected from extrapolation of those observed at faster spreading ridges.
A larger area hosting fractures/ fault systems relative to the extracted magma volume seems to be a likely explanation for this higher activity. Many of the vent fields at the AMOR are associated with axial volcanic ridges (AVR). Strong focusing of magma toward these ridges, deep rifting of the ridges, and subsequent formation of long-lived detachment faults, that are rooted below the ridges, may be the major geodynamic mechanisms causing the unexpectedly high hydrothermal activity (Pedersen et al., 2010a). Hydrothermal venting north of Iceland was first described from the Kolbeinsey Field (Fig. 3.4) (Botz et al., 1999) and the Grimsey Field of the Kolbeinsey Ridge (Hannington et al., 2001). Today, the vent fields along the Kolbeinsey Ridge are well-explored. Further findings from Lena Trough (Snow et al., 2001) and from Gakkel Ridge (Edmonds et al., 2003) followed (Fig. 3.4). Many hydrothermal vent fields were also found and explored from Mohns Ridge: Soria Moria Field, Troll Wall, Copper Hill, Mohn's Treasure and Loki's Castle (Pedersen et al., 2010b), from which the last one was intensively investigated.
Loki's Castle Vent Field (No.7 in Fig. 3.4), which is located at Mohns Ridge at about 2,400 m water depth, was the first black smoker vent field visited at an ultraslow-spreading ridge and in the Arctic waters. The field is located in the vicinity of the area where the striking of Mohns Ridge changes about 80° to a more northerly trend and merges into the Knipovich Ridge. It is additionally situated near the summit of a large AVR. Venting from Loki's Castle Vent Field occurs from the top of two hydrothermal mounds that are around 20–30 m high and approximately 200 m across.

Venting causes a hydrothermal plume in the water column that rises 300–400 m above the seafloor and is characterized by anomalies in Eh, CH_4, and H_2 (Pedersen et al., 2010b; Baumberger et al., 2016). Low-temperature venting also occurs at the flank of the mound and gives rise to a distinct field of barite chimneys (Eickmann et al., 2014). Although Loki's Castle Vent Field is underlain by volcanic rocks, the influence of sediments from the nearby Bear Island sedimentary fan is observed in the fluid chemistry (e.g., high concentrations of methane and ammonia). Lead and likely also S and the $^3He/^4He$ ratio show not only evidence for interactions with the basaltic basement, but also with sediments (Baumberger et al., 2016). Linkage between sedimentary influence and ultraslow spreading resulted in a new type of sediment-influenced hydrothermal system.

Loki's Castle Vent Field hosts an unique Arctic vent fauna represented by siboglinid tube worms (*Sclerolinum contortum*), a putative new species of amphipod, small grazing gastropods and others (Pedersen et al., 2010b). Moreover, a new group of microbes named Lokiarchaeota, was sampled at Loki's castle for the first time. Lokiarchaeota was described in 2015 after the identification of a candidate genome in a metagenomic analysis of the mid-oceanic sediment sample (Spang et al., 2015). This analysis suggested the existence of a genus of unicellular life dubbed *Lokiarchaeum*. Lokiarchaeota became a proposed phylum of the domain Archaea, remarkably, a phylogenetic analysis disclosed a monophyletic grouping of the Lokiarchaeota with the eukaryotes. The analysis revealed several genes with cell membrane-related functions. The presence of such genes support the hypothesis of an archaeal host for the emergence of the eukaryotes.

In addition to the hydrothermal vent fields at Kolbeinsey Ridge and Mohns Ridge, several indications of hydrothermal activity like sulfide deposits and hydrothermal plumes in the water column are known from Lena Trough and Gakkel Ridge (Fig. 3.4). In contrast, hydrothermal activities are not known so far from Knipovich Ridge and Molløy Ridge, except for a single location (No. 8 in Fig. 3.4) at a ridge around 74°47'N (Connelly et al., 2007). At this site, plume signals in the water column were detected using *in situ* optical backscatter sensors suspended from a deep-tow side-scan sonar instrument as it was towed along a 2 km section of survey track from 74°46.7'N, 08°28.1'E to 74°47.7'N, 08°27.0'E over a ridge axis.

3.2 Aims of the Cruise

As part of the research unit "The Ocean Floor as Reactor" of the Bremen Cluster of Excellence "The Ocean Floor – Earth's Uncharted Interface" we used R/V MARIA S. MERIAN cruise MSM109 to investigate hydrothermal fields of the Knipovich Ridge and Molløy Ridge in the Norwegian Greenland Sea west of Svalbard. In contrast to other spreading ridges in the European Northern Sea and the Arctic, these more than 500 km long segments of ultraslow oceanic spreading have hardly been investigated, and active hydrothermal fields on the seabed are yet unknown.

3.3 Agenda of the Cruise

Previous geological investigations and more recent multi-beam echosounder measurements during MSM57 and MSM68 along the Knipovich Ridge show a clear segmentation in the occurrence of igneous rocks that alternate with sediment-covered sections on the seabed. Based on indications

of hydrothermal plumes in the water column, on registered earthquakes, and on detailed multi-beam data, we worked in four different areas: The Molløy Ridge, the Brøgger AVR, die AVR at Logachev Seamount and at the southern Knipovich Ridge. After having identified plumes during dives with the AUV MARUM-SEAL and in the course of CTD stations, detailed investigations and samplings were carried out with MARUM ROV QUEST 4000.

4 Narrative of the Cruise

On **Wednesday, 6 July 2022**, R/V MARIA S. MERIAN left Tromsø bunker pier at 11:00 a.m. local time to set sail for the Norwegian Sea. Marine geological investigations of hydrothermal vents and its distribution at the sea floor of the Knipovich ridge are the focus of mission MSM109.

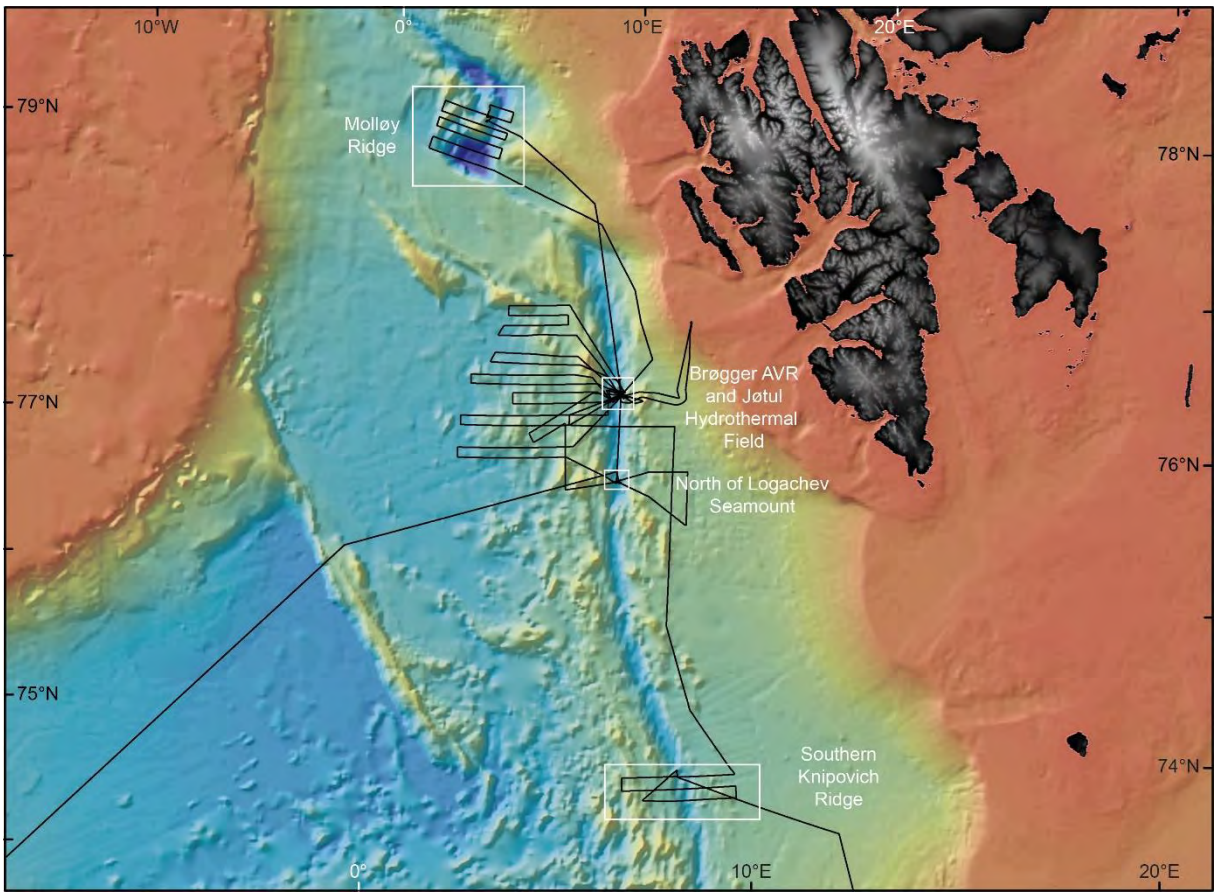

Fig. 4.1 Research areas and track lines of R/V MARIA S. MERIAN cruise MSM109 in the northern Norwegian-Greenland Sea.

The two main devices, the ROV (Remotely Operated Vehicle) QUEST and the AUV (Autonomous Underwater Vehicle) of the MARUM had to be installed on the research vessel during the port time. For this purpose, 8 containers were delivered from Germany to Tromsø, which were partly set up on the ship's deck with a special crane on land. This happened on **Sunday 3 July** and had to be completed in the evening as the ship had to move from pier 24 to pier 25. The arrival of the new scientists and crew members was associated with many short-term changes, since flight operations caused chaotic conditions in some cases due to strikes, threats of strikes, cancellation of flights and a lack of personnel for aircraft and airports. Despite this, the scientists, with the

exception of two stragglers, were able to embark on **Monday, 4 July** after presenting a current negative corona test. Since there are no test centers in Norway some of us were tested for corona by the on-board doctor before boarding the ship. Inside the ship and when people gather on deck, we wear FFP2 masks for the first 7 days on board and have to test ourselves for the Corona virus for the first 5 days in the morning before we are allowed to leave our cabin.

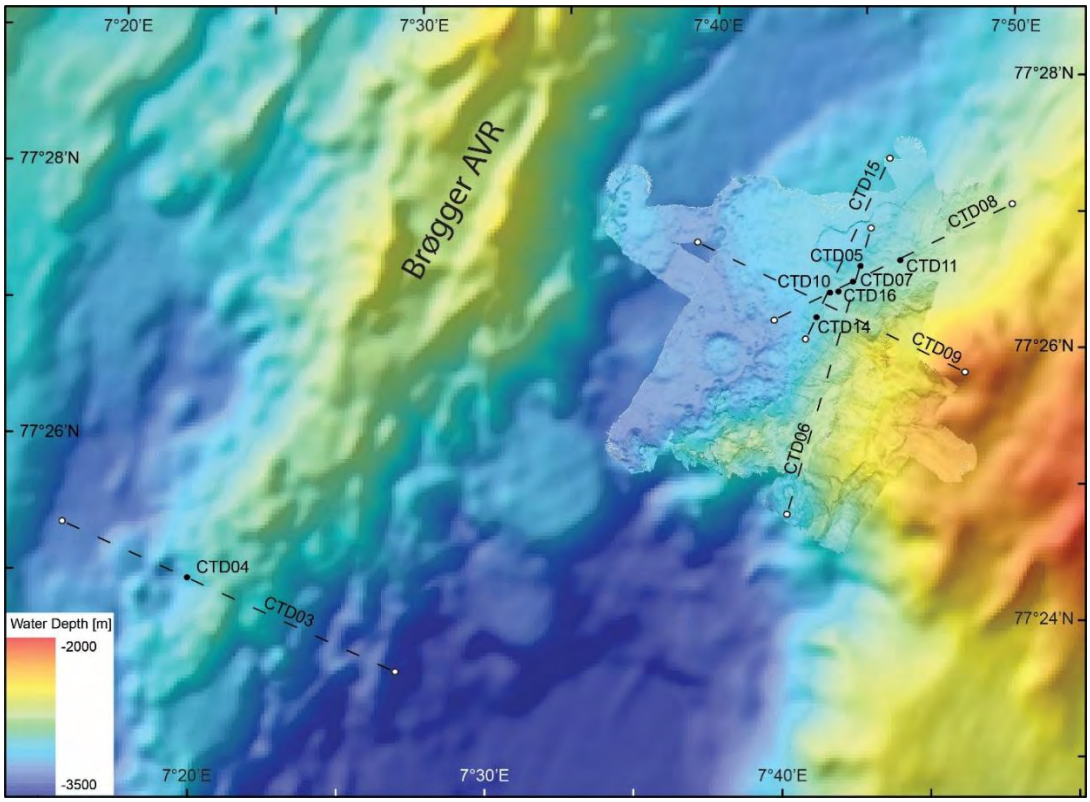

Fig. 4.2 CTD-stations taken during MSM109 at the southern Brøgger Axial Volcanic Ridge (AVR) and in the area of the Jøtul hydrothermal field.

After two nights on the research vessel in the port of Breivika/Tromsø, on **Wednesday, 6 July**, it was time to cast off, and the MARIA S. MERIAN started to move. A 6-hour journey took us first through the 4-5 km wide passage of Grøtsundet and then about 25 km through the fjord landscape of Fugløysundet before we reached the open shelf sea of the Barents Sea. The rain in Tromsø and the dense clouds within the fjords made us expect bad weather, to which we were then exposed when we reached the open sea. Wind speeds of 8 on the Beaufort scale with occasional gusts of up to 9 whipped up the sea and caused some of us to feel unwell, which lasted until mid-morning the following day. Towards evening, the sea had calmed down and everyone was fine again. On the way to our working area, we overran the Håkon Mosby mud volcano on the continental slope to the Barents Sea fan. This mud volcano has been well studied in the past and appears to be characterized by continuous activity of methane leaks. This time, we were able to detect the active escape of gas in the water column above the mud volcano with the ship's hydro-acoustic systems when crossing it. We reached our actual target, the southern Knipovich ridge (Fig. 4.1), on **Friday 8 July**, starting to the South with a CTD-station in an area where signals from a hydrothermal plume could be identified in the water column in previous years. A planned AUV-dive to measure the seabed had to be aborted for technical reasons, and so we decided to alternatively carry out measurements of the seabed further north after a second CTD-station. The Knipovich ridge is about

500 km long and is part of the spreading zone between the North American plate and the Eurasian plate emission sites and hydrothermal vents on the seafloor had not yet been detected from Knipovich ridge. The aim of our expedition was to find hydrothermal signs or even spring outlets at the Knipovich ridge in order to understand their impact on processes to the seafloor.
An expedition by the Norwegian Petroleum Directorate north of 77°24'N last year found signs of hydrothermal activity by measuring the redox potential close to the ground, which we want to examine more in detail now. On the way there, we passed previously uncharted areas of the seabed and mapped the seabed with the multibeam echosounder and the sediment echosounder PARASOUND. We reached the area of potential hydrothermal activity on **Saturday evening 9 July**, and started surveying the water column at midnight with a CTD-station (CTD03, Fig. 4.2) and our Eh-sensors. At a slow speed of only half a knot, we scanned the water column between the seafloor and a water depth of 2,700 m by Tow-yo-like movements of the probe with the ship's wire over a profile length of about 4 nautical miles and took water samples.

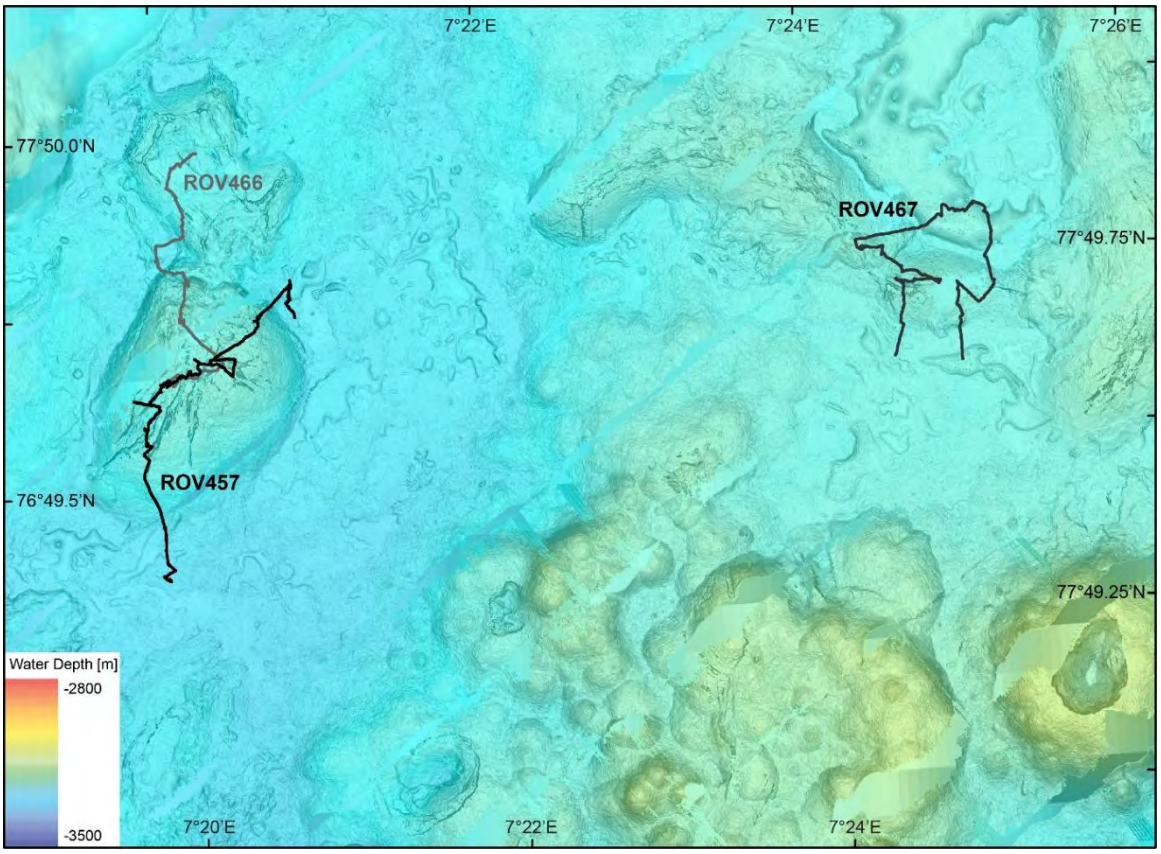

Fig. 4.3 ROV QUEST dives performed in a young volcanic area north of Logachev Seamount (micro-bathymetry data are from Norwegian Petroleum Directorate, Stavanger).

The analysis of the water samples was carried out in the ship's laboratory on **Sunday morning, 10 July**. At the same time, MARUM ROV QUEST dived to the seabed for its first dive during the cruise (ROV455), where we carried out investigations in 3,200 m water depth during the course of the day. We explored a seafloor region at the southern end of the Axial Volcanic Ridge (AVR) at 77°24'N latitude. There, an Eh-anomaly in the water column about 70 m above the seafloor was measured with an AUV during the expedition of the Norwegian Petroleum Directorate last year. The goals of this dive were to find an explanation for this anomaly on the seafloor, but at the same time to understand the bottom composition of the AVR. Unfortunately, the dive had to be cancelled

earlier than planned for technical reasons. We did not find reasons for last year's Eh-anomaly, but we were able to gain important geological insights. Volcanic rocks form the approximately 20 km long and more than 500 m high AVR in the middle of the 3,500 m deep central graben of the Knipovich ridge. The basalts we found at this AVR occur in the form of solidified tubular pillow lavas, which are covered with a relatively large amount of hemipelagic sediment. Despite the sedimentary cover, very characteristic elements of the pillow basalts could be seen,, such as volcanic glass at the outer edge of the pillows and shrinkage cracks caused by the cooling of hot lava in cold seawater. We specifically collected corresponding rock samples from the seabed.

During a second longer dive with MARUM ROV QUEST on **Tuesday 12 July** in this area we were able to investigate a larger area. The pillow basalts form numerous mounds of about 20-40 m in height and 200-300 m in diameter, the areas between the mounds are completely covered with sediment. These hill structures, which are widespread on the AVR, had already been noticed in the high-resolution bathymetric maps of the Norwegian AUV survey, whereby the formation of the hill structures from the dives is now better understood. A second, very prominent axial volcanic ridge (AVR), lies close to the Logachev Seamount, about 50 nautical miles south of the previously studied AVR, in whose extension an apparently young volcanic area appears morphologically (Fig. 4.1). It is mainly characterized by very high backscatter values in the side-scan sonar and backscatter recordings of the AUV multi-beam survey.

We were able to understand that relatively young volcanic activity prevails there during a very extensive ROV-dive (ROV457) on **Wednesday, 13 July** (Fig. 4.3). In contrast to the previously examined AVR, there is significantly less sediment cover and an unexpectedly large variety of cooled volcanic lava rocks were found on the seafloor. In addition to pillow lavas, that are already known, we could also distinguish between ropy lavas and flat and smooth former lava sheet flows, which we also sampled individually. In addition, there were deposits of very rough, sharp-edged lava fragments, which indicate lava that was formerly very gas-rich and are referred to as a'a' lava in Hawaii. Here, a hill structure 50 m high and 500 m in diameter was built up by these magmatic rocks, which, however, showed huge cracks and fissures of several meters deep in the direction of the spreading (Fig. 4.3). In one of those fissures we found hydrothermal precipitates in the form of rock staining and small sulfide smokers for the first time. Due to technical problems with the ROV, we were no longer able to investigate whether there was still low thermal activity. Unfortunately, the technical problems of the ROV continued until the end of the week and it was not until this **Sunday, 17 July**, that we are back on the seabed with the ROV.

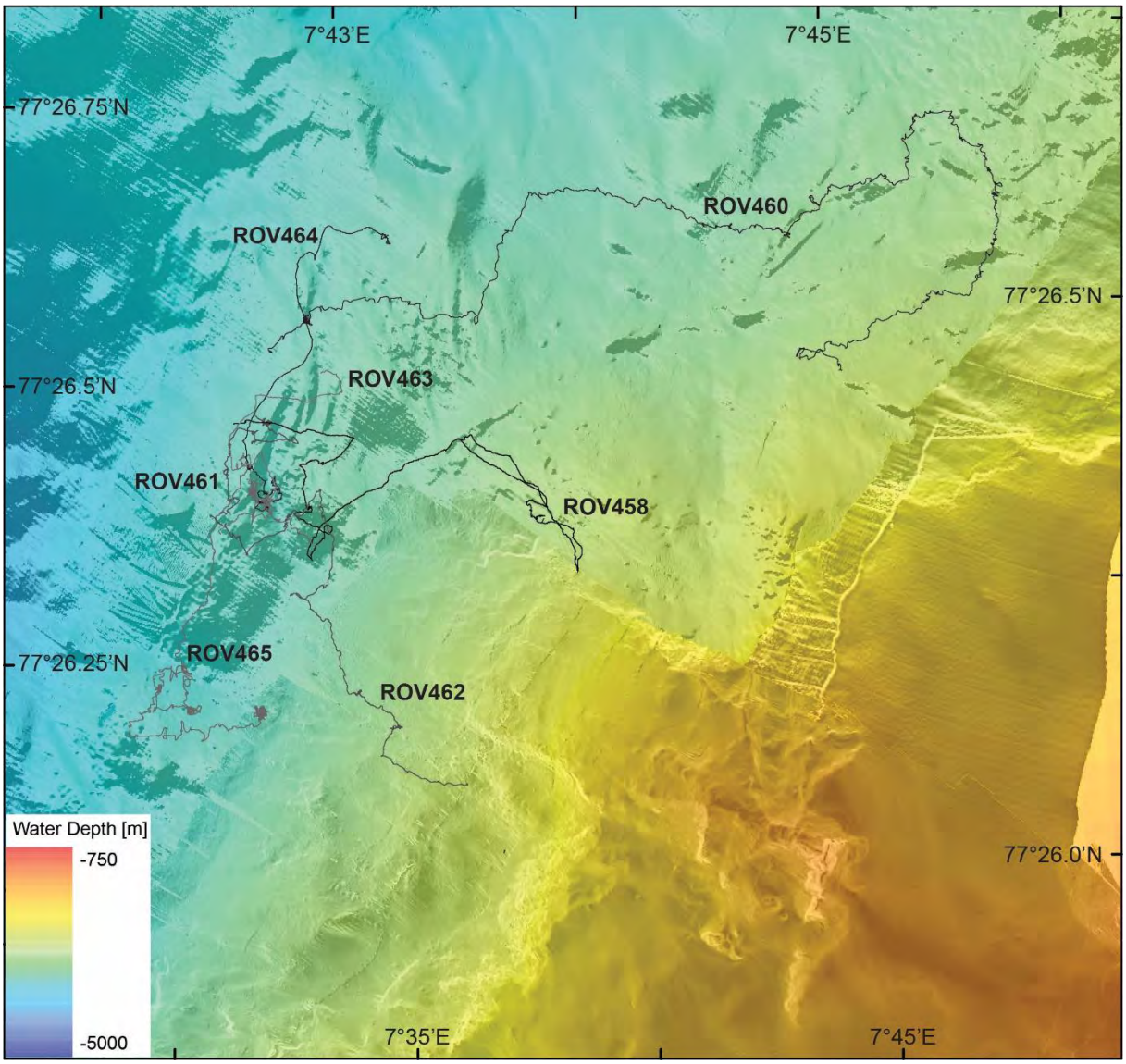

Fig. 4.4 ROV-dives performed during MSM109 in the area of the Jøtul hydrothermal field.

With the AUV, we carried out micro-bathymetric measurements in the area of the slide complex on **Tuesday, 12 July** and **Thursday night, 14 July**. Here, we were guided by an earlier measurement of the redox potential in the water column, too, which we were able to confirm during a CTD measurement with an Eh-sensor. In the meantime, this region has proven particularly attractive to continue searching for hydrothermal activity as we have detected Eh-anomalies and small temperature anomalies in several Tow-yo CTD profiles (Fig. 4.2). In addition, the water samples with levels of 100-1,000 nmol/L have high methane concentrations with otherwise background levels of 2-4 nmol/L. Unfortunately, there were technical issues with both the AUV and ROV in the second half of the week, so we used the ship time for other work. The focus was on surveying with the ship's own multi-beam, especially of the western shoulder of the Knipovich graben (Fig. 4.1) together with the CTD-measurements. On **Saturday evening, 16 July** both diving vehicles, AUV and ROV, were operational, but the weather was blowing too hard with Beaufort 7 winds. The sea only calmed down again this Sunday and we are back on the seabed in the area of the slide complex with the QUEST diving robot. So far, we have found a large number

of white bacterial mats there, mostly at the edges of individual pillow layers, which indicate diffuse escape of fluids.

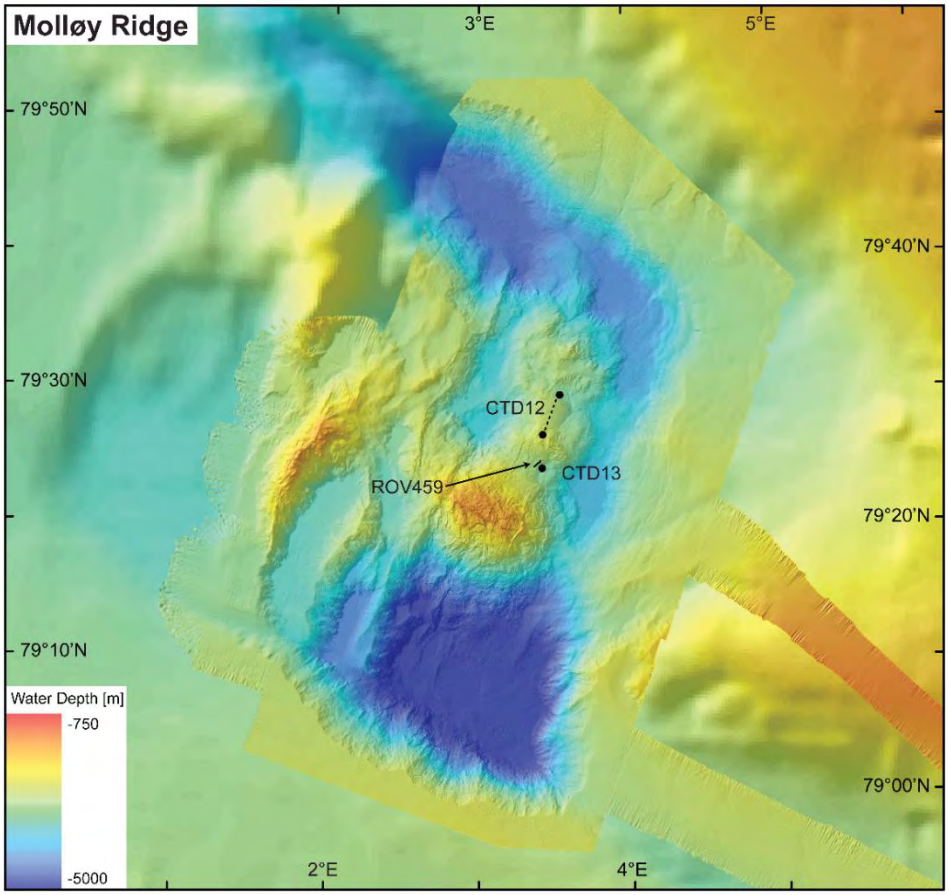

Fig. 4.5 MSM109 station work on Molløy Ridge.

Our 3rd week was the most successful week, because for the first time we were not only able to document but also to measure hydrothermal vents at the Knipovich ridge. Also, the technical problems of AUV and ROV have been overcome. During last Sunday's dive we discovered patchy areas of tubeworms and microbial filaments that gave us the first indications of active fluid outflows in an area of the eastern rim of the graben. To further explore this prospective area, an AUV-dive was conducted during the night and a CTD-station in the morning to measure methane distribution. The following Monday we steamed north into the Fram Strait between Greenland and Svalbard to conduct investigations at the Molløy spreading center (Fig. 4.5). The two weeks before, this area was covered with pack ice, which drifted from the Arctic Ocean into the East Greenland Current via the Transpolar Drift and prevented station work there on the Molløy Ridge. The R/V MARIA S. MERIAN with its ice class PC7 does not have to fear sea ice, but the operations with our ROV and AUV deep-sea vessels require ice-free water. The ice situation allowed us to do all our surveys, station work and dives from **Monday, 18 July** to **Wednesday, 20 July**.

Midweek we steamed out of the Fram Strait back to the Axial Volcanic Ridge (AVR) at 77° 20'N. To distinguish this AVR from the AVR further south near the Logachev Seamount we use the

name of Waldemar Christofer Brøgger, a Norwegian geologist who has become internationally famous not only for his work on the igneous rocks of the Oslo Graben. At the geographical latitude of the now named Brøgger AVR, we had the best chance of finding and documenting hydrothermal activities of the Knipovich ridge at the eastern edge of the graben thanks to our Eh- and methane anomalies and our first observations from a dive. Therefore, during two AUV dives, we added further micro-bathymetry to an earlier AUV map of the Norwegian Petroleum Directorate in order to get as much preliminary information as possible on the morphological phenomena for the diving work with the ROV. We are measuring a last missing bathymetry area on the seabed of this region this Sunday night. We focused on a north-south band at a water depth of 3,000 m in the foot area of the graben's eastern rim, which is characterized by a further subsidence of the seabed to the West up to Brøgger AVR to about 3,500 m.

The AUV map shows that igneous rock bodies are also present in the deepest part, extending to the foot of the eastern graben depression. During the ROV dives on **Friday, 22 July**, and **Saturday, 23 July**, we repeatedly observed outflows from pillow lavas that formerly flowed onto a sedimentary bedrock. Some rift-parallel fissures at a water depth of about 3,000 m also show on the fissure walls that pillow basalt layers stacked on top of each other contribute to the structure of the lower slope area of the rift wall. During the dives we repeatedly found indicators of hydrothermal venting in an approximately 50-70 m wide strip parallel to the slope. These could usually be recognized by white staining, which could be traced from the lower edges of the rock in a vertical direction on the surface of rocks. On closer inspection, tubeworms cloaked in filaments of bacteria can always be found in the area. Very small gastropods and crabs, a few millimeters in size, can usually be seen. Fluid samples showed that methane concentrations of several 100 nmol/L are present there. During dive ROV461 (Fig. 4.4) on **Saturday, 23 July** we sampled an exit site with shimmering fluid that was 8°C and mixed with bottom water at -0.6°C. The methane level rose to almost 2 µmol/L and had a distinct H_2S-odor after recovery. The corresponding chemosynthetic organisms and precipitates from the location were recovered and are being investigated within the Bremen Cluster of Excellence. During the dive we were also able to recover sulfide precipitates and parts of a chimney which was mainly gypsum. The sampled region appears characterized by widespread diffuse venting, which explains the high methane concentrations we measured in the CTD water samples.

After the 3rd week of our expedition was quite successful, the 4th week was associated with even more scientific highlights. We were able to dive during all days, further examining the region of seafloor hydrothermal activity that we had mapped from the methane and Eh-anomalies in the CTD profiles of the water column. On **Monday, 25 July** during ROV-dive 463 we discovered a black smoker whose fluid at a temperature of over 300°C shot out of an almost 20 cm opening. Since the opening was not directed upwards but to the side and the chimney area sat relatively short on a mound of older hydrothermal deposits, it was a great challenge for the ROV pilots to carry out the necessary sampling on the smoker. In addition to the fluid samples at three different points of the outflow, a piece of the sulfide precipitates could be obtained from the edge of the smoker, too. The methane levels, which are in the range of mmol/L, surprised us, but explain why we measured quite high levels of methane in the water of our CTD-casts and -profiles. During Tuesday's dive, we revisited the smoker for temperature and further fluid sampling and mapped

the northward distribution of bottom hydrothermal features. During the night, our AUV Seal 5000 surveyed the area with a higher resolution than before by conducting a dive just 60 m above the seafloor. This map gave us more details that we were able to use during the ROV-dive on **Wednesday, 27 July**. Wednesday's ROV-dive (ROV465) explored the southward extension of the hydrothermal field and amazed us with more findings of active fluid vents.

A complex hydrothermal edifice with numerous chimneys and flanges was found. The hot fluid escaped everywhere, so that the entire structure was completely surrounded by shimmering water, and photo-documentation was extremely difficult. Here, too, the outlet temperature was over 250°C and the methane content was several mmol/L. We were fascinated in such a way by this hydrothermal vent, that we named it Yggdrasil, the term for the tree of life in Norse mythology. With these results of the expedition, we could define a new hydrothermal field, namely the first of the 500-km-long Knipovich Ridge. The field has an extension of about 1 km in north/south direction and with a width of 150-250 m it follows the eastern marginal fault at a water depth of 3,000 m. We called it the Jøtul hydrothermal field, a name for a being that in Norse mythology corresponds to a giant that dwells in a mountain or range. The last two ROV-dives (ROV466 and ROV467), on **Thursday, 28 July**, and **Friday, 29 July**, we dived 50 km to the South in what is probably the youngest volcanic area in 3,200 m water depth (Fig. 4.3). There, too, we had already found hydrothermal relics on an earlier dive, but they were very difficult to find in a 10 m deep and very narrow canyon of mainly piled up pillow lavas. In fact, more hydrothermal relics were found on Thursday with possible sulfide deposits. Friday's short ROV-dive captured an abundance of existing lava structures and morphologies. We were also able to welcome viewers from Germany to this dive at short notice via telepresence, who followed the internet link of the MARUM YouTube channel.

On **Friday, 29 July** at 5:00 p.m., we had to stop station work and set off for Reykjavik. On the transit route to the port, the ship only traveled 10 knots through the water for reasons of energy saving and cost. We use the southbound path in the East Greenland Current, which brought us further advantages in these austerity measures, and arrived in the port of Reykjavik punctually on **Wednesday, 3 August**, where the cruise officially finished, and the scientists and several crew members started their journey back home.

5. Preliminary Results

5.1. Multibeam Mapping (MBES)

(Christian Ferreira, Lara Marschall, Angelly Serje Gutiérrez)

Acquisition Devices and Settings

MBES surveys were conducted with the hull-mounted KONGSBERG EM122 MBES (KONGSBERG EM122, 2013). The shallow and midwater EM712 MBES was not used during this cruise since nearly all surveyed areas where at depths between 1,000 and 5,500 meters.
The EM122 MBES is a well-known deep-sea system operating with 11.25 to 12.5 kHz. Onboard R/V MARIA S. MERIAN, a beam width configuration of 2° (TX) by 2° (RX) is installed. A swath angle of up to 150 degrees and a maximum coverage of 5.5 times the water depth can be reached. During cruise MSM57, the maximum swath width was set to 130 degrees to improve data quality, reduce the amount of noisy data at the outer beams, and increase the ping rate.
Sound velocity profiles (SVPs) were measured with CTD and applied to the raw data during acquisition via the SIS software from KONGSBERG. The storage-intensive water column data have recorded during all surveys of this cruise.

Table 5.1. Settings used for both echosounders

Runtime Parameters EM122	Setting	Reason
Swath Width	130˚	Beyond 120° the outer beam quality is below our specs. Ping rate is higher the narrower the swath width.
Beam Spacing	HD EQST (high density equidistant mode)	432 soundings per ping, equidistant over the swath are achieved then
Ping Mode	Medium AUTO	For flare-search surveys For bathymetric surveys
Dual Swath Mode	ON/AUTO	To increase the along track resolution
Pitch/Yaw stabilization	ON	Improvement of data quality

Processing Methods

The EM122 bathymetry data were processed with the open source software package MB-System (vers. 5.7.9 beta 42; see Caress and Chayes, 1995). The following steps were carried out to the EM122 bathymetry-surveys:

- Converting the data to editable MB-format.
- Applying correct SVP if available.
- Applying tide correction based on the Tidal Prediction Software (OTPS; Oregon State University); integrated in MB-System (mbotps). Tides around Svalbard are part of the semidiurnal cycle around the main amphidromic point located in the central Arctic Ocean. The change in amplitude (max. up to 50 cm) and phase is due to Svalbard location between deep Arctic Ocean and shallow Barents Sea (Kowalik et al., 2015).
- Manual editing of the dataset.

- Correcting amplitude (aka backscatter) and sidescan (beam time series) values based on a function of grazing angle with respect to the seafloor (slope).
- Applying the changes to the raw files, creating processed files, grid the data by using netCDF (GMT) file format.

Preliminary Results

During MSM109 in total 3,975 km of EM122 surveys were conducted. Adding the transits from Tromsø to Svalbard and from Svalbard towards Iceland, the total amount rises to 4,965 km.

Fig. 5.1 Multibeam bathymetry measured during R/V MARIA S. MERIAN cruise MSM109

5.2 PARASOUND

(Katharina Streuff, Lara Marschall, Christian dos Santos Ferreira, Angelly Serje Gutiérrez)

Sediment echo sounders use the principle of acoustic wave propagation to identify differences in material properties, such as density and sound velocity, through which lithological changes can be identified in the sediment column. That way, depending on seafloor characteristics, such

instruments can resolve the upper ~100 m of the seafloor. R/V MARIA S. MERIAN is equipped with an ATLAS PARASOUND sediment echo sounder, which, due to the so-called parametric effect, offers superior lateral and vertical resolution of sedimentary structures compared to conventional echo sounders. The parametric effect describes the interaction between two simultaneously emitted sound waves of finite amplitude, which is caused through the non-linear relationship between density and pressure changes in the water column. Furthermore, when operated at a frequency of 4 kHz, the PARASOUND echo sounder has an opening angle of 4° compared to 20° for conventional echo sounders. As a result, the instrument interpolates across a footprint of only 7% of the water depth, which is a mere 20 % of the area conventional echo sounders integrate over. Accordingly, the imaged data are more accurate and of better quality than those of other sediment echo sounders.

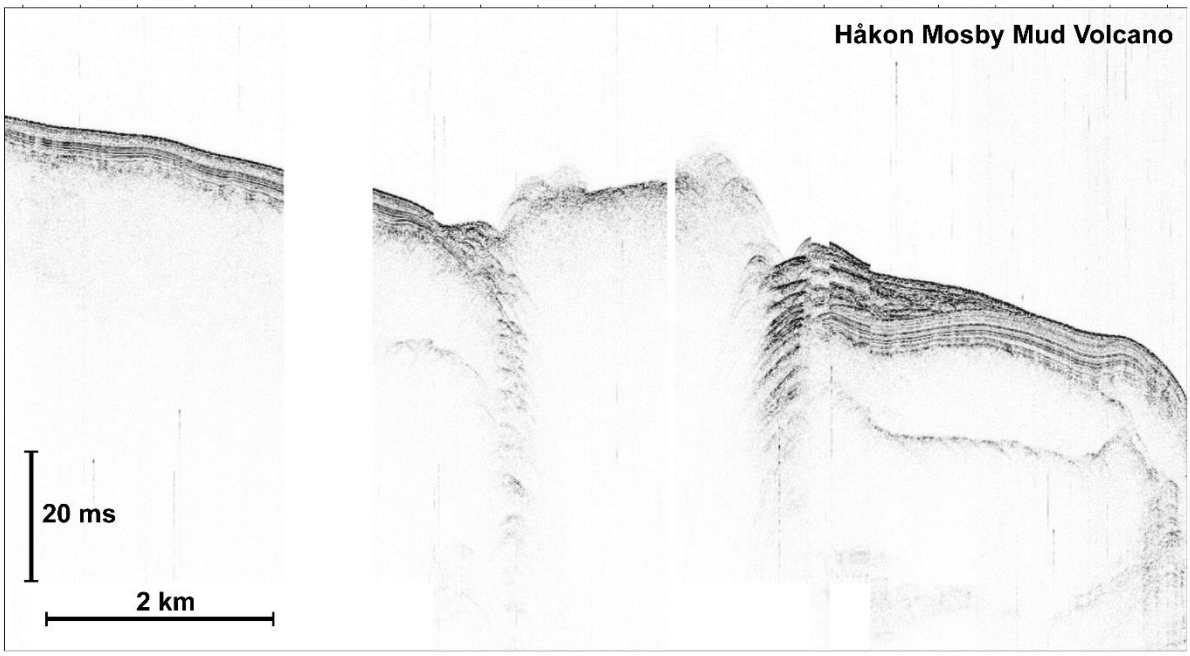

Fig. 5.2.1 PARASOUND sediment echo sounder profile across the Håkon Mosby Mud Volcano. The characteristic pull-down reflections can be observed at the sides. Lighter lenticular bodies at the flanks probably represent a series of mass-flows "erupting" from the volcano.

Methods

The software interfaces ATLAS PARASTORE and ATLAS Hydromap Control Center were used to control the PARASOUND settings during operation. During cruise MSM109, the echo sounder was mainly used with two different frequency signals in order to be able to resolve flares as an indication for gas bubbles in the water column (Primary High Frequency, 18-20 kHz) as well as sedimentary characteristics in the sub-bottom (Secondary Low Frequency, 22-24 kHz). In order to achieve satisfactory quality for the imaging of the sub-seafloor sediments, the sounder was set to operate in Quasi-Equidistant Transmission mode. Using ATLAS PARASTORE, the data, while being recorded, were displayed in two separate echogram windows, where settings could be modified both for the display of the PHF and for the SLF signals. The window length was usually kept at 319 m for the PHF frequency signal and for 500 m for the SLF frequency. Clipping and amplitude were adjusted when appropriate. During cruise MSM109, a total of 221 GB of PARASOUND raw data were recorded (see Table 5.1). Data storage occurred as raw .asd files, which can be replayed should need be, and both, pre-processed .ps3 and .sgy files. Due to their

superior quality, however, only the .ps3 files were used; they were converted into UTM-corrected envelope .sgy files with the help of the software tool PS32SGY. The resulting output files were then imported into SMT The Kingdom Suite v. 2017 for visualization and on-the-fly interpretation. An overview of the surveys imported into SMT The Kingdom Suite is given in Fig. 5.2.1.

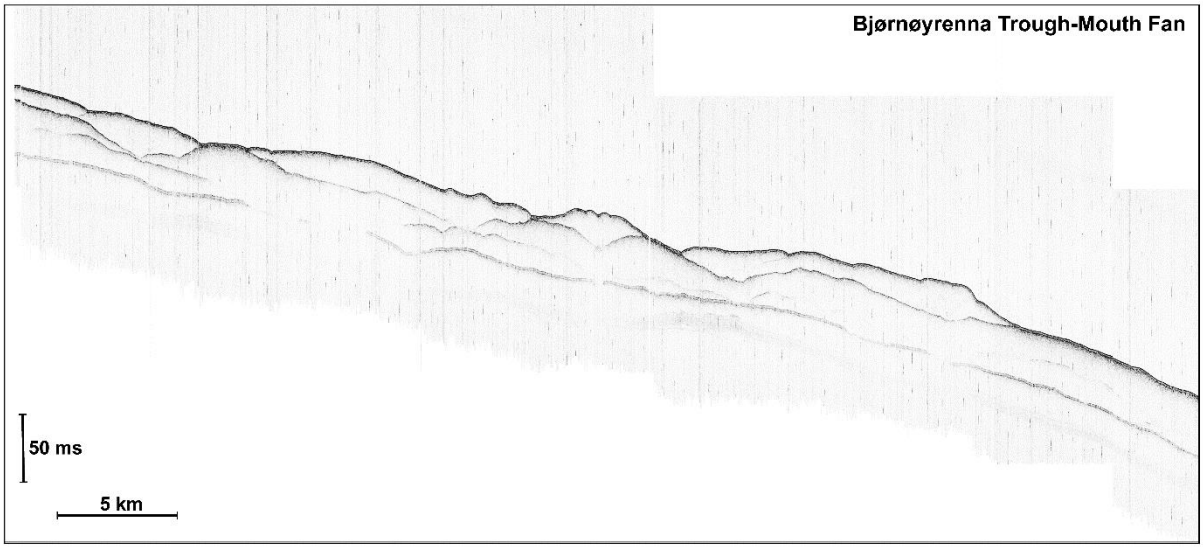

Fig. 5.2.2 PARASOUND sediment echo sounder profile across the Bjørnøyrenna Trough-Mouth Fan. The fan is built from a series of debris-flow lobes deposited in front of a palaeo-ice margin at the shelf edge during the Last Glacial Maximum.

Preliminary Results

During cruise MSM109, 2,829 nautical miles of seafloor were mapped using the PARASOUND sediment echo sounder. The seafloor of the research areas was generally characterized by a very rough appearance, which is unsurprising giving the tectonic history of the Knipovich Ridge. The many pillow lavas and other magmatic rocks observed on the seafloor during several ROV QUEST dives, as well as distinct canyons within the seafloor confirmed a generally hard and resistant substrate, leading to scattered and distorted PARASOUND reflections in these areas. Here, it was therefore often difficult to identify individual sediment layers. Especially directly across and along the ridge, water depths were extremely variable, making it very difficult to obtain a good signal with the echo sounder. In these areas, the seabed was characterized by a discontinuous reflection of highly variable amplitude, often accompanied by refraction hyperbolae and other artefacts.

Furthermore, the system struggled with the sudden changes in seafloor elevation and “lost” the seafloor on numerous occasions, leading to small gaps in the data acquisition. Nevertheless, in areas further away from the Knipovich Ridge and particularly in regions closer to the continental shelf, the PARASOUND echo sounder was able to gather some good data, resolving up to 90 m of the sedimentary structures within the seabed. During the transit from Tromsø to the first research area, the sediment echo sounder not only nicely imaged the Håkon Mosby mud volcano with associated pull-down structures (Fig. 5.2.1), but also showed a succession of stacked mass-flow deposits associated with the build-up of the Bjørnøyrenna Trough-Mouth Fan, that was formed in front of a shelf-wide ice sheet margin during the Last Glacial Maximum (Fig. 5.2.2). Unfortunately, despite the observation of active gas emissions in the form of gas flares in the water column at the site of the volcano, the PARASOUND did not show any indication of free gas,

neither in the water column, nor in the seafloor subsurface. In smoother regions of the research areas as well as in some distinct basins, the echo sounder revealed thick successions of well-stratified, likely pelagic sediments. Due to the tectonic activity at and around the Knipovich Ridge, faults were also commonly observed (Fig. 5.2.3).

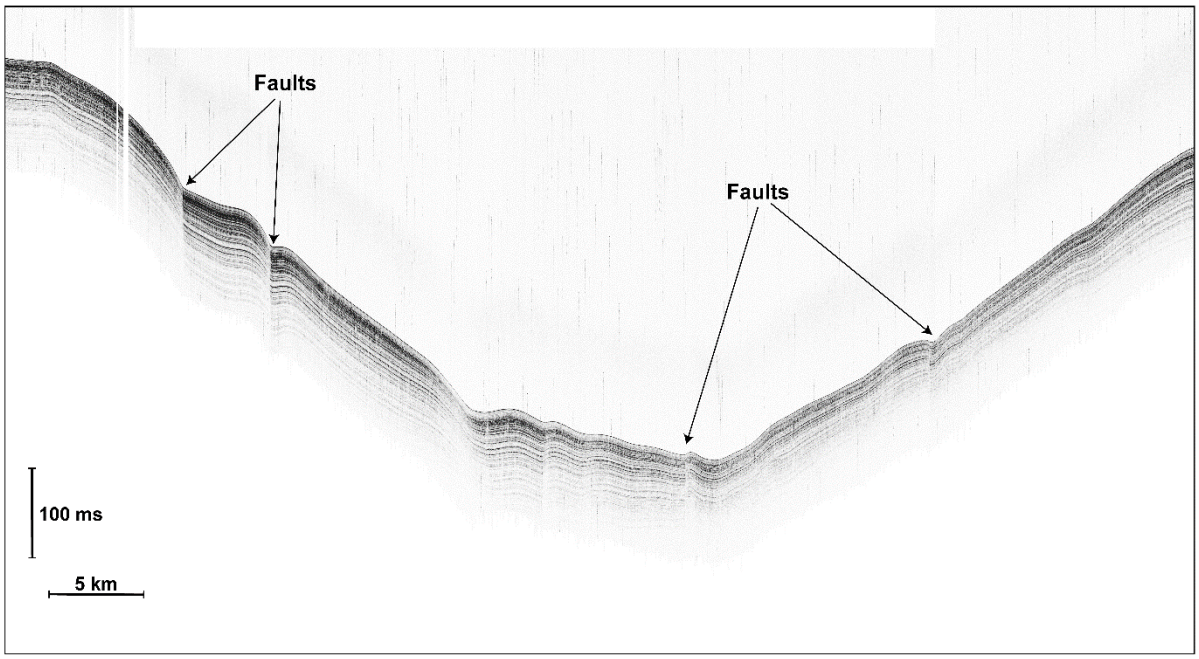

Fig. 5.2.3 PARASOUND sediment echo sounder profile across some faults in the northeastern part of the investigated study areas. The profile is located close to the shelf edge just north of the large Kongsfjorden Trough and orientated NW-SE.

5.3 CTD Work

(Henri Renzelmann, Daniel Smrzka, Jan Kleint, Janice Malnati)

During the MSM109 cruise, 16 CTD stations were conducted. Six of these stations were so-called Tow-yo stations. We found oxidation-reduction potential (ORP) and temperature anomalies in half of the 16 stations (see Table 5.3.1). With each cast 23 water samples were taken, usually between the seafloor and about 400 m above. The water samples were sampled for methane concentrations, and also in 18 cases where we found strong signals with the ORP-sensor, for helium samples.

The CTD probe used was a SEABIRD electronic underwater unit equipped with 2 pressure-, temperature-, conductivity-, and oxygen sensors with 2 separated pumps. During many casts, the sensors of the 2nd pump stopped working for unknown reasons, yet all measurements could still be obtained during these casts. The CTD was also equipped with a turbidity sensor, which was not optimized to detect signals from hydrothermal plumes, and so these data were largely neglected. The CTD probe was attached to an OCEANIC rosette water sampler capable of holding 24 water bottles. Throughout the cruise the last bottle was uninstalled and replaced by a transponder of the "ranger2" system, to obtain exact location of the CTD, especially during Tow-yo casts. For the detection of ORP anomalies by the ORP-sensor was placed onto the rosette (see details in chapter 5.4). In the configuration file M=0,2 and Offset=-500mV as coefficients were given. The raw data were recorded and shown live during the casts by the SeasaveV7 software. After the casts, raw

data were post-processed using the SEABIRD data processing tools (namely: data conversion, wild edit, window filter, align CTD and bin average).

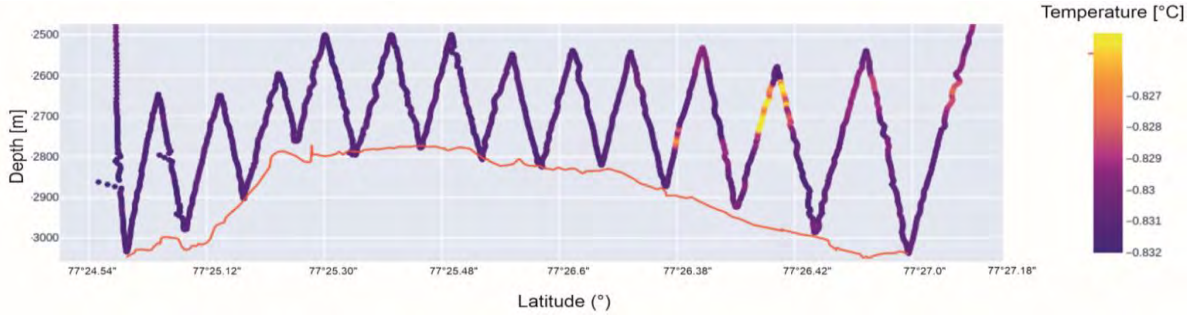

Fig. 5.3.1 Temperature profile of CTD cast 6 in Jøtul hydrothermal field, an example of anomalies in temperature

After attaching the autonomous Eh-sensor, the rosette was lowered with a speed of 1m/s. Two different modes of CTD operation were done. The first was a single cast, where we slowed the speed of the rosette about 100 m above the seafloor down to 0.5m/s. After the rosette reached the seafloor, we closed the bottles every 15 to 20 meters for the first few hundred meters during the upcast. We also did Tow-yo casts, where we lowered the rosette again with 1m/s until we reached an expected depth of plumes in the water column (usually 400 m above the seafloor). From that depth we started steaming with a speed of 0.5 knots along the designated Tow-yo track while lowering and heaving the rosette between the seafloor and ~400 m above it with a speed of 0.5m/s. Each time a signal of a plume was detected with the ORP sensor, bottles were closed in the aforementioned intervals.

Table 5.3.1 Summarized results of CTD casts

Station No.	CTD No.	Latitude	Longitude	Depth [m]	Eh - Anomaly	Temp. Anomaly	Tow-yo
01-1	1	74° 43.093	8° 24.419	3121	no	no	no
02-1	2	74° 43.112	8° 24.470	3310	no	no	no
03-1	3	77° 25.295	7° 16.632	3244	no	no	yes
05-1	4	77° 24.809	7° 20.664	3078	no	no	no
06-1	5	77° 26.726	7° 44.155	2981	yes	no	no
10-1	6	77° 24.994	7° 40.964	3044	yes	yes	yes
12-1	7	77° 26.614	7° 43.865	2954	yes	no	no
13-1	8	77° 26.404	7° 41.159	3142	yes	yes	yes
14-1	9	77° 26.988	7° 38.914	3230	yes	yes	yes
15-1	10	77° 26.549	7° 43.052	2969	yes	yes	no
18-1	11	77° 26.745	7° 45.536	2872	no	no	no
19-1	12	79° 29.877	3° 32.578	2972	no	no	yes
21-1	13	79° 24.461	3° 25.372	3022	no	no	no
29-1	14	77° 26.375	7° 42.516	2984	yes	yes	no
30-1	15	77° 26.261	7° 42.110	3034	yes	yes	yes
33-1	16	77° 26.548	7° 43.342	2942	no	no	no

Station work was done west of the the Brøgger Axial Volcanic Ridge (AVR), the Molløy Deep and most of it in the Jøtul hydrothermal field. The first 2 casts were done to test the CTD. The only region where we found anomalies of any kind was the Jøtul hydrothermal field, distributed within a radius of ~1 nautical mile. The anomalies were ORP and temperature in several casts (see Fig. 5.3.1), and in cast 14 even in salinity. In the latter cast we tried a single cast directly above an active black smoker that we had discovered the day before (see ROV dive 463). There we possibly detected the rising plume of the active smoker, because it was the strongest signal of any CTD cast and less than 100 m above the source.

5.4. MAPR and ORP

(Daniel Smrzka, Henri Renzelmann, Jan Kleint, Angelly Serje Gutiérrez)

Introduction, Technical Details and Modes of Operation

The main target of the cruise MSM109 was to follow up on previous findings of indicators for hydrothermal activity in the study area that included recorded hydrothermal plumes, earthquake activity, and detailed multi-beam data. The primary instrument in order to detect hydrothermal vents during MSM109 cruise was the miniature autonomous plume recorder (MAPR) provided by the Pacific Marine Environmental Laboratory (PMEL) in Seattle (WA, USA). The MAPR is a durable, self-contained instrument that records ambient temperature, pressure, optical backscatter, and the oxidation-reduction potential (ORP) within the ambient water. Because the MAPR data is recorded internally and cannot be accessed or viewed during deployment, a further non-autonomous ORP sensor was installed on the shipboard CTD device in order to record live changes in water column ORP. While the ORP data from the non-autonomous ORP sensors are extracted with the raw data of the CTD, the MAPR data are read out using the MAPR-Terminal software package consisting of the MAPR Terminal serial communication program, and an excel workbook containing macros. The MAPR Terminal software is used to communicate and program the MAPR before deployment, and to read out data and additional information after deployment. A total of two MAPRs (serial numbers 74 and 66), and two non-autonomous ORP sensors were provided, whereby only one of the latter (ORP-12, Fig. 5.4.1) were used during MSM109.

Fig. 5.4.1 (left): The non-autonomous ORP sensor attached to the CTD, (middle) top view of MAPR-74 showing all sensors, (right): MAPR-74 attached to the clamp device with metal rings

The PMEL ORP sensor is equipped with a platinum working electrode and Ag/AgCl reference electrode located on a thermoplastic body. The platinum electrode is exposed to seawater during deployment. A porous barrier separating the seawater from the reference electrode is provided by

a Teflon plug embedded in the cap of the reference cell. The ORP sensor determines the electric potential between the platinum and reference electrodes in the range of -500 to +500 millivolts (mV). The non-autonomous ORP sensor (CTD version) has an output scaled between 0 and 5 volts as required for auxiliary analog sensors on a Seabird 9*plus* CTD.
The CTD-ORP sensor was mounted directly to the CTD frame using plastic zip ties. The sensor was mounted horizontally on the CTD frame in a place where the unobstructed flow of seawater could be guaranteed during casts, and also to enable an easy and quick removal and replacement of the sensor cap. The sensor was coupled to the CTD with a pin-to-pin cable, and was identified by the Seasave Software Instrument Configuration (for details see chapter 5.3. of this cruise report). Both the MAPRs and the CTD-ORP sensors were washed and rinsed with fresh water during each deployment. The flexible vinyl sensor cap of the ORP sensors were initially filled with a potassium chloride solution for shipping, and filled with seawater between casts to prevent the electrode from drying out.

After each deployment the MAPR was connected to the MAPR-Terminal software to check the MAPR status, set the MAPR time for the next deployment, configure the MAPR for sampling, to check battery status, and to download data. MAPR runs with four 9V batteries consisting of three Sensor batteries and one Logic battery. As MAPR performed continuously for several days on one set of batteries, these were changed three times for MAPR-74, and once for MAPR-66 during the entire MSM109 cruise. Batteries were changed when their voltage dropped below 7V by opening the bottom cap using a spanner wrench tool. The MAPR battery pack is secured by a black battery backer plate held by four screws, and separated from the bottom end cap by a foam spacer.

MAPR and ORP Data Visualization and Station List
Because the ORP sensors do not reference the electric potential E to the standard hydrogen electrode, the term E instead of Eh is used throughout. The ORP sensor values all showed a significant drift during deployment, mostly toward more positive E values. The two main reasons for this drift are that ambient seawater during deployment is not at equilibrium, and the sensor continuously moves through it. It is therefore very rare for the sensor to have time to completely come to equilibrium with ambient seawater. The general drift can show either slowly increasing or slowly decreasing values, and is considered normal either way. A significant signal, such as a response to reduced species in hydrothermal plumes, is typified by a dramatic and identifiable decrease in voltage relative to the normal drift. This is usually followed by a slower recovery period with slowly increasing values. Because the recovery is slower than the initial response, this causes significant hysteresis and the "background" seawater values are then even more variable. For this reason, the ORP data recorded by the sensor in E were normalized by the time differential (dE/dt) to identify places where the sensor responded with more rapidly decreasing values. “Delta_ORP” or ΔE is considered to be the magnitude of the overall drop in voltage over the duration of the signal. The logging interval of both MAPRs were set to 5 seconds during all deployments, and for each data point in the graphs (see below) ΔE is calculated from recorded values, representing changes in E over periods of 5 seconds throughout the time of deployment. Particularly during Tow-yo CTD casts the MAPRs show small (<1 mV) drops or shifts in E every time the tow is at depth and changes direction. These changes are most likely related to the change

in winch direction, and not a realistic or significant indication for hydrothermal plumes. Therefore, the interpretation of ORP signals were limited to signals that ΔE exceeded about -2 mV or more. The MAPR is equipped with a strain gauge style pressure sensor that is not temperature compensated, so there is some inherent inaccuracy in the measurements. Therefore, a depth correction of the raw data using an excel macro was conducted in order to determine the atmospheric pressure (zero) value while on deck before deployment. These values were different for each MAPR, and were subject to change from day to day depending on weather conditions. These depth corrections rarely resulted in depth changes greater than 1 meter. The logging frequency of the MAPRs was set to 5 seconds.

Table 5.4.1. List of all MSM109 stations in which MAPRs and ORP sensors were deployed

CTD-03	Brøgger Axial Volcanic Ridge	ORP-12, MAPR-74, Tow-yo CTD
CTD-04	Brøgger Axial Volcanic Ridge	ORP-12, MAPR-74
CTD-05	Jøtül Hydrothermal Field	ORP-12, MAPR-74, ORP anomaly
AUV-102	Brøgger Axial Volcanic Ridge	MAPR-74, ORP anomaly
CTD-06	Jøtül Hydrothermal Field	ORP-12, MAPR-74, Tow-yo CTD, ORP anomaly
AUV-103	Jøtül Hydrothermal Field	MAPR-74, ORP anomaly
CTD-07	Jøtül Hydrothermal Field	ORP-12, MAPR-74, ORP anomaly
CTD-08	Jøtül Hydrothermal Field	ORP-12, MAPR-74, Tow-yo CTD, ORP anomaly
CTD-09	Jøtül Hydrothermal Field	ORP-12, MAPR-74, Tow-yo CTD, ORP anomaly
CTD-10	Jøtül Hydrothermal Field	ORP-12, MAPR-74, ORP anomaly
ROV-458	Jøtül Hydrothermal Field	MAPR-66, ORP anomaly
AUV-104	Jøtül Hydrothermal Field	MAPR-74
CTD-11	Jøtül Hydrothermal Field	ORP-12, MAPR-74
CTD-12	Molløy Ridge	ORP-12, MAPR-74, Tow-yo CTD
AUV-105	Molløy Ridge	MAPR-74
CTD-13	Molløy Ridge	ORP-12, MAPR-74
ROV-459	Molløy Ridge	MAPR-66
ROV-460	Jøtül Hydrothermal Field	MAPR-66, ORP anomaly
ROV-461	Jøtül Hydrothermal Field	MAPR-66, ORP anomaly
AUV-106	Brøgger Axial Volcanic Ridge	MAPR-74
ROV-462	Jøtül Hydrothermal Field	MAPR-66, ORP anomaly
AUV-107	Jøtül Hydrothermal Field	MAPR-74, stopped recording after 30 minutes
ROV-463	Jøtül Hydrothermal Field	MAPR-74, ORP anomaly
CTD-14	Jøtül Hydrothermal Field	ORP-12, MAPR-74 (did not record data)
CTD-15	Jøtül Hydrothermal Field	ORP-12, MAPR-74, Tow-yo CTD, ORP anomaly
ROV-464	Jøtül Hydrothermal Field	MAPR-66, ORP anomaly
AUV-108	Jøtül Hydrothermal Field	MAPR-74, ORP anomaly
CTD-16	Jøtül Hydrothermal Field	ORP-12, MAPR-74
ROV-465	Jøtül Hydrothermal Field	MAPR-66, ORP anomaly
ROV-466	Jøtül Hydrothermal Field	MAPR-66, ORP anomaly
AUV-109	North of Logachev Seamount	MAPR-74, stopped recording after 30 minutes
ROV-467	North of Logachev Seamount	MAPR-66

MAPRs and non-autonomous ORP sensor were deployed in a total of 32 stations during MSM109, and a complete list of these stations is given in Table 5.4.1. MAPR-74 and ORP-12 were exclusively used during CTD casts. MAPR-74 was additionally deployed during AUV dives, whereas MAPR-66 was only used for ROV dives. MAPR-74 was always installed 50 meters above the CTD, and attached to the wire using a clamp device to which the MAPR was attached using metal clamps and one additional zip wire for additional safety. This clamp device was then screwed to the CTD wire and additionally fastened with rope. During AUV dives MAPR-74 was attached to the AUV halfway inside the vehicle hull using an additional clamp device and secured with metal clamps screwed onto the device. The top half of the MAPR containing sensors was left to look out of the hull in order to record data from ambient waters. MAPR-66 was installed on the bottom lower left side of the ROV in a space allowing for seawater to continuously flow by the sensor during dives without obstruction by other devices from the vehicle. MAPR-66 was attached to the ROV frame using metal clamps and zip wires. Figures of all MAPR/ORP data that are not shown in this chapter are given in the appendix.

MAPR and ORP Results – CTD Casts

The MAPRs and ORP sensors were deployed in 16 CTD casts, 7 AUV dives, and 9 ROV dives (Table 1). Of the 16 CTD casts 6 were Tow-yos, and 10 were single casts. Anomalies in E values were recorded in 7 of the CTD casts, of which 4 were Tow-yo CTDs.

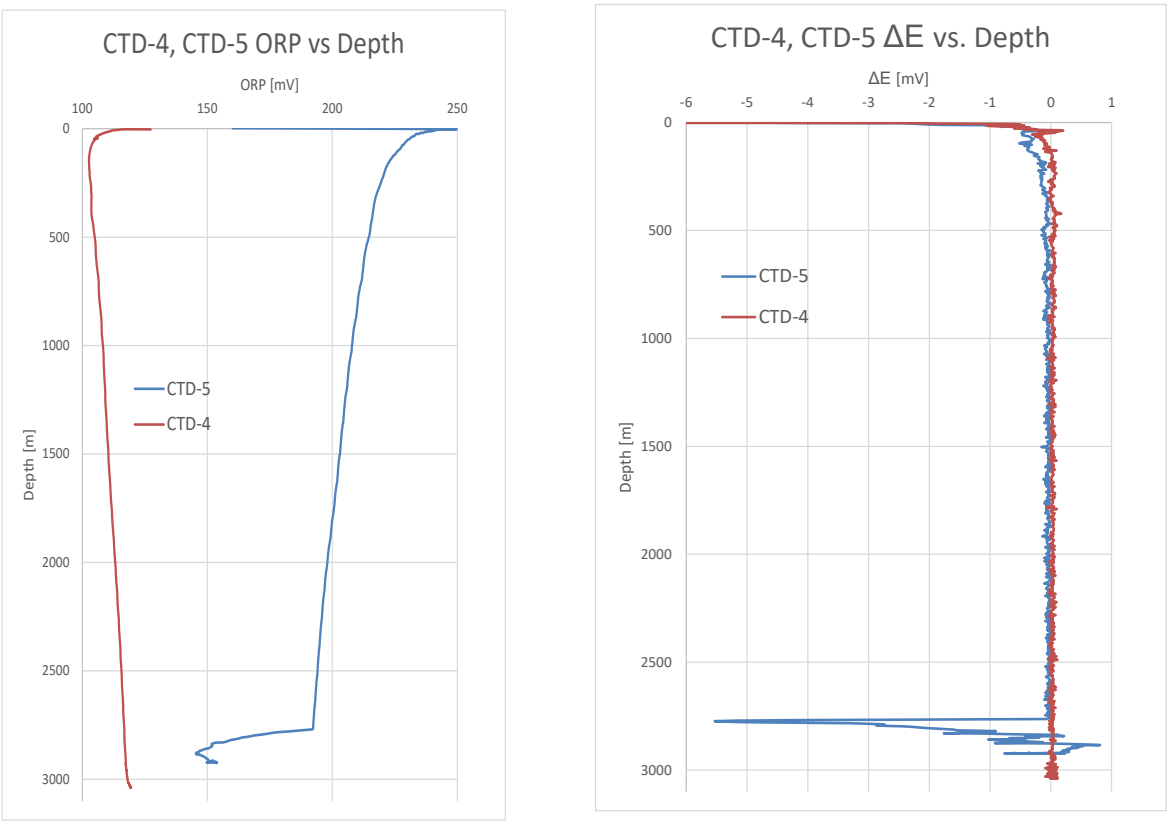

Fig. 5.4.2 Two single cast CTDs over the Jøtul hydrothermal field, CTD-5 showing a clear ORP anomaly at a water depth of 2670 meters. Data shown for MAPR-74.

Anomalies in ORP values were only detected in CTDs deployed over the Jøtul hydrothermal field area, and no anomalies were recorded at Molløy Ridge or in the vicinity of the Logachev Seamount

(cf. Table 5.4.1). For comparison, two single cast CTDs, CTD-4 and CTD-5, are shown in Fig. 5.4.2. CTD-4 shows no ORP anomaly, while CTD-5 picked up the first ORP anomaly during MSM109 at Jøtul hydrothermal field in a depth of around 2,670 meters.
On 14.07.2022 the first Tow-yo CTD was conducted over the area where the above ORP anomaly was detected. This CTD cast (CTD-6) recorded seven clear excursions in E, whereby 4 of these could be clearly ascribed to hydrothermal plumes by their ΔE values between -2 and -3 mV (Fig. 5.4.3). For comparison, the first Tow-yo CTD (CTD-3) is shown in Fig. 5.4.4, where no ORP anomaly was detected.

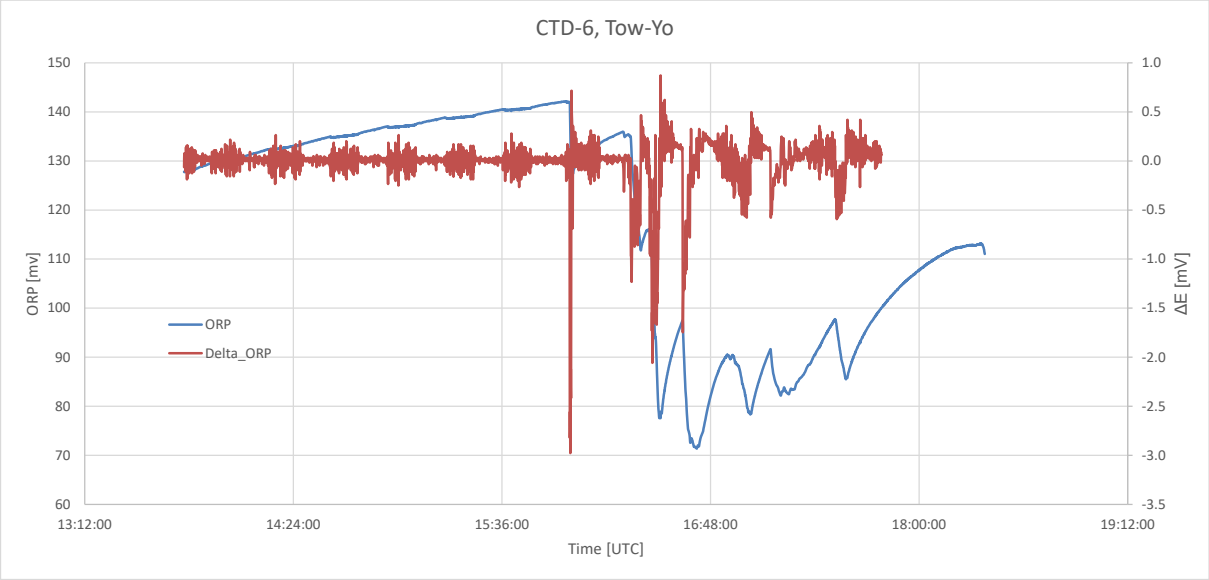

Fig. 5.4.3 ORP and ΔE values of Tow-yo CTD-6 over Jøtul hydrothermal field.

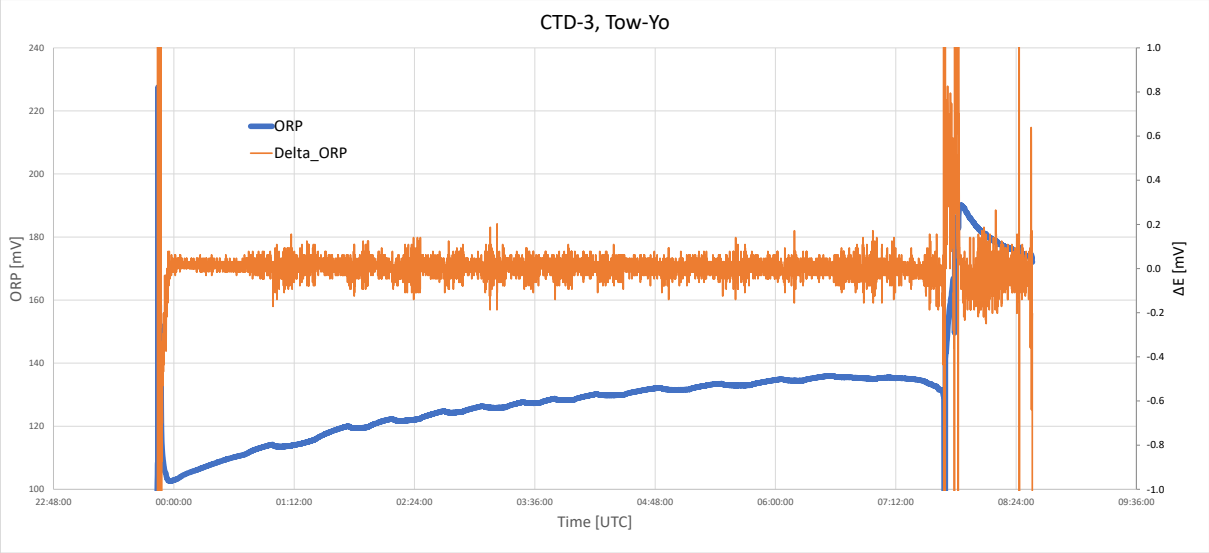

Fig. 5.4.4 ORP and ΔE values of Tow-yo CTD-3 over the southern end of the Brøgger Axial Volcanic Ridge

In order to pinpoint the location of the ORP anomalies as best as possible, E and ΔE values were plotted against depth and either latitude or longitude (depending on the direction of the Tow-yo track). Additionally, the bathymetry along the Tow-yo path is plotted as well. These plots for CTD-6 are shown in Figs. 5.4.5 and 5.4.6, respectively.

As can be seen from Figures 5 and 6, the ΔE value gives more precise information on where changes in E occurred in the water column, and can help detect the emission site of the hydrothermal, reduced fluids. Figures 5 and 6 also show how several plume signals were picked up along the Tow-yo track. Figure 5 shows the initial strong response of the ORP sensor to more reducing plume fluids, after picking up a second strong signal and then relaxing slowly toward the end of the Tow-yo. Comparing figure 3 with figure 6 it can be seen that there are four strong ΔE signals along the Tow-yo track. Aside from CTD-6, CTDs 8, 9, and 15 were three further Tow-yos that recorded significant ORP anomalies, all of which are within the Jøtul hydrothermal field. The Tow-yo tracks of these CTDs are shown in Figs. 5.4.6 to 5.4.9.

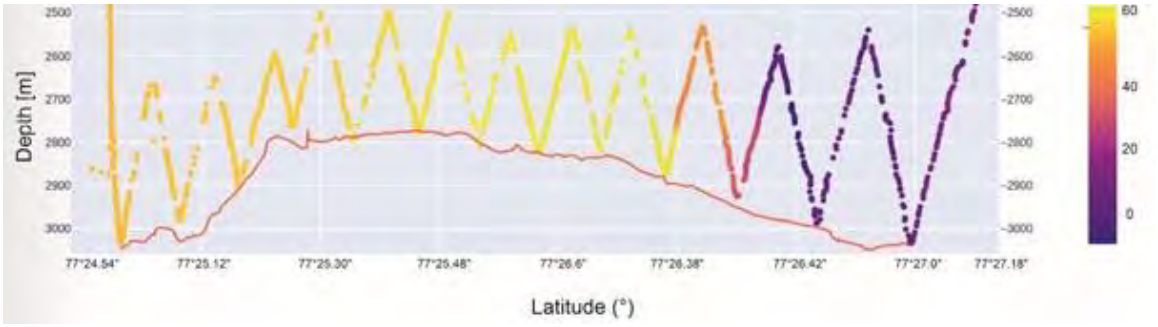

Fig. 5.4.5 ΔE values of Tow-yo CTD-6 over Jøtul hydrothermal field plotted against depth, latitude, and the bathymetric profile across the latitude.

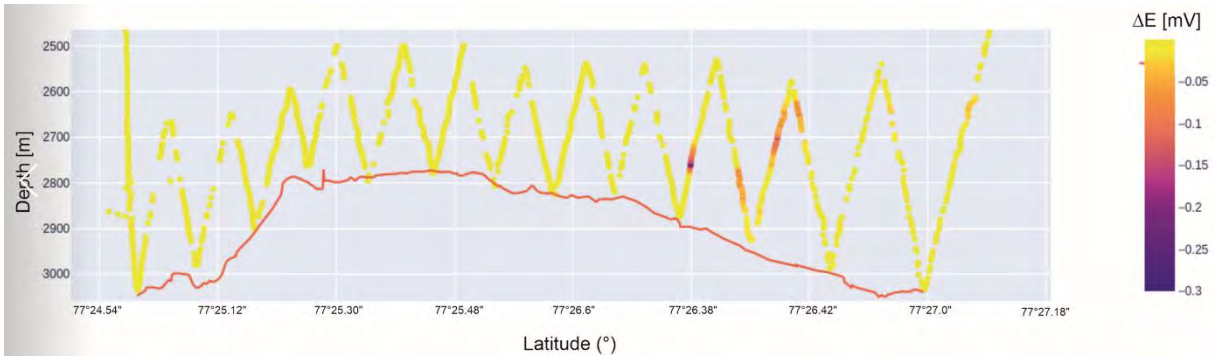

Fig. 5.4.6 ORP values of Tow-yo CTD-6 over Jøtul hydrothermal field plotted against depth, latitude, and the bathymetric profile across the latitude.

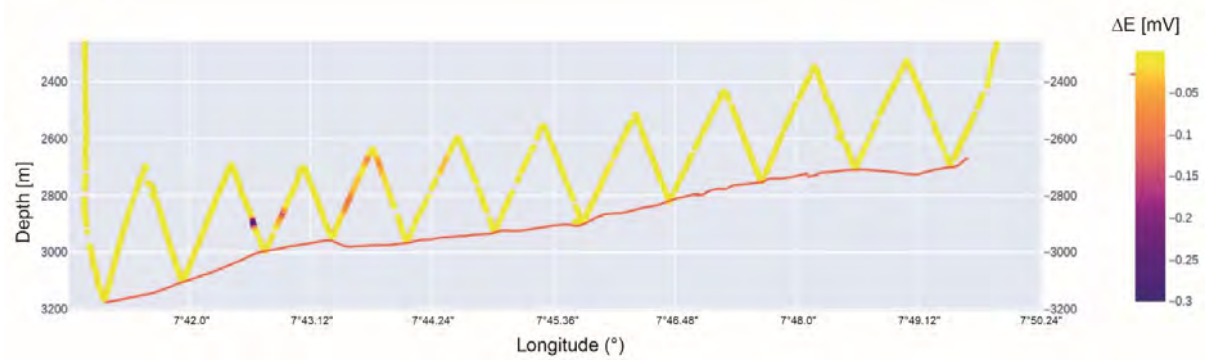

Fig. 5.4.7 ΔE values of Tow-yo CTD-8 over Jøtul hydrothermal field plotted against depth, longitude, and the bathymetric profile across the longitude.

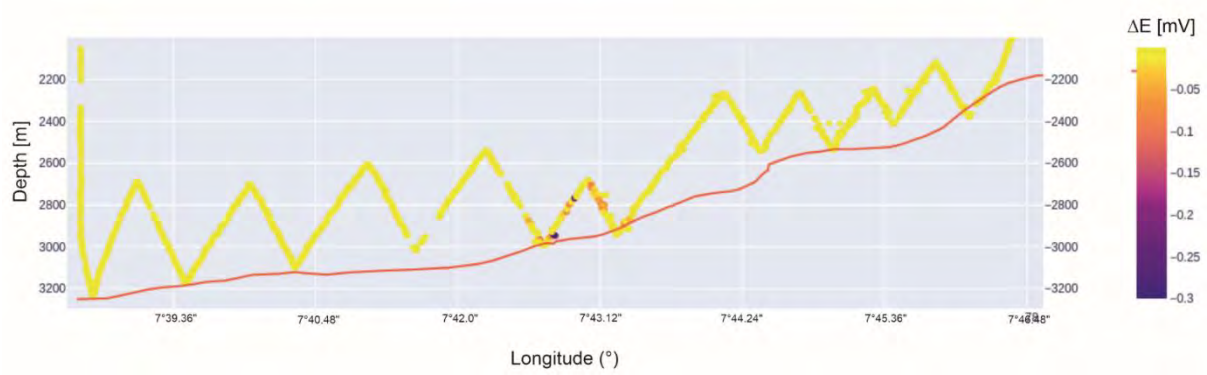

Fig. 5.4.8 ΔE values of Tow-yo CTD-9 over Jøtul hydrothermal field plotted against depth, longitude, and the bathymetric profile across the longitude.

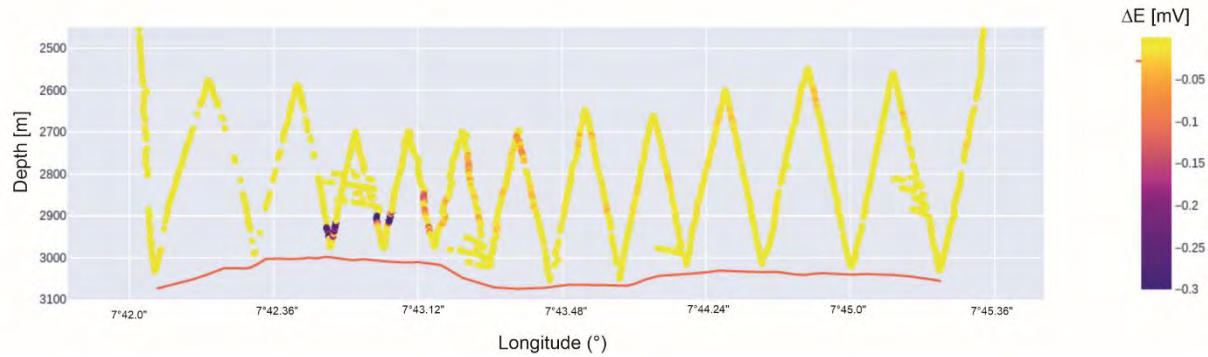

Fig. 5.4.9 ΔE values of Tow-yo CTD-15 over Jøtul hydrothermal field plotted against depth, longitude, and the bathymetric profile across the longitude.

MAPR and ORP results – AUV Dives

MAPR-74 was deployed on 6 AUV dives within the Molløy area and the Jøtul hydrothermal field (Table 5.4.1). Three dives (AUV-104, 105, and 106) did not show any ORP anomalies, whereby AUV-104 and 106 were conducted over the Jøtul hydrothermal field, and AUV-105 targeted the Molløy area (Table 5.4.1). In two further dives (AUV-107, 109) MAPR-74 stopped logging data after 30 minutes for yet unknown reasons, and no ORP data are therefore available for these dives. In three dives (AUV-102, 103, and 108), clear ORP anomalies could be identified in the water column. As an example, MAPR data from AUV dive 103 are shown in several figures below. During this dive two clear ORP anomalies were detected in water depths of approximately 2800 and 2900 meters (Figures. 5.4.10, 5.4.11).

In addition, very slight temperature peaks were recorded during both ΔE peaks, suggesting the presence of hydrothermal fluids at ~130 meters above the seafloor. In addition, the strongest ΔE peak coincides with the strongest increase in temperature over the dive. As can be seen in the turbidity data from MAPR (Fig. 5.4.12), turbidity data are erratic and do not increase significantly with ΔE values throughout the dive. This holds true for most of the MAPR data from the AUV dives.

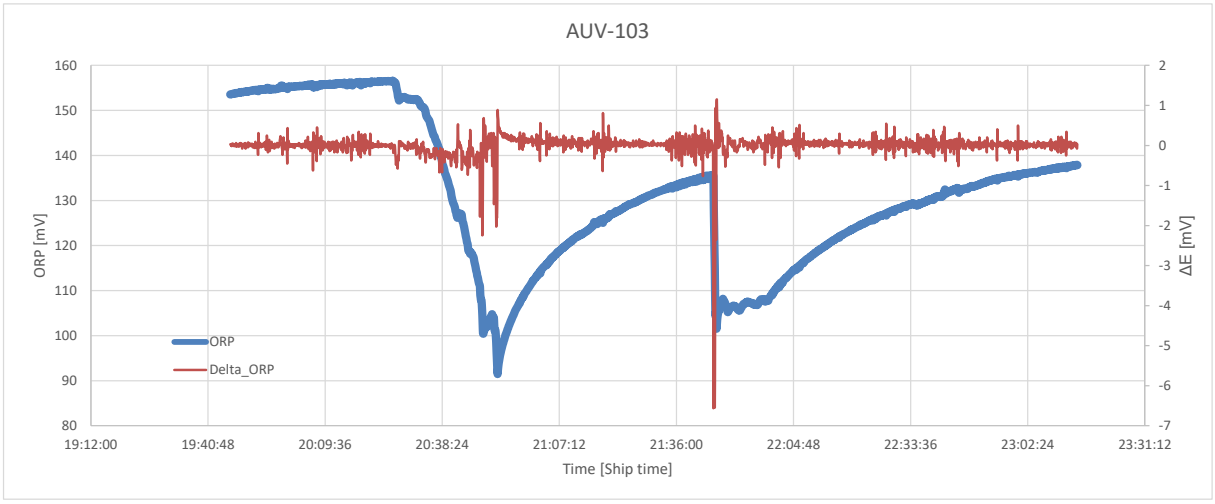

Fig. 5.4.10 ORP and ΔE values of AUV dive 103 over the southern End of the Axial Volcanic Ridge

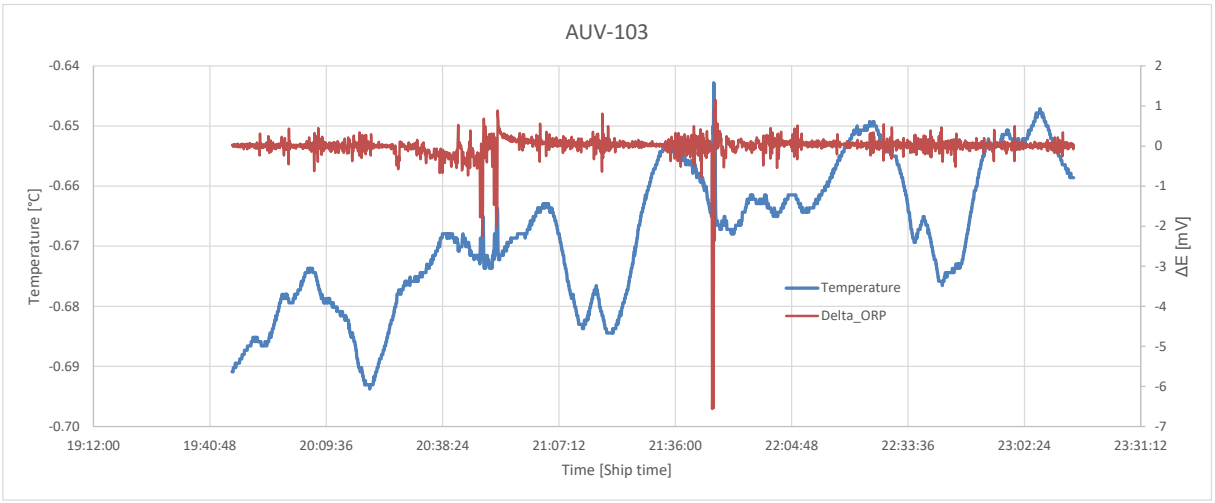

Fig. 5.4.11 ORP and depth values of AUV dive 103

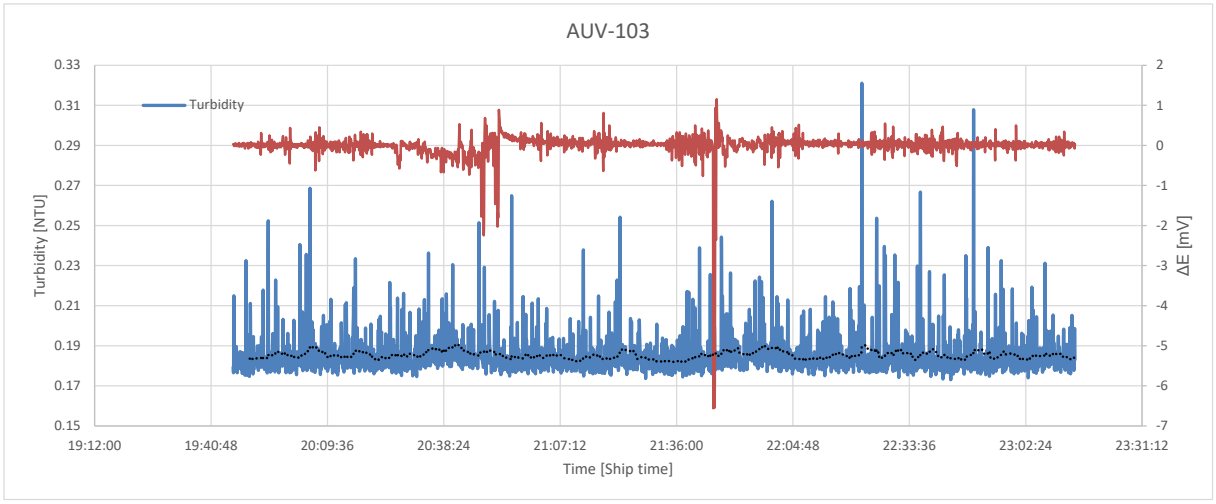

Fig. 5.4.12 ΔE and turbidity values of AUV dive 103 over the southern End of the Axial Volcanic Ridge

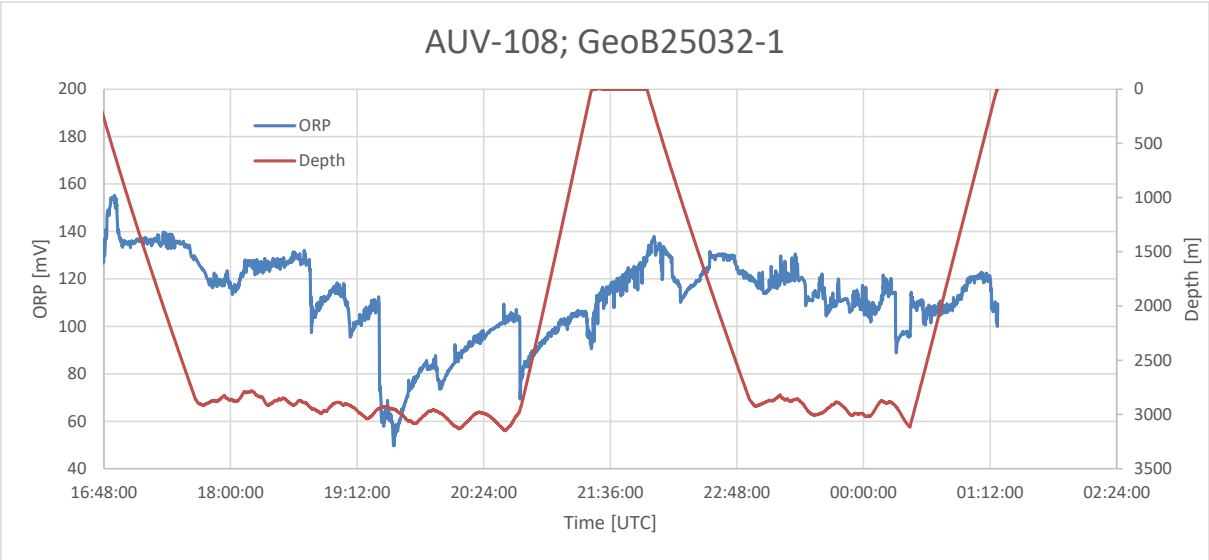

Fig.5.4.13 ORP and depth values of AUV dive 108 over the southern End of the Axial Volcanic Ridge

AUV dive 108 at the slide complex show up to 4 ORP anomalies that may be caused by the emission of hydrothermal fluids from the seabed. As with AUV dive 103, there are distinct anomalies in ΔE and temperature that identify the presence of hydrothermal plumes above the seabed (Fig. 5.4.13).

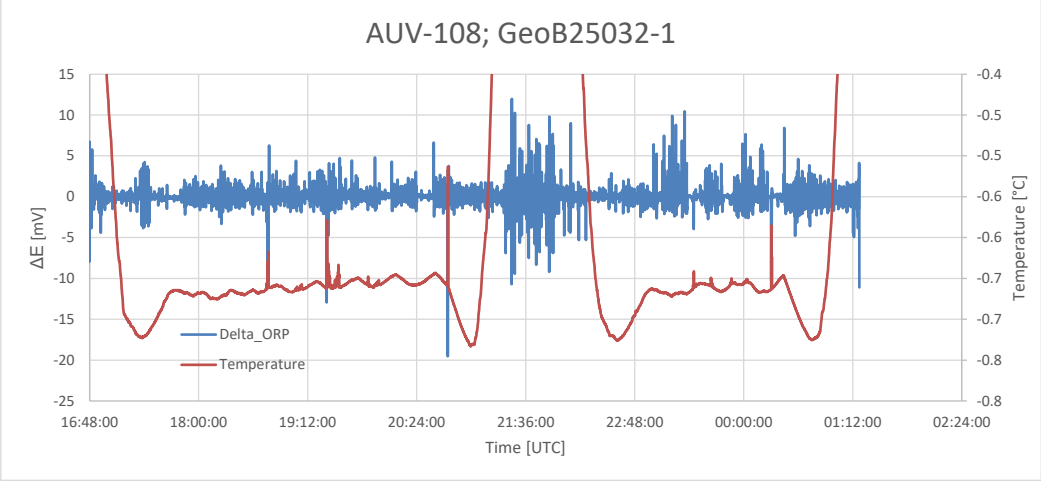

Fig. 5.4.14 ΔE and temperature values of AUV dive 108 over the southern End of the Axial Volcanic Ridge

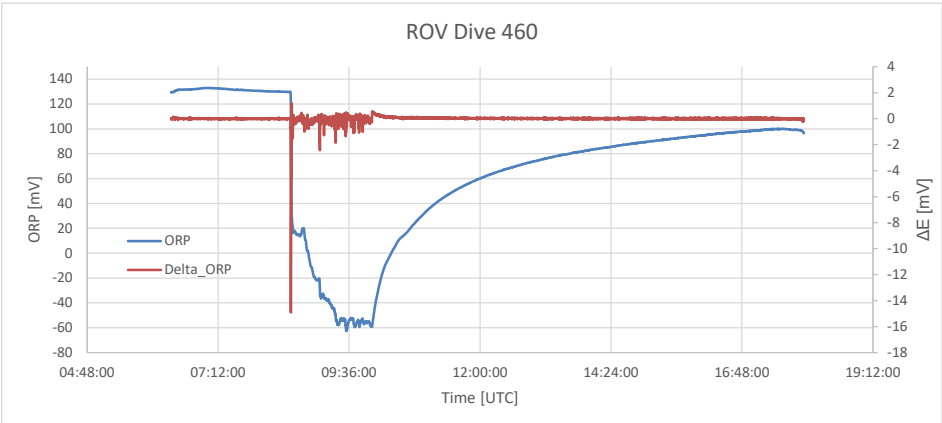

Fig. 5.4.15 ORP and ΔE values of ROV dive 460 over Jøtul hydrothermal field

Further, the more erratic and frequent ORP anomalies occur after the vehicle's descent towards the seafloor, and the ORP sensor relaxes during the intermediate ascent (Fig. 5.4.13). There is also a period of relaxation during an intermediate AUV ascent (Fig. 5.4.14), as well as recurring temperature anomalies coinciding with ORP anomalies (Fig. 5.4.15).

MAPR and ORP Results – ROV Dives

The MAPR was deployed on ROV QUEST in a total of 9 dives (Table 5.4.1). Except for ROV-Dive 459 at Molløy Ridge, and the last dive (ROV-467) all ROV-dives showed multiple ORP anomalies close to the seafloor. During most ROV dives to the Jøtul hydrothermal field the MAPR recorded continuous and repeating smaller and larger ORP anomalies, testifying that this area is highly active and emits reducing fluids from the seabed, even when no fluid venting or shimmering water is observable. These anomalies are not recorded when the ROV was flying more than 1 or 2 meters above the seafloor, suggesting that these emission signals are confined to a very shallow depth above the seafloor. Similar to the AUV data, MAPR recorded slight temperature increases that coincide well with ORP anomalies (Fig. 5.4.17). As an example, ROV dives 460 and 464 (cf. Table 5.4.1) are chosen to showcase typical ORP and temperature anomalies during the ROV dives.

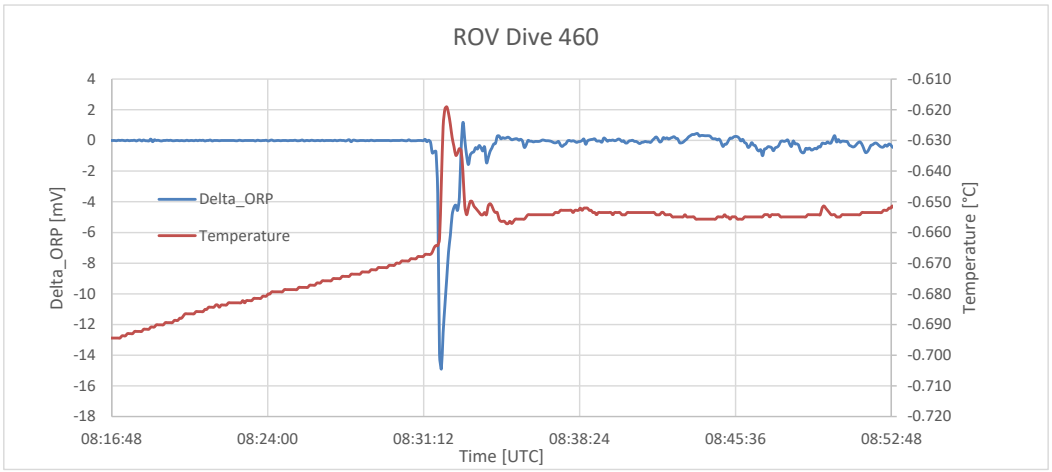

Fig. 5.4.17 Detail of ORP and ΔE values of ROV dive 460 over Jøtul hydrothermal field

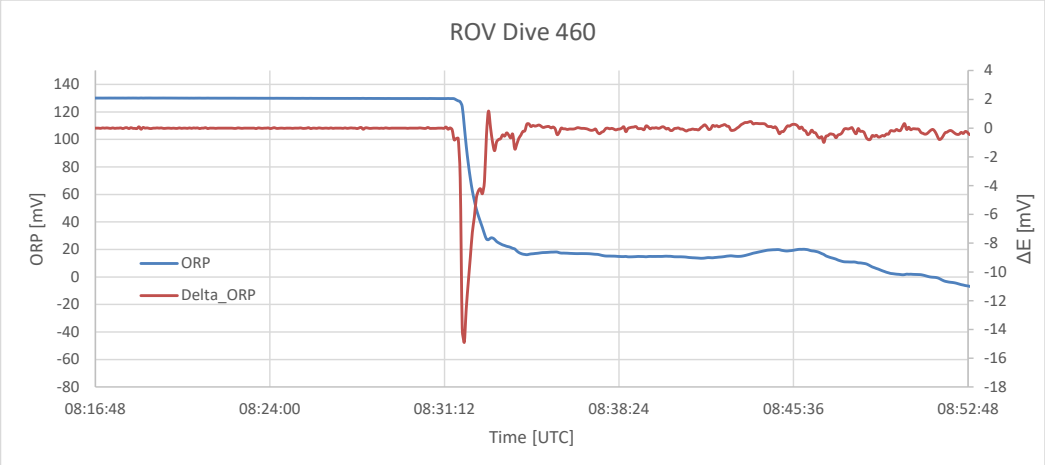

Fig. 5.4.18 Detail of ΔE and temperature spikes during ROV dive 460 over Jøtul hydrothermal field

In many of the ROV dives, a pronounced ORP anomaly was detected immediately upon touching the seafloor at the beginning of the dive. These anomalies were some of the strongest recorded during all stations, reaching ΔE values of up to -20 mV (Figures. 5.4.16, 19). In the case of ROV dives 460 and 464, many of these anomalies were accompanied by distinct temperature changes (Fig. 5.4.18).

ROV dive 460 is an example of recording one strong anomaly as the vehicle approached the seafloor (Fig. 5.4.19), yet other ROV dives recor8ded multiple ORP and temperature anomalies from the point of reaching the seafloor to the end of the dive. ROV dive 464 recorded multiple anomalies during the dive accompanied by temperature and turbidity anomalies (Figures 5.4. 20, 21, 22). The latter, however, should be treated with caution when interpreting them as hydrothermal signals, as the movement of the vehicle close to the seafloor frequently stirs up sedimentary material that may likewise cause strong turbidity spikes.

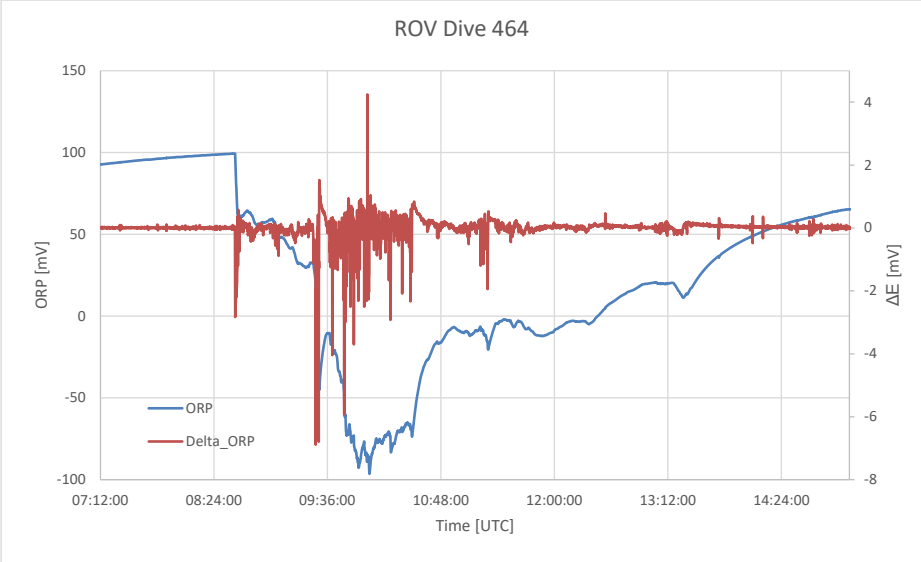

Fig. 5.4.19 ORP and ΔE values of ROV dive 464 over Jøtul hydrothermal field

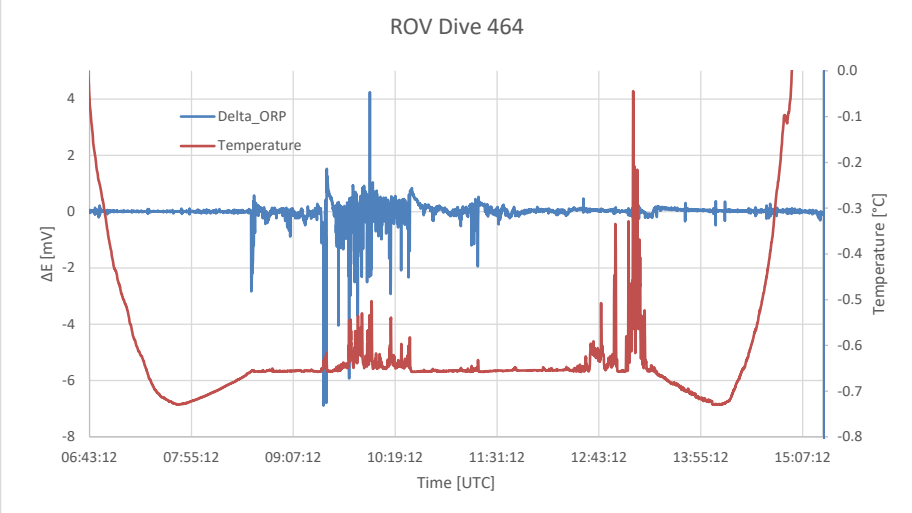

Fig. 5.4.20 ΔE and temperature of ROV dive 464 over Jøtul hydrothermal field

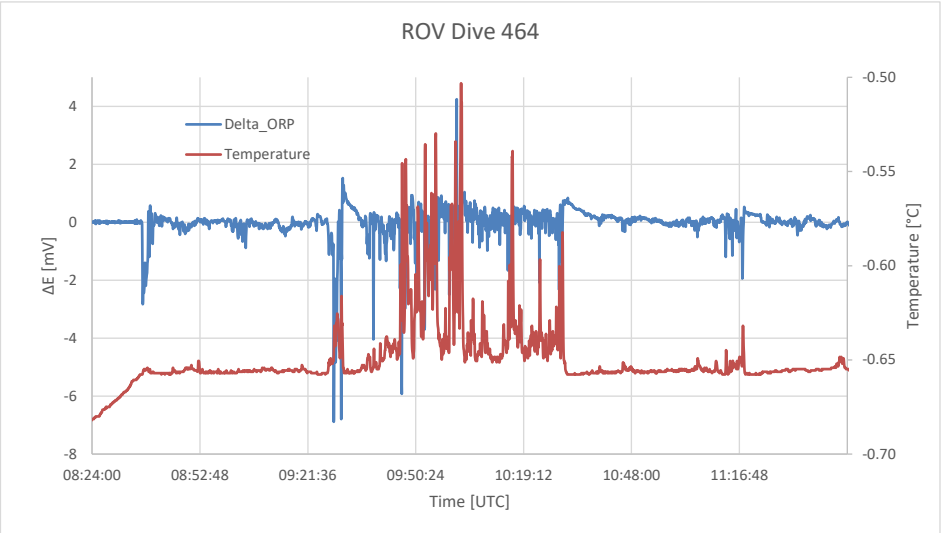

Fig. 5.4.21 ΔE and turbidity of ROV dive 464 over Jøtul hydrothermal field

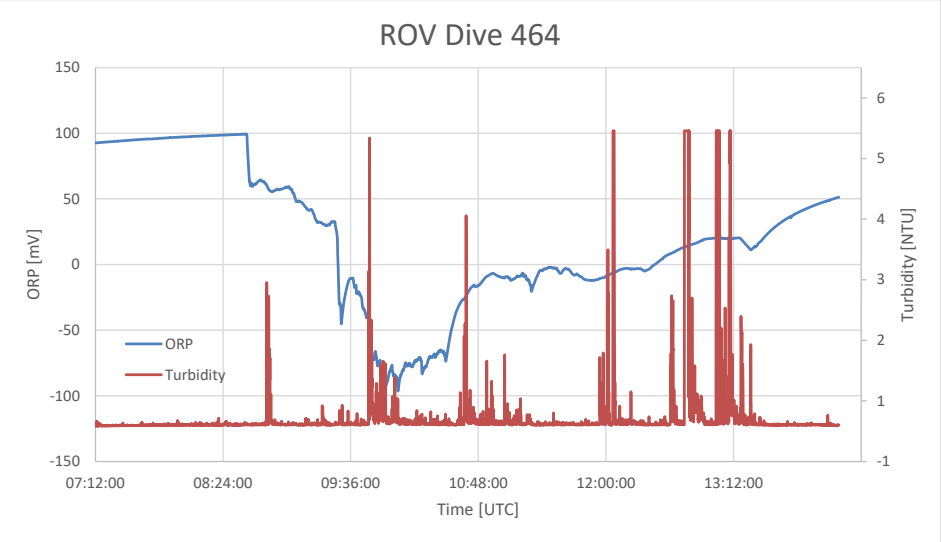

Fig. 5.4.22 Detail of ΔE and temperature of ROV dive 464 over Jøtul hydrothermal field

5.5 Gas Chemistry of Seawater and Fluid Samples

(Janice Malnati, Thomas Pape)

Introduction

The gas chemical works during the expedition focused on two main topics:

- Determination of concentrations of dissolved methane in the water column, identification of methane-rich hydrothermal plumes, and localization of seafloor emissions of hydrothermal fluids
- Analysis of compositions of volatiles in hydrothermal fluids for source assignments

Methods

Preparation of Seawater and Hydrothermal Fluid Samples

Discrete seawater samples were collected with the CTD/rosette water sampling system during 15 of the 16 CTD stations carried out during MSM109. For water sampling, 23 Niskin bottles attached

to the frame of the system were available. Preparation of water samples immediately after arrival of the system on deck and analysis of methane concentrations followed the procedure described by Mau et al. (2020). Briefly, 100 mL-aliquots of the water were immediately transferred from each Niskin bottle into two 140 mL-syringes using silicone hoses. The syringes were carefully flushed and filled with water while avoiding turbulence and introduction of bubbles from atmospheric air. Subsequently, the syringes where closed with a valve at their tip.
A headspace volume was generated in each syringe by drawing 40 mL of 'Zero Air' (hydrocarbon-free air) into the syringe. The syringes were shaken vigorously for more than 1.5 minutes to allow for equilibration between water and headspace. To minimize the risk of water injection into the measurement chamber of the analytical instrument, the 40 mL headspace gas each from both syringes were collected in another gas-tight syringe via a Luer Lock adapter.

Hydrothermal fluids discharged at the seafloor were sampled with the KIPS (Kiel Pumping System) fluid sampling system during four dives (461, 463, 464, 465) of the MARUM ROV QUEST. Aliquots of the fluids were immediately transferred into 250 ml-glass vials, which were closed with butyl rubber stoppers and crimp-caps. Due to ongoing gas exsolution a gas headspace formed in the glass vials.

Analysis of Seawater and Fluid Samples
Quantifications of concentrations of methane dissolved in seawater were done on board with a Greenhouse Gas Analyzer (GGA, Los Gatos Research). The instrument uses laser absorption spectroscopy, where the absorption of the infrared laser beam directed through the sample is used to calculate the mole fraction of methane in the gas. The GGA was installed in the dry lab on R/V MARIA S. MERIAN and calibrated with standard gasses (1 ppm to 100 ppm CH_4 in N_2; Air Liquide). During the period of scientific program, precision of the instrument was checked daily with 1 ppm and 10 ppm methane standard (AirLiquide).
The combined headspace gas volume of 80 mL prepared from the two syringes was injected in the GGA. This was followed immediately by injection of 60 mL of 'Zero Air', as needed to provide a gas volume of 140 mL in the measurement chamber required for analysis with the GGA.

The molecular composition of volatiles in head space gas, that has accumulated by exsolution from the hydrothermal fluid samples in the glass vials, was analyzed onboard by gas chromatography. A defined volume of the gas was withdrawn with a gas-tight syringe and directly injected into a three-channel gas chromatograph (Agilent Technologies, 7890B) equipped with a flame ionization detector (light hydrocarbons, C_1–C_6) and two thermal conductivity detectors (TCD1: N_2, CO_2, CH_4; TCD2: N_2, O_2, CH_4). As an exception, fluids collected during dive ROV-461 (GeoB25024-1) were measured on methane concentrations with the GGA only, but not by gas chromatography.

Preliminary Results
Concentrations of Dissolved Methane in Discrete Water Samples

Knipovich Ridge South
A single vertical CTD/rosette water sampler (CTD/ro) station (CTD-2) was performed at Knipovich Ridge South (Fig. 5.5.1). Relatively low methane concentrations (≤4 nmol/L) in

discrete water samples were measured throughout the water column. Such low concentrations do not suggest significant emission of hydrothermal methane-rich fluids in the area at the time of investigation. This conclusion is in line with the signals of the oxidation-reduction potential (ORP) that did not record any anomaly indicative for input of dissolved reduced species in the water column.

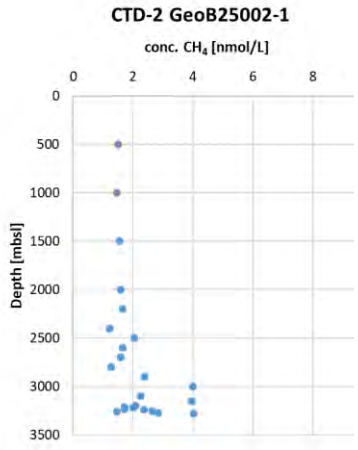

Fig. 5.5.1 Concentrations of dissolved methane in water samples collected during vertical CTD/ro station CTD-2 vs. water depth at Knipovich Ridge South.

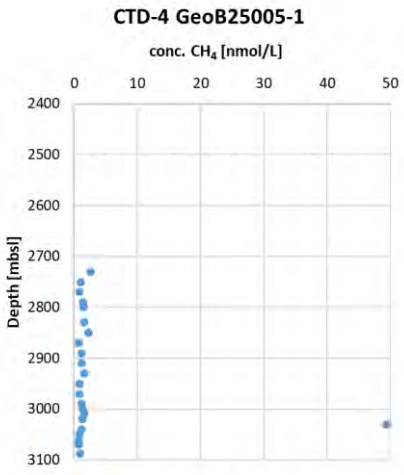

Fig. 5.5.2a Concentrations of dissolved methane in water samples collected during vertical CTD/ro station CTD-4 vs. water depth at Brøgger AVR.

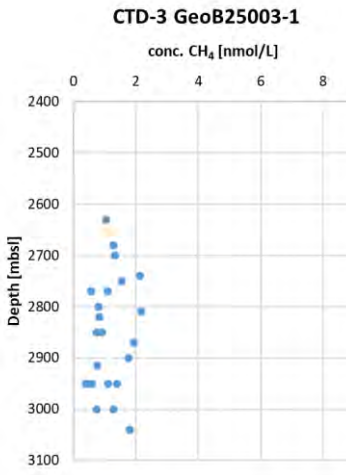

Fig. 5.5.2b Concentrations of dissolved methane in water samples collected during Tow-yo CTD/ro station CTD-3 vs. water depth at Brøgger AVR.

Brøgger Axial Volcanic Ridge

At the Brøgger Axial Volcanic Ridge (Brøgger AVR) two CTD/ro stations, a vertical station (CTD-4) at a restricted site and a tow-yo station (CTD-3) covering a larger area and crossing station CTD-4, were carried out (Figures. 5.5.2a and 5.5.2b). Discrete water samples were collected from the 2,620 – 3,087 m depth interval. Relatively low methane concentrations in the samples (<2.6 nmol/L) were measured throughout the water column, except for a single sample (~49 nmol/L, CTD-4, 3,030 mbsl). The cause for the methane enrichment in a single sample is unknown so far. However, as all other water samples were very low concentrated in methane, and anomalies in the ORP signals were not recorded, significant emission of hydrothermal methane-rich fluids in this area at the time of investigation is unlikely.

Jøtul Hydrothermal Field

During MSM109, the majority of CTD/ro stations was conducted in the Jøtul hydrothermal field. In total six vertical stations (Fig. 5.5.3) and four Tow-yo stations (Fig. 5.5.4) were carried out, and discrete water samples were collected in the 2,186-2,981 m (CTD-9, CTD-14) depth range. Enrichments in methane exceeding 10 nmol/L were found at all stations conducted in the area, with the exception of the two stations CTD-11 and -16. For most stations, significant enrichments in methane were observed below ~2,600 mbsl and maximum concentrations were detected at Tow-yo station CTD-15 (4,991 nmol/L, 2,920 mbsl). This clearly indicates that seafloor discharge of methane-rich fluids is widespread in the Jøtul hydrothermal field. In accordance with the methane

enrichments, anomalies of the ORP signal were detected at all stations in the field except stations CTD-11 and CTD-16.

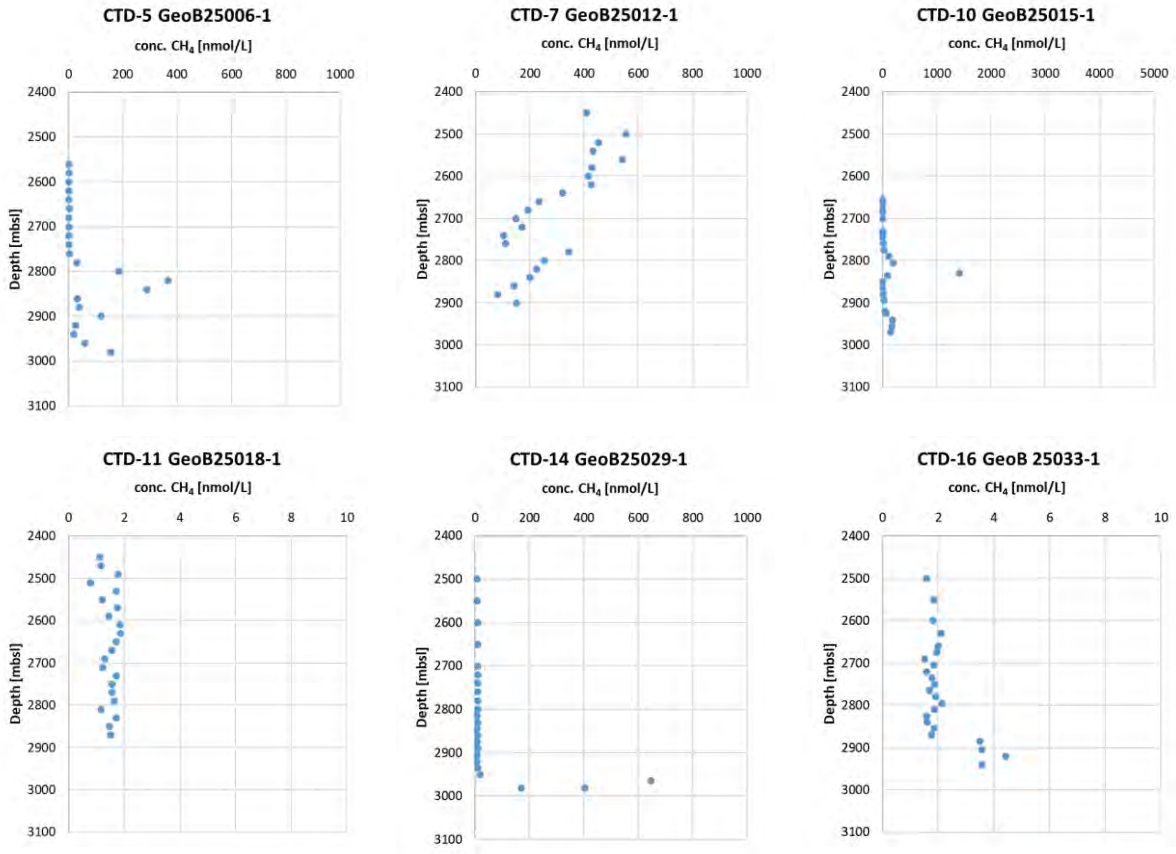

Fig. 5.5.3 Concentrations of dissolved methane in water samples collected during vertical CTD/ro stations CTD-5, -7, -10, -11, -14, and -16 vs. water depth at Jøtul hydrothermal field. Note the different axis scales used for concentrations.

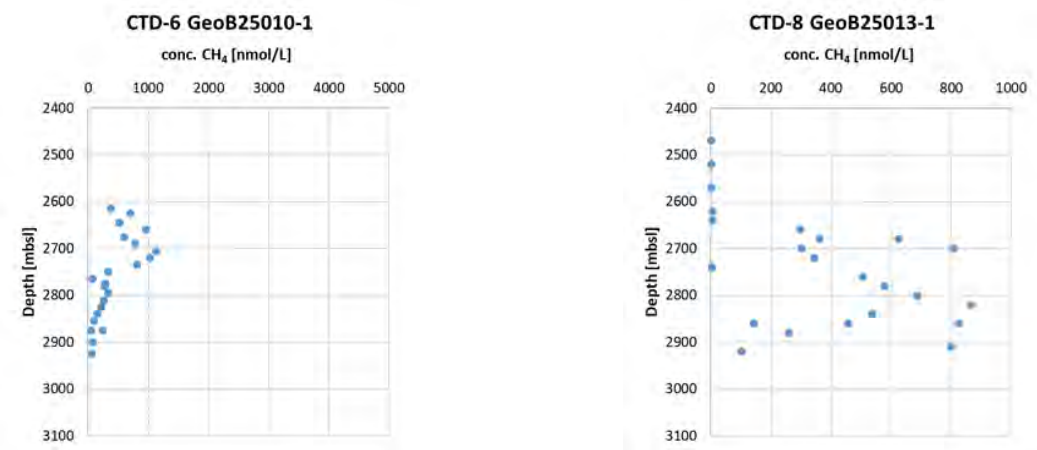

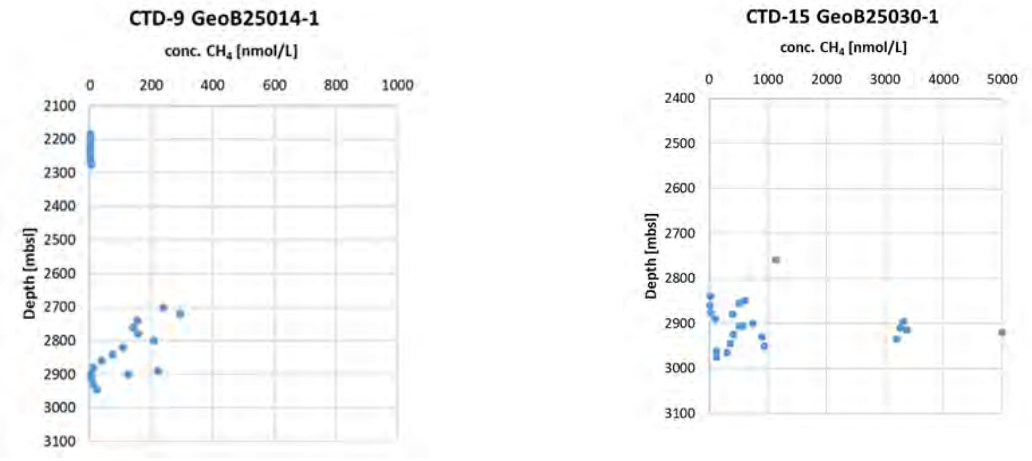

Fig. 5.5.4 Concentrations of dissolved methane in water samples collected during Tow-yo CTD/ro stations CTD-6, -8, -9, -15 vs. water depth at Jøtul hydrothermal field. Note the different axis scales used for concentrations.

Molløy Ridge

Two CTD/ro stations, the vertical CTD/ro station CTD-13 (close to the positions of ROV dive 459) and the northeasterly Tow-yo station CTD-12, were carried out in the water column above the Molløy Ridge (Figures 5.5.5a and 5.5.5b). Discrete water samples were taken in waters between 2,075 mbsl and 3,020 mbsl. At both stations an increase in concentrations of dissolved methane with increasing depth was observed. However, overall methane concentrations <8 nmol/l suggest that no significant amounts of methane-rich fluids were discharged from the seafloor during MSM109. This interpretation is supported by the absence of anomalies in the ORP signal.

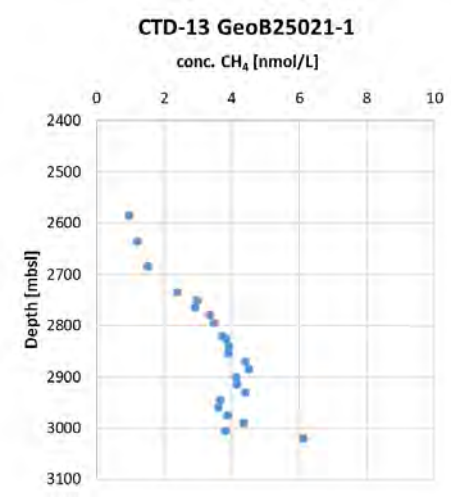

Fig. 5.5.5a Concentrations of dissolved methane in water samples collected during vertical CTD/ro station CTD-13 vs. water depth at Molløy Ridge.

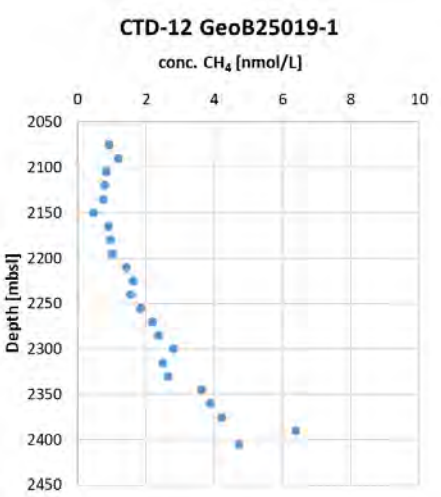

Fig. 5.5.5b Concentrations of dissolved methane in water samples collected during Tow-yo CTD/ro station CTD-12 vs. water depth at Molløy Ridge.

Compositions of Hydrothermal Fluids

Molecular compositions of headspace gas were analyzed for hydrothermal fluids collected during dives ROV-463, 464, and -465, all of which have been carried out in the Jøtul hydrothermal field. Here we focus on the distributions of C_1- to C_3-hydrocarbons. In general, methane concentrations

of all fluid samples ranged between 0.48 and 12.26 mmol/L (Table 5.5.1), and measured concentrations are likely influenced by variable mixture with proportions of seawater. Light hydrocarbons of the fluids were strongly dominated by methane (>99.04 mol-% C_1-C_3), followed by ethane (≤0.81 mol-%) and propane (≤0.17 mol-%,). The resulting hydrocarbon ratios (calculated as C_1/C_2-C_3 or C_1/C_2, respectively) suggest prevalence of non-microbial sources (e.g., Etiope and Sherwood Lollar, 2013).

Table 5.5.1 Compositions of light hydrocarbons in samples collected with the KIPS at the Jøtul hydrothermal field.

ROV dive	GeoB	Feature	C_1/ (C_2-C_3)	C_1/C_2	CH_4 [µmol/L]	C_2H_6 [µmol/L]	C_3H_8 [µmol/L]
463	25028-4	Black smoker (vent center)	102.8	124.3	2.301.7	18.5	3.9
463	25028-5	Black smoker (vent rim)	140.9	163.0	1.537.7	9.4	1.5
463	25028-6	Black smoker (50 cm above)	438.7	507.4	4.786.9	9.4	1.5
464	25031-2	Black smoker (vent center)	119.9	140.8	4.934.8	35.1	6.1
464	25031-3	Black smoker (30 cm above)	181.1	223.6	1.765.3	7.9	1.9
464	25031-4	Black smoker (100 cm above)	168.3	207.2	1.909.1	9.2	2.1
465	25034-3	Shimmering water	n.a.	194.4	477.3	2.5	n.d.
465	25034-8	Shimmering water	105.1	122.8	12.264.9	99.9	16.9

n.a. – not analyzed; n.d. – not detected

All samples will be investigated onshore for stable C and H isotopic compositions of methane and stable C isotopic compositions of carbon dioxide for profound source assignments.

5.6. *In situ* Mass Spectrometer (ISMS)

(Jan Kleint)

Within the Cluster of Excellence "The Ocean Floor – Earth's Uncharted Interface" at MARUM (University of Bremen, Germany) a new *in situ* mass spectrometer (ISMS) is developed in a cooperation between MARUM and Max Planck Institute for Marine Microbiology (MPIMM). Its development is based on a system designed to operate at hydrothermal vents (GirguisLab, Harvard University, US) that is suitable for deep-sea ROV deployments and provides real-time information and guidance for water and sediment sampling during field campaigns. The original instrument quantifies all dissolved volatiles of masses up to 100, and it is suitable for water depths of up to 4,000 m and for the analysis of fluids with temperatures up to 350°C. It has provided significant contributions to our understanding of the coupling of the dynamics of gas emissions and biological community composition and metabolism at hydrothermal vents and cold seeps, respectively (Frank

et al., 2013; Olins et al., 2013; Perner et al., 2013; Petersen et al., 2011; Wankel et al., 2012; Wankel et al., 2010a; Wankel et al., 2011; Wankel et al., 2010b). However, in its initial configuration, the ISMS was strongly limited to the application in gas-rich environments and could not develop its full potential. In order to overcome this limitation, we considerably modified the initial setup of hardware components, and also the software architecture to e.g. lower the limit of detection turning the instrument basically into a new prototype.

A first attempt for testing basic functions in the marine environment of the German sector of the North Sea in late February 2021 (HE591) was thwarted by heavy storms that hindered R/V HEINCKE from reaching the working area. However, shipboard testing of the instrument in particular under real *in situ* deep-sea conditions is required before it can be integrated as an essential tool deployment during future research cruises. For this, the ISMS was deployed on ROV QUEST during this cruise to test the overall function and performance of the new instrument with its technical modifications introduced for improving the limits of detection and the *in situ* calibration in the deep sea.

Methods

Underwater mass spectrometer or ISMS were introduced by several groups in the last decades (Bell et al., 2007; Boulart et al., 2010; Schlüter & Gentz, 2008; Short et al., 2006; Wankel et al., 2010; Wenner et al., 2004), and the general setup of these systems still remain unchanged: the design of an underwater ISMS is based on the extraction of gases through a membrane by applying a vacuum and the subsequent detection by a quadrupole mass spectrometer. The modifications of the new MPIMM/MARUM ISMS compared to its precursor system developed by Pete Girguis at Harvard University, mostly relate to (a) integration into the MARUM fleet, (b) the installation of cryotrap that reduces the water vapor content within the analytical vacuum system permeabilities (see Gentz et al. 2014, Gentz and Schlüter, 2012), (c) change of the membrane material and its backing structure, (d) the modification of the cooling architecture in the pressure housing to reduce the power consumption and by this increase the performance of the entire system, and (e) the implementation of a completely new hardware and software architecture, in order to enable detailed real-time monitoring of both the instrument performance and the obtained *in situ* data, such as gas concentrations, pH and temperatures in the analyzed water. In the laboratory, the new ISMS was tested for methane (CH_4) determinations under various physical conditions, such as changing water temperatures and pressures (0 to 400 bar). To verify the future pre-cruise laboratory calibrations, we developed a new *in situ* calibration system with gas standards dissolved in seawater, stored in gas-tight bags that are measured at depth for *in situ* verification of the ISMS. This will allow the calculation of the *in situ* gas concentration from the obtained raw mass spec data in real-time.

During this cruise, the ISMS was installed on the port side of the ROV QUEST (see Fig. 5.6.1). Sampled seawater was pumped from the titanium sample nozzle, that was actively positioned using the ROV manipulator, to the KIPS fluid sampler and subsequently to the ISMS. The water was passively cooled by ambient water using a copper cooling loop and temperatures were monitored by 4 temperature probes along the flow path to the ISMS to estimate the temperature gradients within the tubing and prevent possible damage at the membrane while sampling of high-temperature vents. From a bypass in the main tubing system, water was constantly pumped at a

flow rate of 10 ml min^{-1} to the membrane inlet system of the ISMS by an external peristaltic pump. Up to two three-way magnetic valves allow the selection between the sampled water or the standard solutions in the gas-tight bags for *in situ* calibration/validation of the ISMS.

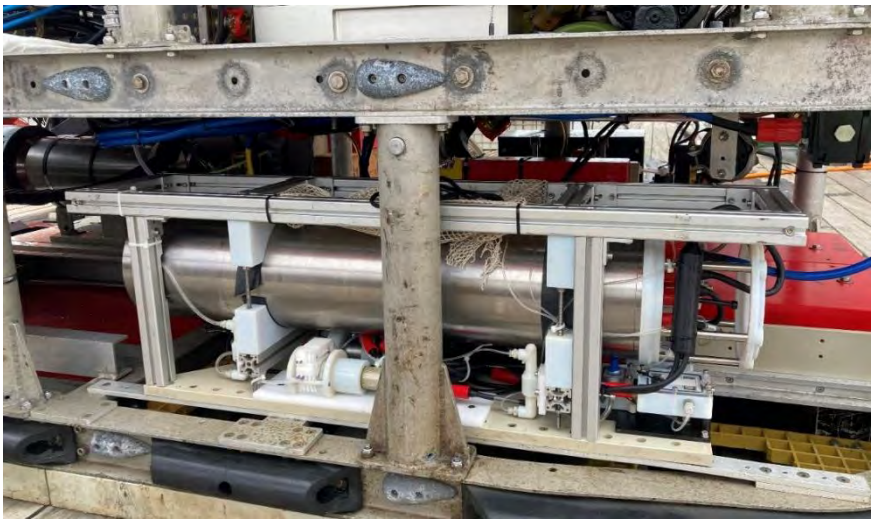

Fig. 5.6.1 The MPIMM/MARUM *in situ* mass spectrometer (cylindrical pressure housing) with its peripheral devices and sensors in its frame deployed on ROV QUEST during MSM109.

Preliminary Results

The ISMS was deployed during all 13 successful ROV QUEST dives and provided real-time data during the first 10 dives. No measurements could be carried out during the last 3 ROV QUEST dives (dives 465, 466 and 467) due to electrical problems, most likely in the connection to the ROV QUEST.

During the successful deployments, the ISMS was running smoothly and no major issues were detected. The pressure housing of the ISMS, the membrane unit and all additional peripheral devices have withstood the pressure of up to 330 bar (3300 m water depth). The power supply and communication were stable all time, and temperatures within the pressure housing were in the expected range (less than 30°C). The controlling software developed in-house specifically for the ISMS ran smoothly and the dashboard, which is making real-time MS and additional *in situ* data such as temperatures accessible for every user onboard, also worked successfully. On the other hand, the proprietary software, which is needed for controlling the quadrupole mass spectrometer in the ISMS, froze up frequently and will therefore be replaced by a new software upgrade of the in-house developed controlling software for future deployments. This upgrade was already developed a few weeks prior to this cruise and the tests during the last dive were very promising.

The in-house built peripherals such as the external peristaltic pump or the external temperature sensors worked as expected. The tests of two different magnetic valves provided valuable input for the final design of the *in situ* calibration system. The final version will be improved with regard to (a) the valve types used, (b) the pressure compensation which is also suitable for water temperatures <0°C and (c) the space usage to simplify and speed up maintenance work between consecutive ROV dives.

The sampling of low- and high-temperature vents with max. temperatures of 8°C and 317°C at the outflow, respectively, showed no concerning temperature increases at the membrane inlet, as the

water was sufficiently cooled by the cooling loop along its flow path: to ambient water temperatures for low-temperature vent sites and to less than 20°C at the high-temperature vent site in Jøtul hydrothermal field. However, these temperature differences at the membrane inlet tend to change the membrane properties and by this the gas permeability through the membrane, resulting in complex, pressure and temperature-dependent calculations of the actual *in situ* gas concentrations. The implementation of a temperature-controlled ("heated") membrane inlet might be a future option to provide qualitative and quantitative concentration data, since the new ISMS will be deployed in different marine environments with changing temperatures. A more detailed evaluation of the data as well as technical realization of this new and additional feature will be carried out after this cruise.

At all sampling sites, the ISMS showed very reasonable results of the gas contents and composition: e.g. high CH_4 and/or H_2S signals, accompanied by low O_2 signals. A selection of the obtained mass spec data is shown in Fig. 5.6.2. The peak in CH_4 signal in Fig. 5.6.2a was obtained at a low-temperature vent (8°C - ROV dive 461) and corresponds to a CH_4 concentration of ~2µM. The analysis of the black smoker fluid in the Jøtul hydrothermal field (316°C – dive 465) revealed a signal for CH_4 that exceeded the background signal by a magnitude of 5 and corresponds to CH_4 concentration of ~5-10mM. A final statement concerning the actual *in situ* gas concentrations is not possible at this time, as the calibration and characterization work of the ISMS in the laboratory is still ongoing for these gases and will be finalized within the next months.

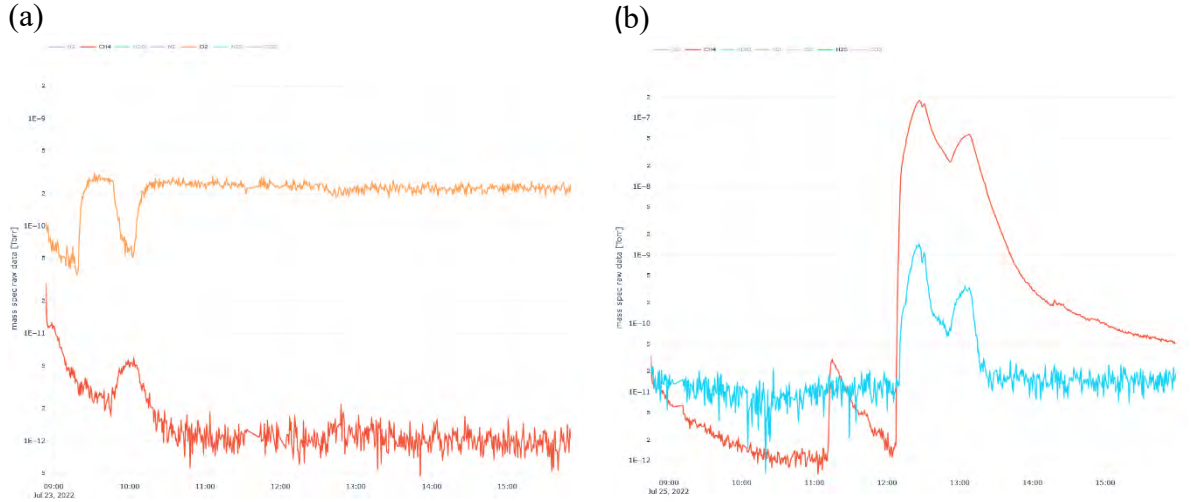

Fig. 5.6.2 Raw and uncalibrated mass spec data for methane (red) and (a) oxygen (orange), as well as (b) hydrogen sulfide (blue) during ROV dives 461 (low-temperature vent – 8°C) and 465 (high-temperature vent – 316°C), respectively, in the Jøtul hydrothermal field. Note the different scale for the mass spec raw data.

This cruise was the first shipboard testing of the new MPIMM/MARUM ISMS in particular under real *in situ* deep-sea conditions, and the results show that the instrument is technically ready for operation in the deep sea. The integration into MARUM ROV QUEST is finalized and the instrument operated as expected. In addition, the tests of the peripheral devices were either successful or provided valuable input for further improvements. A detailed evaluation of these improvements as well as the technical realization will be carried out in the upcoming months. Scientific deployments will follow in summer 2023 during M190 (DIVEMAR / ROV QUEST) and M192 (BRIDGEHELL / ROV SQUID).

5.7 Station Work With the Autonomous Underwater Vehicle (AUV) MARUM SEAL 5000

(Jens Renken, Pooja More, Daniel Hüttich, Ulli Spiesecke)

Introduction

In the year 2006 the MARUM ordered a deep diving autonomous underwater vehicle (AUV), designed as a modular sensor carrier platform for autonomous underwater applications. The company "International Submarine Engineering"(I.S.E.) built this AUV in Canada. In June 2007 the AUV "SEAL" was delivered to MARUM and tested afterwards on the French vessel R/V SUROIT (June 2007) and the German R/V POSEIDON (November 2007) in the Mediterranean Sea. Since then, the AUV is in operational mode and was used 14 times on field cruises on-board research vessels (R/V SONNE, R/V METEOR, R/V MARIA S.MERIAN, R/V POSEIDON, R/V SUROIT, R/V OR5) and 2 times in Lake studies (Lake Constance, Lake Neuchatel). This R/V MARIA S. MERIAN cruise MSM109 is the 19th field cruise of MARUM SEAL 5000.

SEAL Vehicle – Basics

The MARUM SEAL is No. 5 of the Explorer-AUV series from the company I.S.E. The AUV is nearly 5.75 m long, with 0.73 m in diameter and a weight of 1.35 tons. The AUV consists of a modular atmospheric pressure hull, designed from 2 hull segments and a front and aft dome. Inside the pressure hull, the vehicle control computer (VCC), the payload control computer (PCC), 8 lithium batteries and spare room for additional "dry" payload electronics are located. Also, the inertial navigation system PHINS and the Kongsberg multibeam-processor are located as dry payload here. The tail and the front section are flooded and made out of GRP. In the tail section the motor, beacons for USBL, RF-radio, flashlight, IRIDIUM antenna and DGPS antenna are located. In the newly designed aluminum front section the Seabird SBE 49 CTD, the Sercel MATS 200 acoustic modem, the DVL (300 kHz), Kongsberg Pencil beam (675 kHz), the recently implemented Kongsberg EM2040 (200, 300, 400 kHz), the PAROSCIENTIFIC pressure-sensor and the BENTHOS dual frequency (100/400 kHz) side scan sonar are located. Actually, the SEAL AUV has a capacity of approx. 15,4 KWh of battery power installed, which enables the AUV for approx. 70 km mission-track lengths. Although the max. track length on bottom is a bit shorter than with the formerly installed Reson 7125, the outcome in surveyed area increased significantly with the new multibeam, as the AUV is flying with greater altitude resulting in a larger beam width and an increased line spacing for the survey.

Now the AUV is able to survey an area of approx. 10 km² in one dive with an even better data quality than with the Reson. For security aspects, several hard- and software mechanisms are installed on the AUV to minimize the risk of malfunction, damage and total loss. More basic features are dealing with fault response tables, up to an emergency drop weight, either released by the user or completely independent by the AUV itself. MARUM puts special emphasis on an open architecture in hard- and software design of the AUV, in order to be flexible in vehicle operations as well as in repair and maintenance. Therefore, the VCC is based to a large extent on industrial electronic components and compact-PCI industrial boards and only very rare proprietary hardware boards have been implemented. The software is completely built QNX 4.25 – a licensed UNIX derivate, that is to a large extent open for user modifications. The payload PC is built on

comparable hardware components, but running either with Windows and/or Linux. On the support vessel, the counterpart to the VCC is located on the surface control computer (SCC).

It is designed as an Intel based standard PC, also running with same QNX OS and a Graphic User Interface (GUI) to control and command the MARUM SEAL AUV. Direct communication with the AUV is established via an Ethernet-LAN, either by hard-wired 100 mb LAN cable plugged to the AUV on deck, or by the Ethernet-RF-LAN modem – once the vehicle is launched. The typical range of the RF-link is around 1 – 2 km distance between the ship and the vehicle. Within this range the user has all options to operate the AUV in Pilot-Mode, e.g. to maneuver the AUV on water or change vehicle settings. Once the AUV is submerged, all communication links are shut down automatically and the AUV is in mission-mode, means it is working based on specific user-defined missions. Despite being in mission-mode it is necessary to communicate with the AUV when it is under water, i.e. asking for actual position, depth and status. To achieve this, onboard the support vessel an acoustic underwater modem with dunking transducer has to be installed (SERCEL MATS modem) communicating with the counterpart on the AUV, on request. Due to limited acoustic bandwidth only rare data sets are available.

Mission-Mode

The AUV - as dedicated autonomous vehicle - has to be programmed before operated under water. As mentioned, only at the surface a real-time control by the pilot is possible - once it dives, it will lose any real-time communication and therefore must be in a defined mission-mode. Initialized correctly, fault prevention mechanisms take action in the case that the AUV maneuvers into a dangerous scene. Simplified, an AUV mission is a set of targets; clearly defined by its longitude, latitude, and a given depth/altitude that the vehicle should reach/keep at a given speed in a distinct time. The AUV needs to be in a definite 3-dimensional underwater space to know exactly its own position over mission time, in order to actively navigate on this.

To achieve this basic scenario, the AUV is working with best position updates possible, e. g. DGPS position at the surface. Once it dives, it takes the actual position as starting point of navigation, looks for its own heading and the actual speed and calculates its on-going position change based on the last actual position, e.g. method known as dead reckoning. To achieve highest precision in navigation, a combination of Motion Reference Unit (MRU) and Inertial Navigation System (INS) is installed on the MARUM AUV SEAL – the PHINS inertial unit made by IXSEA. Briefly, the MRU is measuring any acceleration of the vehicle in all 3 axis (x,y,z). The INS is built on 3 fibre-optic gyros (x,y,z) and gives a very precise/stable heading, pitch and roll information, based on rotation-changes compared to the axis. Even on long duration missions, the position calculated by the AUV will be very accurate based on that technique. Once the AUV is close to the seabed, the DVL delivers accurate navigational data on the vehicle's motion relative to the seafloor. In mission planning principle, the VCC of the AUV accepts a simple list of waypoints as targets for the actual mission (the list has to be in a specific syntax). In order to arrange it more efficient and convenient, a graphical planning tool is used for this mission planning. The MIMOSA (© Ifremer) mission-planning tool is a software package specially designed to operate underwater vehicles (AUVs, ROVs, Glider). The main goal of this software is to plan the current mission, observe the AUV once it is underwater and to visualize gathered data from several data sources and vehicles.

MIMOSA is mainly built on 2 software sources, an ArcView 9.1 based Graphical Information System (© ESFRI ArcGIS) and a professional Navigation Charting Software (© Chersoft UK). In order to plan a mission, the user has to work on geo-referenced charts with a given projection (UTM); either GIS-maps, raster-charts or S-57 commercial electronic navigational charts (ENCs). These basic charts could be easily complemented with user specified GIS projects and with already gathered data, e.g. multibeam data, or different points of interest. Once installed in MIMOSA, the user can create AUV missions by drawing the specific mission by mouse or by using the implemented set of tools (MIMOSA planning mode). Missions created in that way are completely editable, movable to other geographical locations and exportable to other formats. In order to be interpretable by the MARUM AUV SEAL, the created mission will be translated into the I.S.E. specific syntax; a set of targets, waypoints, depth information and timer will be created and written into an export path. From here the mission file can be uploaded via the SCC (support vessel) onto the VCC (AUVs control PC). From here on the AUV has its mission and is capable to dive, based on a valid mission plan.

Mission Observing/Tracking

The MIMOSA planning tool is also used for supervision, in order to monitor the vehicle at sea surface and under water (MIMOSA observation mode). The MIMOSA software is client based, that means one dedicated server is used for planning, while the others are in slave/client mode, referring to the actual mission. Therefore, position data strings (UDP broadcast data) from the support ship (i.e. R/V MARIA S. MERIAN position and heading) are being sent to the local network and fed into the MIMOSA software. The same protocol is active for the AUV position data, e.g. DGPS signal once it is at surface. During the dive the AUV can be tracked automatically via ship-borne ultra-short baseline systems (USBL), e.g. SONARDYNE RANGER, using the on-board AUV installed USBL transponder beacon. In addition to that the vehicles own calculated (VCC) position can be displayed also. This position is supplied by transmitted data strings from the MATS underwater acoustic modem, which is only sent by the AUV on user request. To summarize, the following navigational data is displayed in tracking mode:

- position of support vessel (lon/lat and heading)
- either DGPS of AUV during surface track, or
- USBL position (RANGER, GAPS or POSIDONIA)
- and MATS position (underwater acoustic on request)

Operational Aspects

MARUM SEAL was used at least 19 times on field cruises so far. Thus, different research vessels have served as a base and on each of them the handling of the AUV is slightly different. Generally, the A-frame or ship side crane with a range of more than 10 m outboard is supposed to be the best position to launch and recover the AUV, because the tendency to hit the ship is minimized based on experiences.

On R/V MARIA S. MERIAN, the AUV was successfully launched and recovered with the starboard side crane close to the stern. In principle, the AUV can be operated out of the lab, just with a simple laptop. On this cruise the AUV operations were run out of a 20" operation/workshop van, located on the main deck, midships. Not only the file-server and several displays, but also a printer, a workbench, tools and different spares are installed in this container. In addition to the control van, a transport van was set that comes with all the bigger spares, tools and the AUV itself. The SERCEL MATS acoustic transducer was installed in the moon pool. For USBL positioning, the ship owned RANGER system was used. Prior to every launch of the AUV, the PHINS INS (onboard the AUV) needs to be calibrated. In order to do so, the INS is reset and the support vessel must hold its position for at least 5 minutes. After that initial phase (INS coarse align), the ship needs to sail a course with quasi rectangular heading alterations – either a square-like course, 3 minutes @ 3-5 knots each line (INS fine align) or a stair-like course. At the end of that calibration procedure, the PHINS is in a so-called "normal mode", which means it has its highest position quality.

Station Work on R/V MARIA S. MERIAN

During cruise MSM109, we had 8 dives. SEAL successfully recovered water-column-, backscatter- and micro-bathymetry- data, as well as geo-referenced CTD and MAPR (NOAA sensor package for hydrothermal plume detection) sensor mapping data. The rough seabed with many alternating steep gradients is a big challenge for mapping with constant altitude. Facing this challenge and some technical problems, most of the missions could be completed successfully. Errors could be identified and partially dealt with via remote access when the AUV was interrupting the mission and reached the surface. The preparation of several mission scenarios for each Dive made it possible to send the AUV back to the mission when challenging slopes have aborted the dive. Jumping in mission steps during the dives made it possible to steer SEAL around difficult obstacles.

In total, 243 km of track lines have been surveyed at bottom. Most of the surveys were conducted with a line spacing of 300 m at an altitude of 130 m above seafloor. The high altitude with wide lines spacing was chosen in order to search hydrothermal plumes on large areas. Beam width is then approx. 450 m and frequency chosen was 200 kHz.

Additional two areas were mapped with 60 m altitude using 400 kHz frequency which results in an even higher resolution of the target area. In this way, detailed analysis of the found hydrothermal vents will be possible. Water column data was recorded in order to find potential gas flares. All multibeam data shown here are raw and unprocessed data.

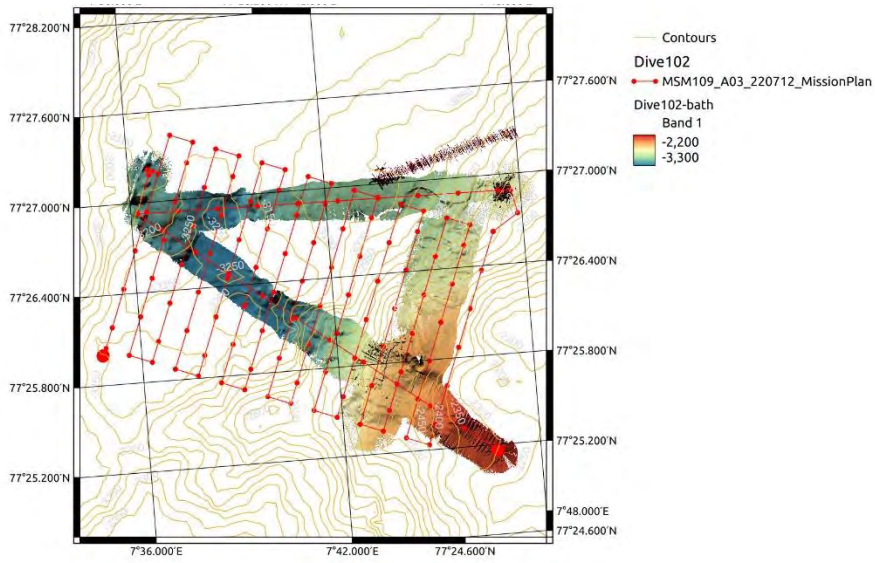

Fig. 5.7.1 **Dive No.102** The Mission started at 17:49 UTC on 12 July 2022. Electronic errors and a blocking of the thruster at 2100 m water depth made it the third attempt for dive 102. After changing the thruster Motor twice, the AUV performed the first successful dive on MSM109. At 20:50 UTC the AUV was not able to flow over the seabed holding the altitude without getting too close to the seafloor. At 1:44, the Seal was recovered with success.

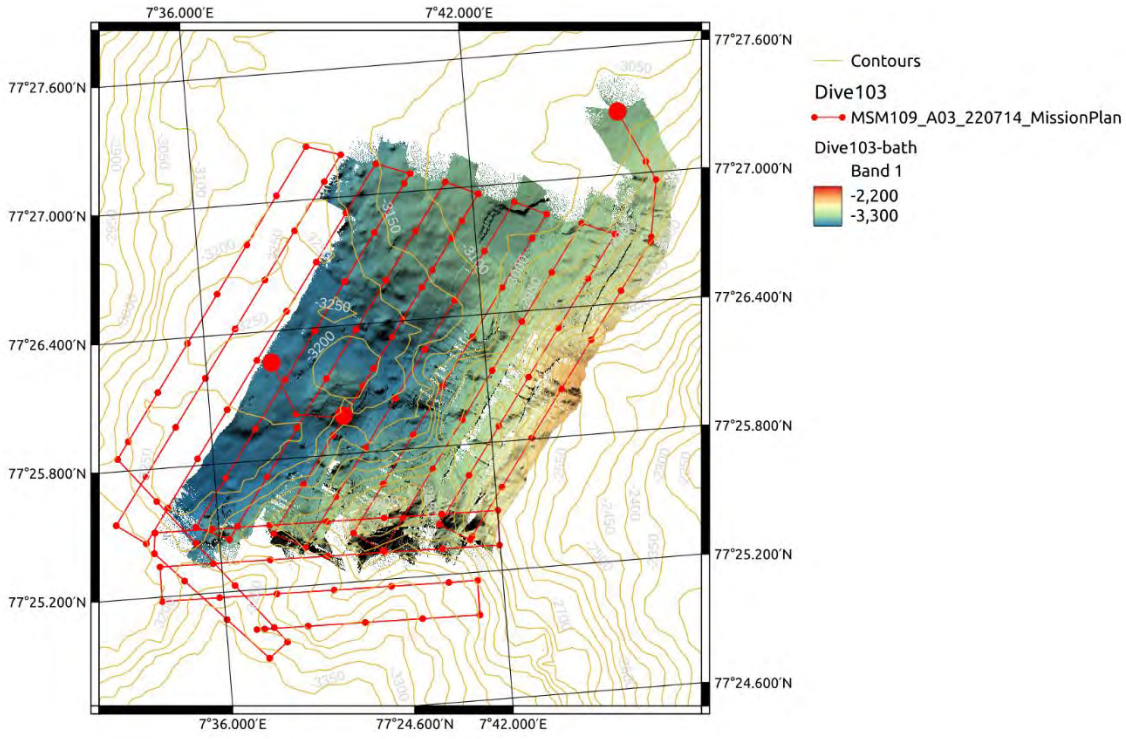

Fig. 5.7.2 **Dive No. 103** The Mission started at 18:04 on 14 July 2022. Analyzing the dive behavior of Dive 102, the weight and balancing of the AUV was changed to make it easier to follow the slope. The MAPR sensor pack was placed in a better hydrodynamic position. Diving over the same area like that

of Dive 102, the AUV was now able to stay within the altitude range for mapping. At 3:06, the AUV was recovered after mapping the missed areas of the last dive.

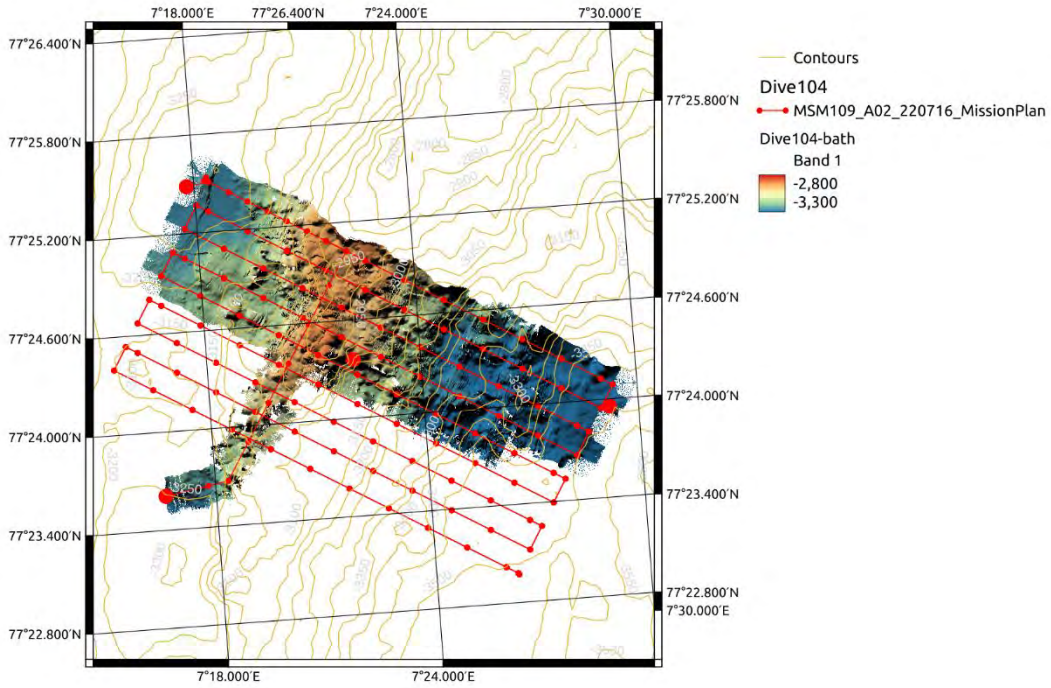

Fig. 5.7.3 **Dive No. 104** The mission start was postponed from 16 to 17 July 2022 19:23 UTC due to sea state change. Additional adjustment in the ballast improved the diving behavior. At 2:54 UTC the Mission was interrupted when the flooding sensor of the main hull detected water. The emergency system released 25kg weight and the AUV was recovered at the surface. The alarm was triggered by moisture formed by condensation on the pressure hull wall that was cooled by the seawater. To prevent the system to run in the same failure we evacuated and refiled the electronic housing with dried air.

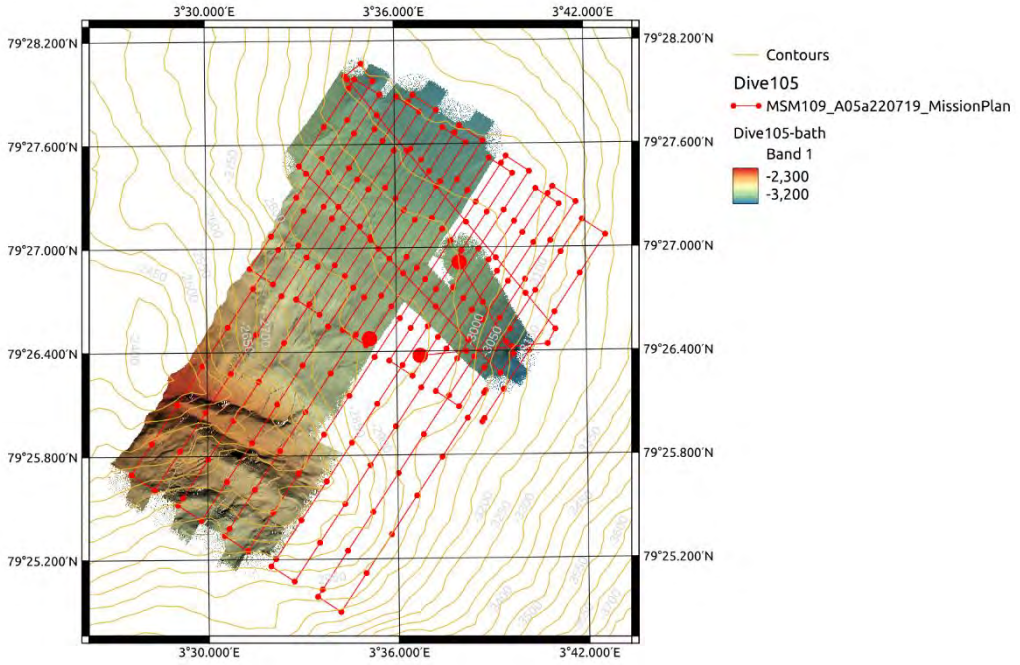

Fig. 5.7.4 **Dive No. 105** The Mission to the extreme North took place on 20 July 2022 at 20:13 UTC. In foggy weather the AUV was recovered after completing the mission at 3:35 UTC.

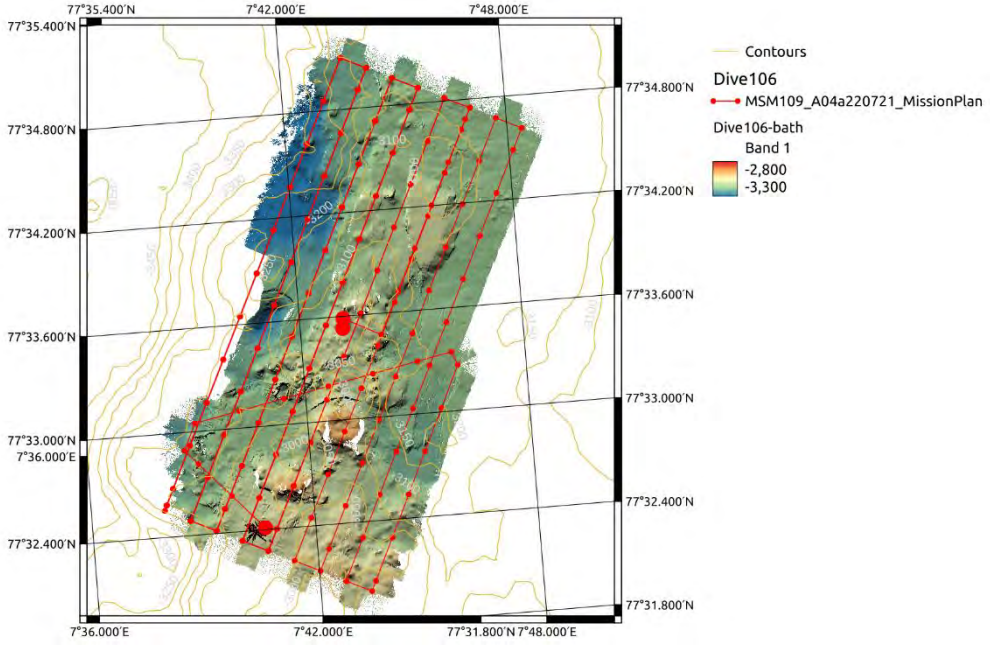

Fig. 5.7.5 **Dive No. 106** On 23 July 2022, SEAL was sent on mission at 19:20 UTC. It performed well and was recovered at 5:25.

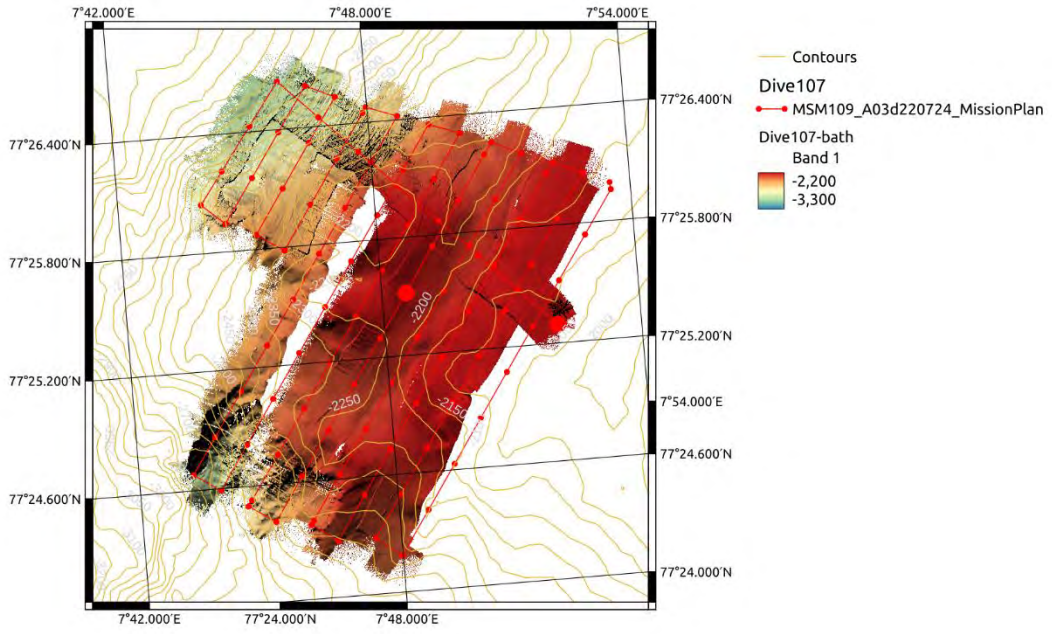

Fig 5.7.6. **Dive No. 107** On 24 July 2022 the AUV went on mission at 18:52 UTC. The terrain was difficult and the current forced the AUV to dive close to a very steep slope. SEAL needs at least 1 m/s speed thru the water to be able to steer with the planes. When the water current comes from the aft, it is possible that the hydrodynamics of the AUV plans become instable. At 23:02 the Mission was interrupted but SEAL could be resent for executing the mission successfully till 6:05 UTC.

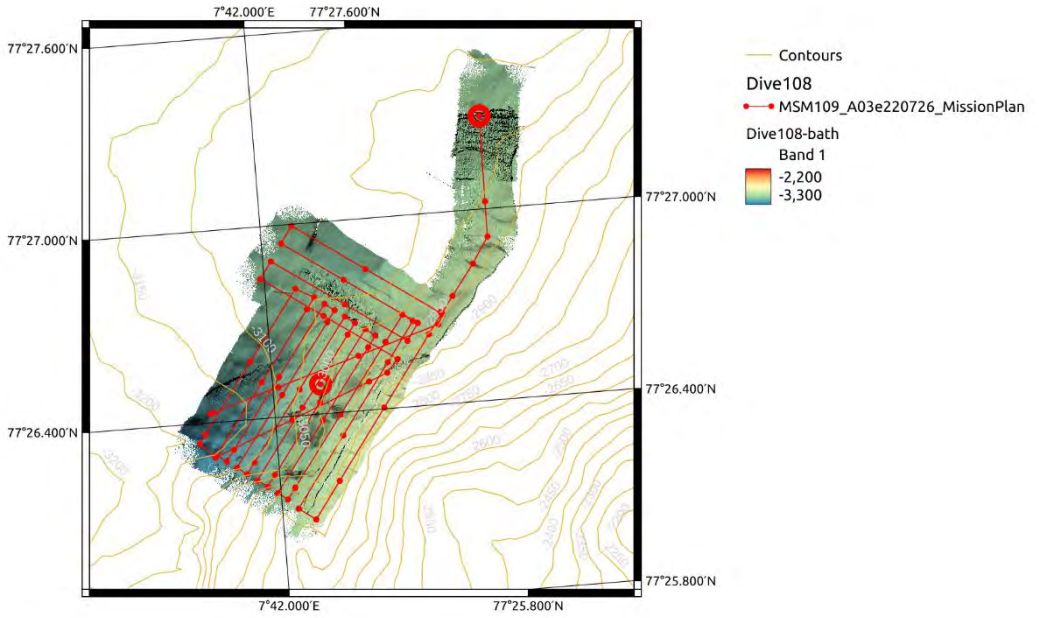

Fig. 5.7.7 **Dive No. 108** On 26 July 2022, SEAL was sent on the mission at 16:40 UTC. We programmed the AUV to fly at 60m altitude using 400kHz multi-beam frequency. Since big cracks in the sea bottom made the mission execution quite difficult, the AUV had to interrupt the mission at 20:44 UTC. We could resend the AUV back to the seafloor, and mapping this difficult structure from another direction resulted in a successful dive. The task was competed and SEAL was recovered at 0:26 UTC.

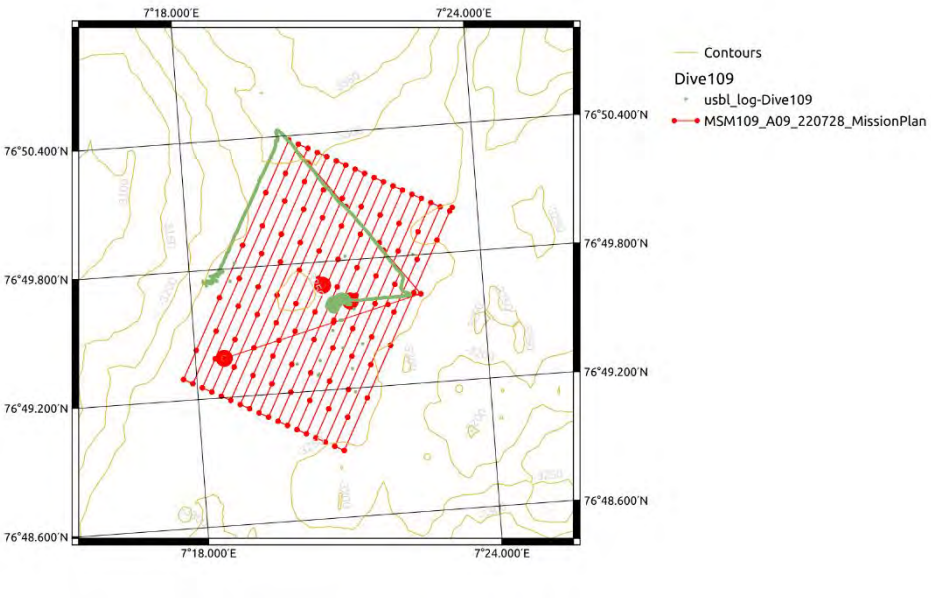

Fig. 5.7.8 **Dive No. 109** At 17:38 UTC on 28 July 2022, SEAL began its last mission planned for this cruise. After finishing the first three lines, the main controlling computer had a malfunction. The AUV was recovered dead at 19:26 UTC. Due to the error, the multi-beam data will be downloaded after fixing the AUV Computer in Bremen.

Table 5.7.1 Dive Overview MSM109

Dive	Location	Date	Mission Start UTC	Bottom Log UTC	End (loss of Bottom Log)	Bottom Time [h]	Distance [km]	Area [km²], approx.	Mission End
102/1	Jøtul Field	12.07. 2022	17:49	18:33	20:42	2,2	11,3	6,000	Low Altitude
102/2	Jøtul Field	13.07. 2022	23:29	00:12	01:44	1,5	8,1		Low Battery Voltage
103	Jøtul Field	14.07. 2022	18:04	19:04	03:06	8,0	42,1	8,340	Low Battery Voltage
104	Southern Brøgger Ridge	17.07. 2022	19:23	20:25	02:34	6,1	31,9	8,000	Water Alarm Main Hull
105	Jøtul Field	20.07. 2022	20:13	20:25	03:35	7,2	34,2	8,100	Low Battery Voltage
106	Jøtul Field	23.07. 2022	19:20	20:18	05:25	9,1	48,9	12,300	Low Battery Voltage
107/1	Jøtul Field	24.07. 2022	18:52	20:02	23:02	3,0	14,2	9,000	Low Altitude
107/2	Jøtul Field	25.07. 2022	00:38	01:23	06:05	4,7	25,2		Time Break
108/1	Jøtul Field	26.07. 2022	16:40	17:40	20:44	3,1	15,8	1,710	Low Altitude
108/2	Jøtul Field		21:51	22:56	00:26	1,5	7,9		Mission End
109	Southern Brøgger Ridge	28.07. 2022	17:38	18:39	19:26	0,8	3,9		VCC Switch-off
Sum						**47,2**	**243,5**	**53,450**	

5.8. ROV Work

5.8.1 Technical Description and Performance During MSM109

(Hauke Büttner, Abraham Tibebu, Ralf Rehage, Christian Reuter, Ousmane Coulibaly, Tobias Schade, Marcel Schröder, Daniel Hüttich)

Objectives

The scientific deep water ROV (remotely operated vehicle) “MARUM QUEST 4000m” was used aboard R/V MARIA S. MERIAN during cruise MSM109. The system is hosted at and operated by MARUM, Center for Marine Environmental Sciences at the University of Bremen, Germany. The ROV QUEST is based on a former, commercially available 4,000 m rated deep water robotic vehicle designed and built by Schilling Robotics, Davis, USA. Since installation at MARUM in May 2003, it was set up as a mobile system specifically adapted to the requirements of scientific work aboard marine research vessels for worldwide operation. Today, QUEST has a total record

of 467 dives during 41 expeditions, including this cruise. During MSM109, QUEST performed 13 dives to depths between approx. 2,800 m and 3,300 m.

Dive tasks included rock and fluid sampling, geological sampling, high quality photographic and HDTV video documentation, optical 3D structure reconstruction and online *in situ* measurements of fluid temperatures around hydrothermal vents. QUEST was operated by a team of 8 pilots/technicians on a 12-hour basis.

The good weather conditions during the cruise allowed almost permanent diving. When diving, close cooperation between ROV team and ship's crew through all departments allowed a safe and routinely performed handling especially during deployment and recovery, as well as precise navigation, underwater positioning and an always clear and friendly communication prior and during dives.

Fig. 5.8.1 ROV QUEST setup for MSM109

QUEST System Description

The total QUEST system weighs about 45 tons (including the vehicle, control van, workshop van, electrical winch, 5,000 m umbilical, Launch and Recovery System, and transportation vans) and can be transported in four standard ISO 20ft containers. Using an electric storage winch to manage the 5,000 m of 17.6 mm NSW umbilical, no hydraulic connections are necessary to host the entire handling system. For installation on R/V MARIA S. MERIAN, the launch and recovery frame (LARS) has to be mounted on a traversal adapter structure in the A-Frame, providing mechanical mounts to host LARS and umbilical block. The ship's A-Frame hydraulic lift winch assembly is needed in addition.
The QUEST uses a Doppler velocity log (DVL, 1200 kHz) to perform Stationkeep, Displacement, and other auto control functions. The combination of 60-kW propulsion power with DVL-based auto control functions provides exceptional positioning capabilities at depth. Designed and operated as a free-flying vehicle, QUEST system exerts such precise control over the electric propulsion system that the vehicle could maintain relative positioning hold within decimeters.

Absolute GPS-based positioning is carried out using the shipboard Sonardyne Ranger USBL positioning system.
The QUEST control system provides transparent access to all RS-232, network data and video channels. The scientific data system used at MARUM feeds all ROV- and ship-based science and logging channels into a real-time database system (DSHIP-ROV), a version of the database software commonly used aboard the German research vessels.
During operation, data such as the navigation, CTD and high temperature data, sonar screen, and underwater video including two HDTV and one 3DHD feed are distributed to the vessel's conference room. The tiled pilot video screen was distributed to the ship's intranet. Due to the limited space in the control van, the ship's conference room was set up to allow scientists to take part in the dive with access to all images and data, including a QGIS client and acoustic intercom to communicate with the 2 scientists and pilots inside the control van.

Table 5.8.1 Overview data of ROV Dives MSM109

No.	Dive No.	Date	Site Lat	Site Lon	Depth max. (m)	Time Launch	Bottom hours	Total Dive hours
1	455	7/10/2022	77°24.816'N	007°20.620'E	3146	6:20	**2.68**	**8.20**
2	456	7/12/2022	77°24.816'N	007°20.620'E	3182	6:05	**5.37**	**10.37**
3	457	7/13/2022	76°49.724'N	007°20.816'E	3316	7:55	**6.77**	**11.23**
4	458	7/17/2022	77°26.449'N	007°42.430'E	3055	8:00	**5.13**	**10.10**
5	459	7/21/2022	79°24.616'N	003°22.178'E	2912	7:50	**3.77**	**8.33**
6	460	7/22/2022	77°26.534'N	007°42.584'E	3029	6:10	**7.20**	**11.90**
7	461	7/23/2022	77°26.450'N	007°43.474'E	3036	6:40	**6.63**	**11.50**
8	462	7/24/2022	77°26.364'N	007°42.315'E	3043	8:13	**4.90**	**9.70**
9	463	7/25/2022	77°26.349'N	007°42.350'E	3046	7:30	**5.77**	**10.50**
10	464	7/26/2022	77°26.356'N	007°42.789'E	3034	6:00	**4.45**	**9.38**
11	465	7/27/2022	77°26.361'N	007°42.638'E	3082	6:01	**7.75**	**12.15**
12	466	7/28/2022	77°49.666'N	007°42.437'E	3276	6:02	**4.82**	**10.57**
13	467	7/29/2022	78°49.666'N	008°42.437'E	3301	5:57	**4.07**	**9.07**
				Max. Dive depth (m):	**3316**		**69.30**	**133.00**

During MSM109, the following scientific equipment was used onboard MARUM ROV QUEST:

ROV based standard tools, installed on vehicle:

- 2 hydraulic manipulators for sampling and experiment handling
- 2 hydraulic drawers for probe and sample storage
- Tool skid center section setup for vertical mapping with cameras and lights
- ROV starboard-side basket frame for rock and fluid sampling
- high temperature probe "T-Lance" with logger and online data display
- various nets and shovels with T-handles

MSM109 specific payloads, installed on vehicle:

- MAPR autonomous sensor loggers
- KIPS fluid sampler (Fig. 5.8.2.)
- new developed ISMS *in situ* mass spectrometer (in-house development MARUM/MPI, first deployment)

New Developments Used During MSM109

- Zeus camera upgrade to 4k including new control panels in the control van
- new fluid sampler storage management system
- Enhanced 4k video tiling, overlay and distribution system, with integrated recording
- hydrophone electronics upgrade for lower distortion
- 3D Stereo HDTV camera
- inhouse 3D mapping software for enhanced on the fly 3D mapping
- first Telepresence video streaming and participation of land-based scientists and the general public in ROV dives at R/V MARIA S. MERIAN in low bandwidth mode

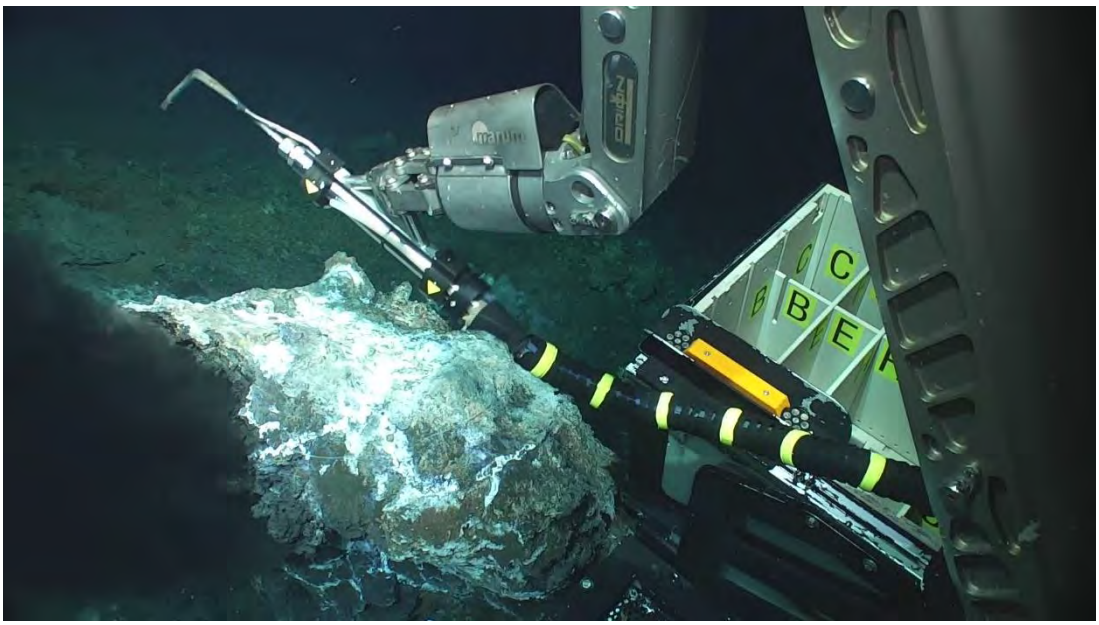

Fig. 5.8.2 New temperature fluid sampling management system

To enhance the video imaging capabilities of QUEST and to be prepared for high quality documentary filming tasks required during MSM109, a number of developments were undertaken and tested in Bremen prior to the cruise and were installed over the duration of the expedition onto the ROV. Among these the most important ones are the 4K Zeus camera rebuild, and the integration of our Sony still camera in a new housing with corrected optics, a 3D HTV stereo camera, as well as the integration of the recording into the video tiling system.

For safer and less time consuming fluid sampling, our high temperature probe and sampling nozzle was redesigned with an easier cable and hose management system. Allowing fast and easy grabbing and storing of the sampler with the ROV's ORION hydraulic arm.

Telepresence transmission of underwater video was tested during this cruise for the first time on R/V MARIA S. MERIAN. The setup relies on a stable C-Band internet connection and the possibilities of network routing and traffic shaping in the ship's intranet. During MSM109, we tested our setup with the standard ship's bandwidth of approx. 1,2 Mbs up and 5 Mbs downstream. With the limit of the 1,2 Mbs upstream, we were able to stream a stable video with 700 kbs and additional remote audio for on-shore scientist participation. Results show that the infrastructure aboard R/V MARIA S. MERIAN is capable of real-time telepresence application, yet higher bandwidth will be required for high quality transmission without affecting ship's regular internet connection in future.

5.8.2 Dive Reports

ROV Dive 455 (GeoB25004-1; Station MSM109/04-1)
Area: Southern tip of Brøgger Axial Volcanic Ridge (AVR)
Date: Sunday, July 10, 2022
Start bottom (UTC): 10:24
End bottom (UTC): 12:27
Bottom Time: 02:03
Start bottom (Lat/Long/Depth): 77°24.824'N/07°20.792'E/3076 m
End bottom (Lat/Long/Depth): 77°24.780'N/07°20.460/3073 m
Responsible scientist: Gerhard Bohrmann

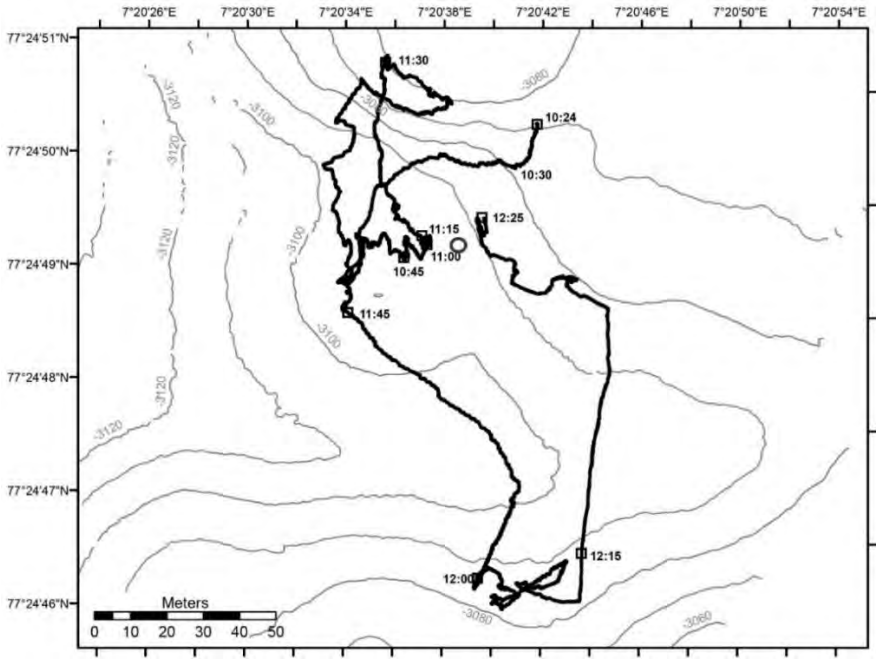

Fig. 5.8.3 Area of ROV Dive 455 at the southern tip of Axial volcanic ridge north and track of the seafloor observation.

Key Results

Basalt pillows were observed in mostly sediment covered areas. Stacked pillow layers along a steep cliff suggest the interpretation that isolated mounds were formed by very locally occurring volcanic activity, despite being mostly covered by sediment. Problems with the compass and the USBL navigation do not allow a good positioning of the observations.

Table 5.8.2 Samples during ROV dive 455

GeoB No	Instrument	UTC Start	Latitude Longitude	Depth m	Comment
25004-2	ORION manipulator	11:05	77°24.799'N 07°20.757'E	3125	Rock sample
25004-3	ORION manipulator	11:07	77°24.799'N 07°20.757'E	3125	Rock sample

Dive Description

The dive was planned at the southern tip of the Brøgger Axial Volcanic Ridge AVR because an Eh anomaly was measured during an AUV dive of the NPD expedition 2021. The dive started at 10:24 on sediment covered sea floor from which in some areas parts of volcanic rocks outcropped. The way of the ROV was taken to the Southwest uphill, and we climbed more than 50 m in height (Fig. 5.8.3) to reach the summit of the hill. On the top, we sampled two pieces of rock (Table 5.8.2). We moved to the north where we saw a steep wall composed of sheeted pillow basalts partly covered with sessile organisms. Steaming to the South brought us back to sediment covered sea floor. Navigation data documented that we moved at around noon to the south where again pillows were seen (Fig. 5.8.4 and 5.8.5). However, we doubt the accuracy of the navigation data and watch the position data with great caution. Unfortunately, the dive had to be cancelled after 2 hours due to technical problems with the ROV.

Fig. 5.8.4 Tubular pillow basalt with flow texture.

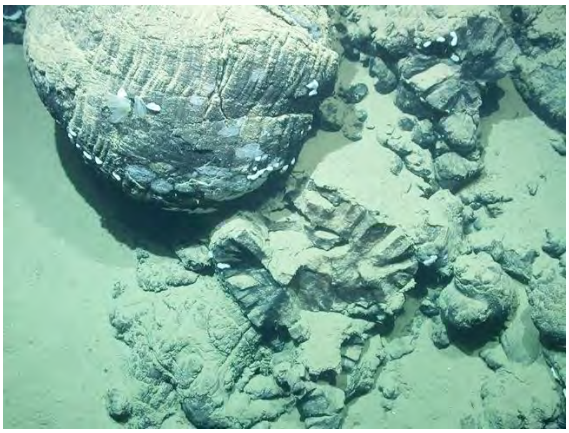

Fig. 5.8.5 Basalt pillows with typical shrinking cracks of the outer layer.

ROV Dive 456 (GeoB25007-1; Station MSM109/07-1)

Area: Southern tip of Brøgger Axial Volcanic Ridge (AVR)
Date: Tuesday, 12 July 2022
Start bottom (UTC): 08:55
End bottom (UTC): 13:58
Bottom Time: 05:03

Start bottom (Lat/Long/Depth): 77°24.818'N / 07°20.592'E / 3.136 m
End bottom (Lat/Long/Depth): 77°°24.967'N / 07°20.407'E / 3.138 m
Responsible scientist: Gerhard Bohrmann

Key Results

Observations from the dive before were confirmed. The volcanic rocks formed at the Brøgger AVR are intensively covered by sediments. The Eh-anomaly found by the NPD AUV-survey could be confirmed by seafloor observations.

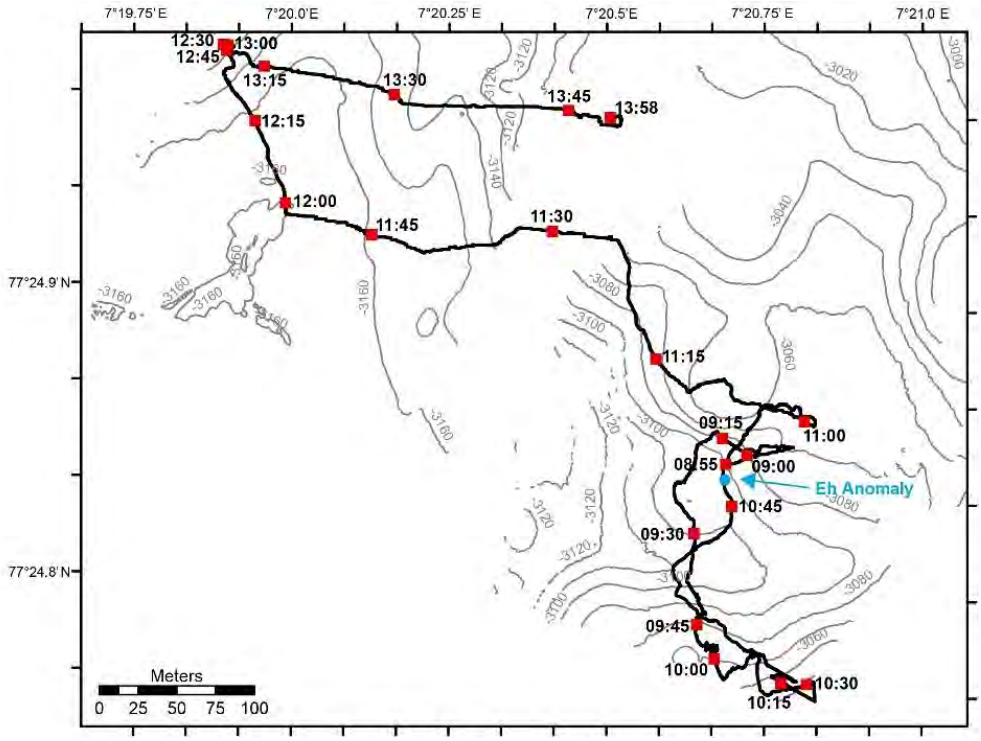

Fig. 5.8.6 Area of ROV Dive 456 at the southern tip of AVR north

Table 5.8.3 Sample taken during ROV dive 456

GeoB No	Instrument	UTC Start	Latitude Longitude	Depth m	Comment
25007-2	Scoop sample	12:55	77°24.974'N 07°19.841'E	3,108	Soft sediment

Dive Description

The dive started at 8:55 at the same launching position as dive 455 (Fig. 5.8.6). After surveying this place on a volcanic hill we explored the area south, first at a water depth of around 3,100 m and then to shallower depth up to 3,040 m where pillow lava was extensively available at the seafloor. Around 10:30 we moved back to the explored the area north and east of the launching position. Until 12:00 we moved to the West on a shallower plateau in 3,160 m water depth and then to the north. On the edge of the plateau, pillow basalts were more common and in the northwestern part we sampled unknown sediments with a scoop (Table5.8.3). The rest of the dive brought us to the East, for a longer time in sediment-covered areas and close to the end to a pillow lava field. The dive was aborted at 13:58 UTC.

ROV Dive 457 (GeoB25009-1; Station MSM109/09-1)
Area: High backscatter area north of Logachev AVR
Date: Wednesday, 13 July 2022
Start bottom (UTC): 10:00
End bottom (UTC): 16:49
Bottom Time: 06:49
Start bottom (Lat/Long/Depth): 76°49.243'N / 07°17.991'E / 3.126 m
End bottom (Lat/Long/Depth): 76°49.399'N / 07°19.854'E / 3.315 m
Responsible scientist: Gerhard Bohrmann

Key Results

During the dive a volcanic mound of 50 m high and 500 m in diameter was explored. Various types of lava (ropy, pillow, sheeted, a'a' lava) were recognized and sampled. Impressive fissures are shown on the AUV-map mainly striking in about NE/SW direction and are partly developed as canyons up to 10 m deep and 8-12 m broad. Sediment coverage is less than in other areas of the Knipovich Ridge which is well represented by high backscatter values of the AUV multi-beam data. At the bottom of one of the fractures, hydrothermal activity was proved by the presence of small sulfide chimneys and a color staining at the surface of some rocks. Recent hydrothermal activity could not be documented due to reduced maneuverability of the ROV.

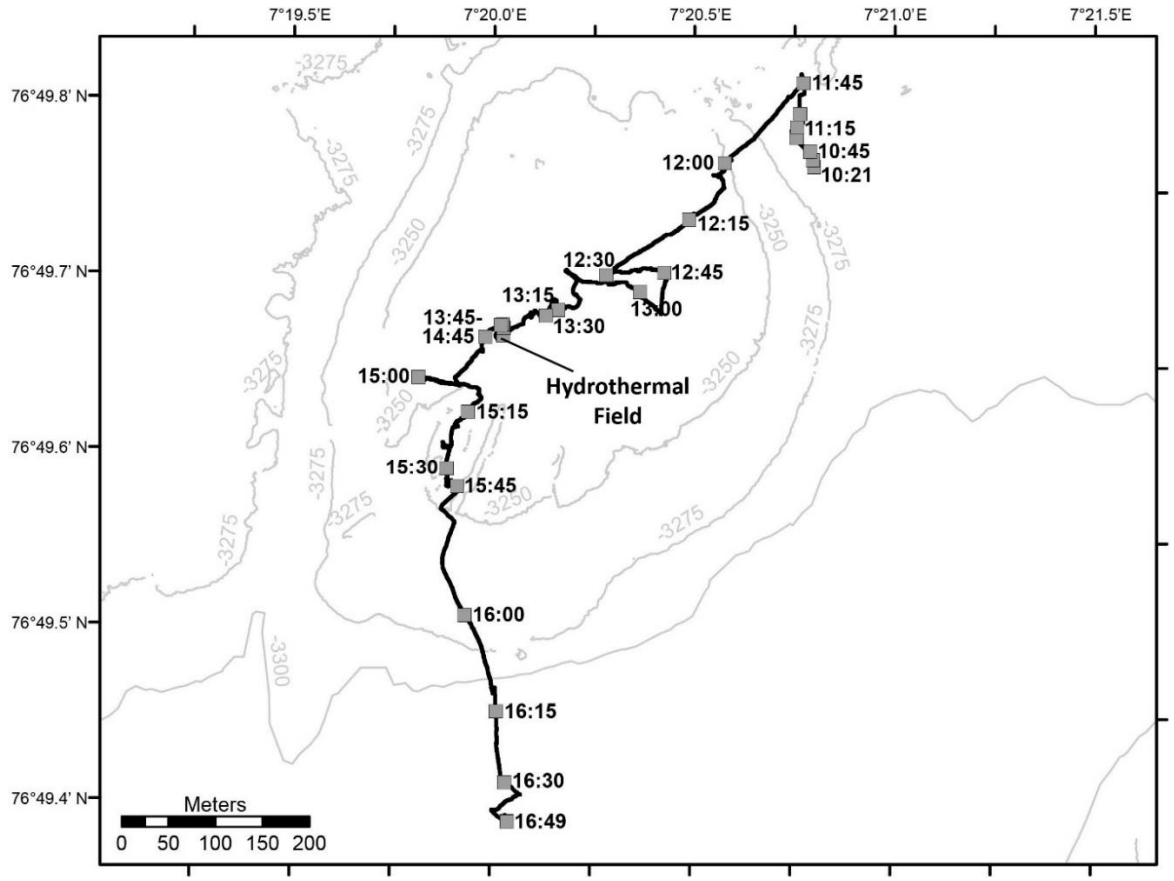

Fig.5.8.7 Area of ROV Dive 457 at in the high backscatter area

Table 5.8.4 Samples during ROV dive 457

GeoB No.	Instrument	UTC Start	Latitude Longitude	Depth m	Comment
25009-2	ORION manipulator	10:42	76°49.242'N 07°17.977'E	3.003	Ropy lava sample
25009-3	ORION manipulator	11:34	76°49.277'N 07°17.901'E	3.284	Layered rock
25009-4	ORION manipulator	13:24	76°49.166'N 7°17.27'E	3.252	A'a lava sample
25009-5	Net sample	14:32	76°49.649'N 07°19.977'E	3.261	Sulfide Chimney

Dive Description

Due to an electrical short circuit, numerous elements of the ROV could not be used. This mainly affected the mobility of the drawers and the Rigmaster arm. The ORION manipulator arm could be used for rock sampling. The seafloor observation started in 3,284m water depth at the NE rim of the volcanic mound (Fig. 5.8.7). The seabed was initially relatively flat and covered with sediment. A number of cracks in the seabed were observed, and ropy lava rocks increasingly appeared on the way to the north (Fig. 5.8.8). Two samples were taken, a ropy lava with a glassy rim and a layered volcanic rock that lay broken in several pieces on the seabed (Fig. 5.8.9). At approximately 11:45 UTC the ROV changed direction and headed southwest up the slope of the volcanic mound. At the beginning on the lower slope we often crossed screes of lava pieces and sheeted rocks, partly covered by thin sediment. More pillow fragments were found in the upper slope area. At around 12:00 UTC a first gaping fracture was encountered in stacked pillow basalts. The fracture cuts the pillows off sharply, and we saw vertical walls leading deep down.

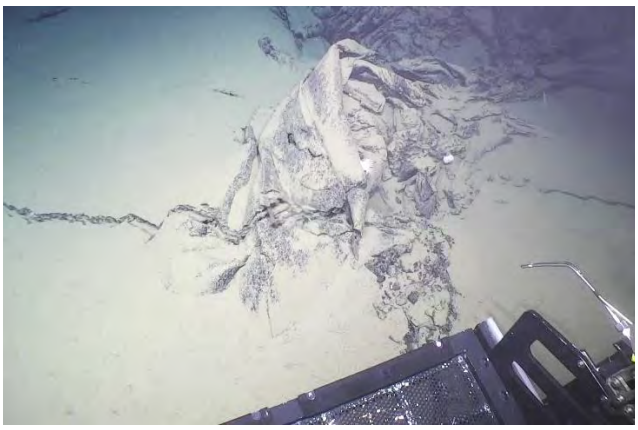

Fig. 5.8.8 Ropy lava pile on flat seafloor. A relative you crack is running from left to right and is cutting through the pile.

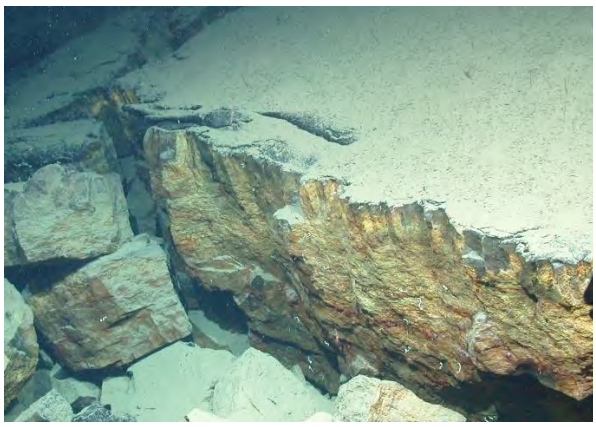

Fig. 5.8.9 Layered unknown volcanic rock with shrinking cracks at the surface and thin sediment cover.

On the way to southwest, on the top of the volcanic mound, we crossed several fissures and deep cracks (Figs. 5.8.10 and 5.8.11). Large areas of the flat summit appear to be covered or formed by pillow basalts with thin unconsolidated sediments often covering the pillows. As of approximately 12:30 UTC, ROV QUEST turns east for fifteen minutes and then turns south to cross another fissure running NW-SE. After that, we changed direction several times to cross numerous widened crevasses and canyons and generally followed the SW direction again from about 13:15 UTC. In this area of the hill, massive deposits of very rough volcanic components have been found which

can be attributed to a formerly gas-rich lava. A sample that we took with the manipulator at 13:24 UTC clearly showed that it can be described as a'a' lava (Table 5.8.4).

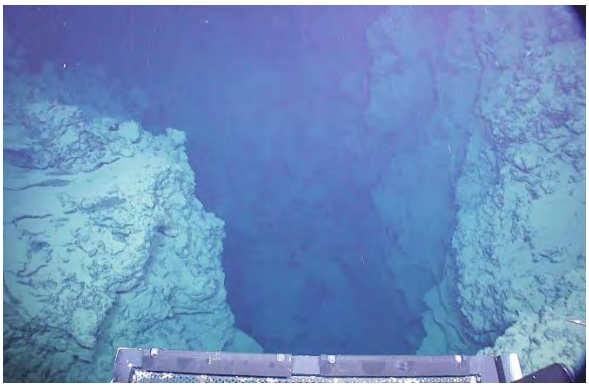

Fig. 5.8.10 Tectonic open crevasse with steep flanks on both sides.

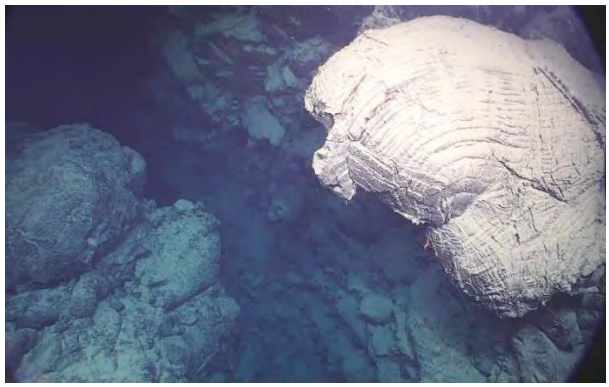

Fig. 5.8.11 Deep fissure in a thick sequence of pillow lavas.

At around 13:35 UTC we dove with ROV QUEST in one of the fissures that went down about 8-10 m deep. A yellowish staining in one spot in the wall made us curious, and we dove down to the bottom where a branching chimney was seen (Fig. 5.8.12). This spot we explored in the following minutes (13:44 UTC) and found several small dark smokers, but they were not releasing any smoke at the time. In addition to the smokers, an orange staining in some areas of the seafloor gave indications that it is a hydrothermal field. We could not determine how active this field is at the moment, since both the temperature sensor and the fluid sampler could not be used on this dive. With the ORION manipulator arm, the pilots tried to recover one of the chimneys (Fig. 5.8.13), which was then successful with a net (14:18 UTC). An inspection of the sample onboard showed that it was a sulfide smoker.

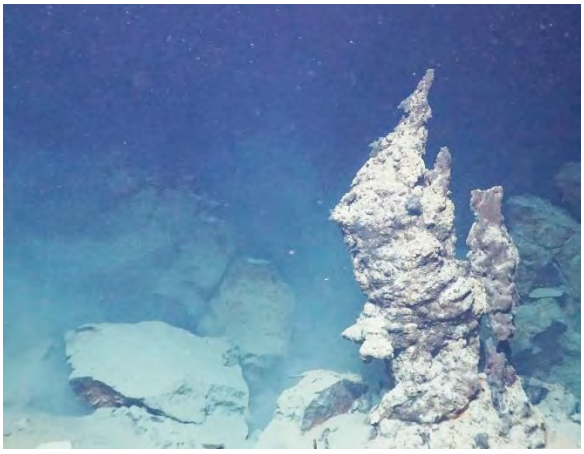

Fig. 5.8.12 Irregular chimney with sediment cover on the bottom of a deep canyon-like fracture.

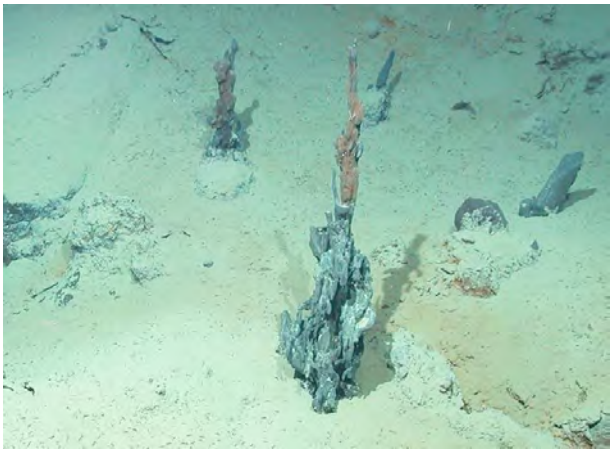

Fig. 5.8.13 Sulfide chimney with several branches, which was sampled during ROV dive 457. Smaller chimneys in the neighborhood.

After emerging from this narrow submarine canyon, we continued our way southwest. The path led again over numerous pillow lavas, which alternated with mixed scree from different volcanic fragments. Several times we crossed crevasses again as well as open fissures without exploring

the ground of the canyons. We followed now southwards along the southern slope of the hill. Large-scale pillow basalts were found on the lower slope of the mound, slightly more heavily covered with sediment but still showing the shape of the pillows.

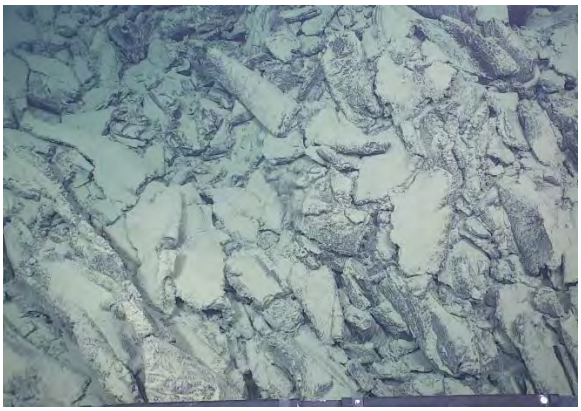

Fig. 5.8.14 Debris of ropy lava clasts with thin sediment cover.

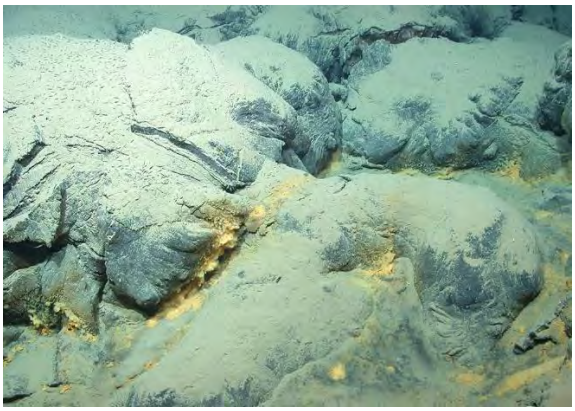

Fig. 5.8.15 Lobate lava flows with yellow staining and microbial filaments on the edges indicating most probably low-temperature hydrothermal activity.

From 16:09 UTC the pillow basalts were replaced by ropy lava flows, some of which showed smooth surfaces, some of which contained screes of volcanic fragments (Fig. 5.8.14). Moving further south, these lavas were replaced by pillow basalts at around 16:22 UTC. Orange staining was observed in numerous places on the lower edges of the pillows, which, on closer inspection, showed that they were filaments of microbes that moved with the movements of the surrounding water (Fig. 5.8.15). A few flakes swam in front of the ROV cameras. After another trip to the South, which showed rocks on the bottom, which were also encountered at the beginning of the dive, the dive was terminated at 16:49 UTC on the seabed.

ROV Dive 458 (GeoB25016-1; Station MSM109/16-1)
Area: Jøtul hydrothermal field
Date: Sunday, 17 July 2022
Start bottom (UTC): 10:59
End bottom (UTC): 15:59
Bottom Time: 05:00
Start bottom (Lat/Long/Depth): 77°26.449'N / 07°42.434'E / 3053 m
End bottom (Lat/Long/Depth): 77°26.424'N / 7°43.386'E / 2952 m
Responsible scientist: Stig-Morten Knutsen

Key Results
The dive investigated the flank of the central graben of the Knipovich Ridge. The location is to the East of an axial volcanic ridge (AVR) and in an area with several observations of increased Eh- and methane readings from CTD measurements. Several elongated bathymetric features, potentially representing fractures or faults, mainly N-S trending, combined with seabed morphology possibly indicating mass-movements, are characteristic for the area. The dive covered an area of about 800 – 1000 meters in an overall shallowing trend, transecting non-active faults or

fractures as observed from the bathymetry. Areas of pillow- and fractured lava-flows were observed with several observations of white staining and apparent bacterial activity, interpreted to represent hydrothermal activity. No change of temperature was however associated with these patches of apparent hydrothermal activity, maybe indicating that the activity is not continuous but perhaps happens in pulses. Registration of Eh during the ROV gave increased measures (anomalies) mainly in the lower part of the dive transect (shown in yellow at the map below). The reason for the distribution of Eh-registrations are uncertain, but one hypothesis is that it is associated with increased fault / fracture activity in the lower part of the dive, and that these fractures might be conduits for (some) hydrothermal activity.

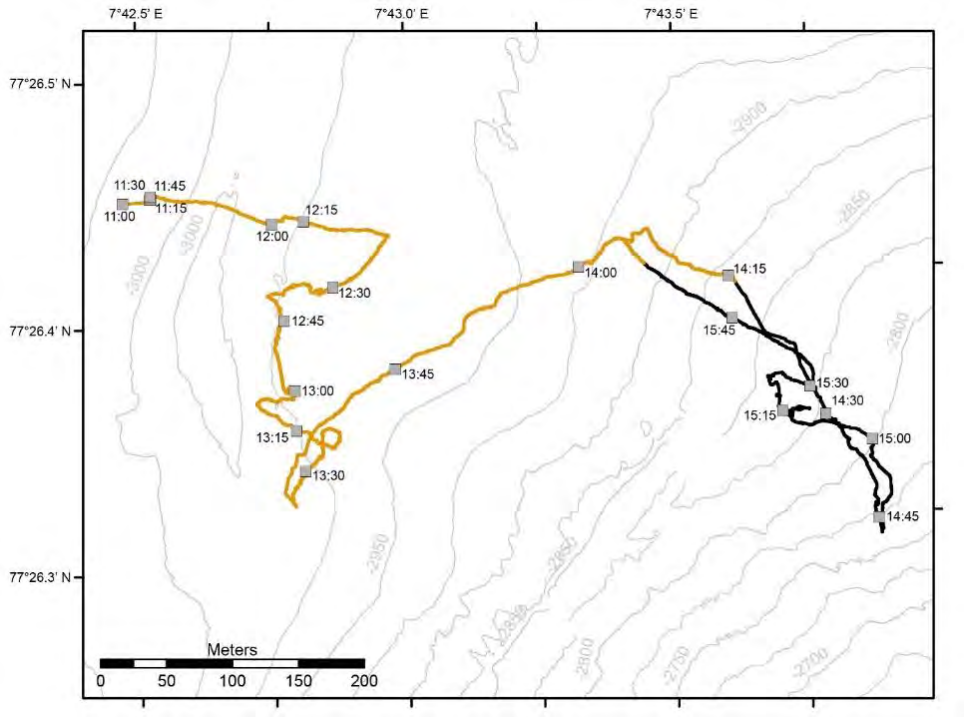

Fig. 5.8.16 Area of ROV Dive 458 – showing transect of dive with time in black and yellow, where yellow indicate areas of Eh-anomalies.

Table 5.8.5 Samples during ROV dive 458

GeoB No	Instrument	UTC Start	Latitude Longitude	Depth m	Comment
25016-2	ORION manipulator	11:29	77°26.450'N 07°42.484'E	3046	Rock + whitish precipitate
25016-3	ORION manipulator	11:45	77°26.450'N 07°42.484'E	3047	Whitish precipitate

Dive Description

Seabottom was dominated by fine-grained pelagic (hemipelagic) material and local black clasts. Observed pillow lavas with white staining and what appeared to be bacterial activity (Figure 2). Acquired sample with the ORION manipulator arm of black pillow lava with a thin, up to approximately 0.5 cm coverage, of white material of unknown origin. The sample also showed clear indication of biological activity in the form of what could be small sponges but will need to be classified with more certainty.

Fig. 5.8.17 Pillow lava on mainly flat seafloor. White areas / staining with associated bacterial activity observed on the base (central-right) part of the picture.

Fig. 5.8.18 Applying the temperature probe on the ROV did not measure any changes associated with the white patches / staining.

Moved eastwards and observed more white staining on lava, both pillow-lava and more fractured fragments on otherwise sediment-covered seabed. The white staining appears to occur mainly on the bottom side of the deposits. Attempted to take another sample of the white substance but this being very soft, it mainly fell apart and got dissolved in the ORION manipulator arm. Did however manage to get some back to sample box. The substance became harder when dried, and further analysis is needed to decide composition and possible origin.
By applying the temperature probe on the ROV, the patches of white staining and adjacent bacterial activity did not seem to be associated with any changes in temperature (Fig. 5.8.18).

Continued moving eastward. At about 11:56 UTC the ROV crossed fractures (faults?) several meters wide and up to more than 10 meters deep. Apparently, these are oriented in an N-S-direction and are observable also on the bathymetric maps. The presence of sediments draping the flanks and the fractures themselves, suggest that these are not currently highly active. Flanks of fractures are made of black blocks and occasional pillows, all suggesting a volcanic origin of the structures.
The topography and environment outside the fractures are dominated by fine-grained pelagic (hemipelagic) material. The sediments are mainly unconsolidated, but with local indications of stratification and layering.
After about 200 meters, at 12:24 UTC, the ROV moved more to the South for about 200 meters, approximately at the 2,975-meter contour – at or close to a fracture / fault which, when crossing over, has a relief (depth) of more than 10 meters.
No major observations of hydrothermal activity were observed, and the topographic and sedimentary environment continued very much as described above: occasional pillow-lava and fragments / fractured blocks of lava generally with a thin carpet of sediment drape, and with occasional indications of white material along smaller fractured patters / pillows (Fig. 5.8.19).

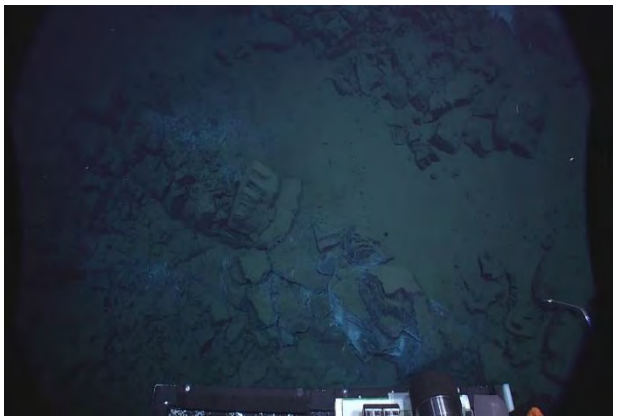

Fig. 5.8.19 Fractured and broken pillow lavas with indications of white staining, possibly associated with hydrothermal activity.

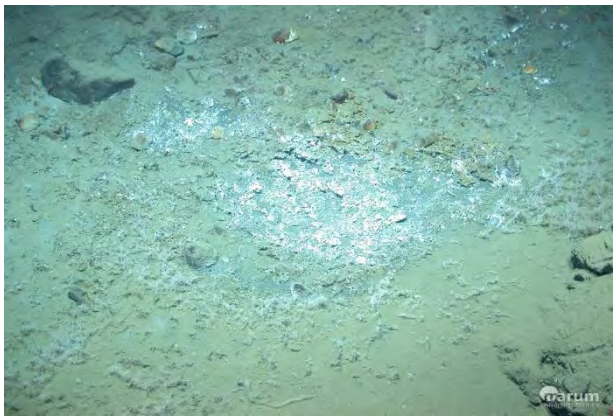

Fig. 5.8.20 Occasional observations of white, possible bacterial matter, on areas with less sediment coverage on the seafloor.

Locally and apparently at the flanks or minor "high" associated with this fracture / fault, indications of white material and assumed biological activity were observed on the seabed (Fig. 5.8.20). These "patches" of white staining and biological activity seemed to occur where there for some reason (currents?) were less sediments, and harder substrate (but not necessarily pillows) on the seafloor.

After following the fracture until about 13:37 UTC, the ROV moved in an N-E-direction for about 400 meters and shallowing to about 2,900 meters. No major topographic features observed. Seabed dominated by fine grained sediments with just occasional fragments of lava – both as blocks and pillows.
From about 14:04 UTC the ROV direction shifted more to the SE/E moving to still shallower parts of the seabed in an E/NE-direction. For this part of the dive, the seabed environment was very much as described above: non-consolidated fine-grained sediments with occasional volcanic clast / pillow lava.
From the bathymetric maps some elongated mainly E/SE to W/NW-oriented features can be observed. From ROV-observations these appear mainly as ridges, dominated by the same type of seafloor environment as described above. Along with these larger elongated features, some fractures or faults oriented more SW-NE and dipping to SW can be observed as "walls or ridges" made-up of broken-up lava and pillow-lavas.

Trying to further investigate the E/SE to W/NW-features, the ROV at 14:48 UTC shifted to a N/NW-direction. However, still no significant changes of sedimentary, structural or topographic environments were observed. The dive was aborted approximately at 16:00 UTC.
During the dive Eh was registered (Fig. 5.8.16), and several changes / (small) anomalies were observed. By plotting the location of these Eh registrations (anomalies) on the ROV-track, it appears that the Eh-response is present in the westernmost (deepest) part of the ROV-dive area (Fig. 5.8.16). It is however not easy to determine if there are increased Eh associated with the fractures / faults, or if this western area of the dive in general has an increased "background" Eh-response.

ROV Dive 459 (GeoB25022-1; Station MSM109/22-1)
Area: Depression on the central Molløy Ridge
Date: Thursday, 21 July 2022
Start bottom (UTC): 10:25
End bottom (UTC): 13:58
Bottom Time: 03:33
Start bottom (Lat/Long/Depth): 79°24.630' N / 3°22.205' E / 2891 m
End bottom (Lat/Long/Depth): 79°25.084' N / 3°24.694' E / 2842 m
Responsible scientist: Katharina Streuff

Key Results

The central parts of the Molløy Ridge are covered by a thick layer of homogeneous, likely fine-grained sediments with very few scattered rock fragments. The latter were probably transported down-hill into a depression showing striations thought to be characteristic of detachment faults. Due to an accumulation of unfortunate circumstances, the dive was aborted prematurely.

Dive Description

The purpose of the dive was to investigate the northern flank of the central parts of the Molløy Ridge in a water depth between 2,875 and ~2,375 m. The Molløy Ridge is orientated in a general NE-SW direction and is roughly 56 km long and 17.5 km wide. It has a unique morphology with its highest point on top of a large and round dome-shaped feature with a hummocky surface (Fig. 5.8.21), that flattens on both ends. Northeast of the dome, the ridge shows an approximately 4 km-wide and 300 m-deep depression characterised by numerous SE-NW-trending "striations" (Fig. 5.8.21), thought to be implicating a detachment fault. ROV dive 459 was intended to follow an approximately 4 km-long transect from the deepest part of the depression back to the ridge top to investigate the nature of these striations and associated seafloor material. Unfortunately, however, strong bottom currents and problems with the cable orientation caused the ROV QUEST to proceed extremely slowly along the transect. During its total bottom time of approximately three and a half hours, the ROV QUEST managed to cover only a fraction of the profile, which showed a smooth and even seafloor thickly covered with fine-grained, homogeneous sediments with no notable characteristics. Very few scattered rocks were observed, which likely were transported down-slope into the depression. Total bottom time was interrupted by a period of nearly one hour between 12:29 and 13:23, during which the ROV QUEST ascended to a depth of ~2,820m in order to gain some speed and move further along to the next planned waypoint. Upon re-descent the integrated cameras showed no changes in the composition and nature of the seafloor, which, alongside problems with the correct navigation, as well as with the wire, eventually lead to the decision to abort the dive prematurely.

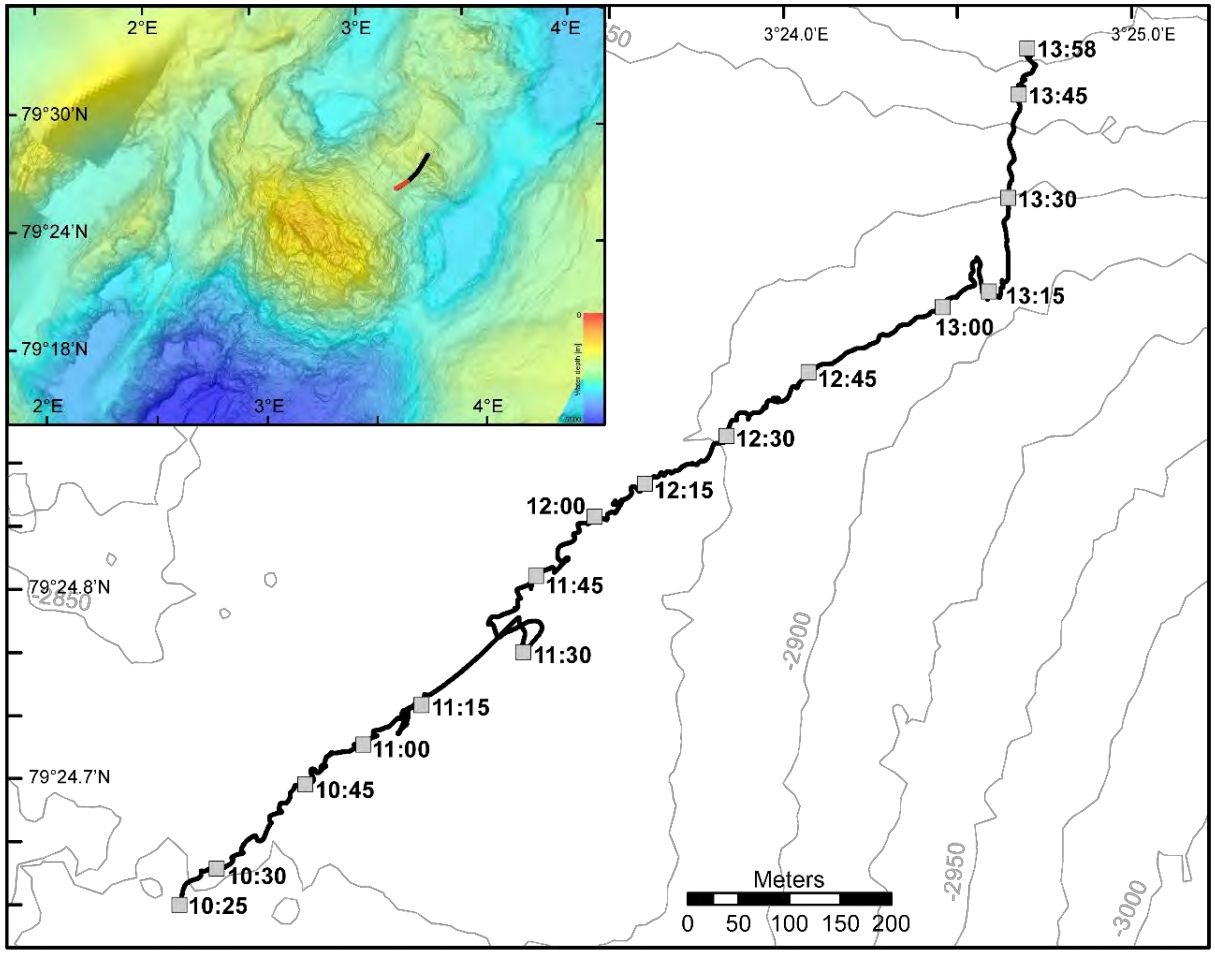

Fig. 5.8.21 Area of ROV Dive 459 at Molløy Ridge. A) Overview map of the Molløy Ridge and the investigated depression. The planned transect is indicated in black, the real track in red. B) Map of the ROV's actual track during the dive with quarter-hourly timestamps.

ROV Dive 460 (GeoB25023-1; Station MSM109/23-1)
Area: Jøtul hydrothermal field
Date: Friday, July 22, 2022
Start bottom (UTC): 08:47
End bottom (UTC): 15:48
Bottom Time: 07:01
Start bottom (Lat/Long/Depth): 77°26.512' N, 7°42.622' E, 3024 m
End bottom (Lat/Long/Depth): 77°26.455' N, 7°44.966' E, 2762 m
Responsible scientist: Katharina Streuff

Key Results

The seafloor in the plain and its adjacent slide complex at the eastern flank of the Knipovich graben are characterized by a mostly smooth appearance imparted by the presence of a thick and widespread cover of fine-grained sediments, rock fragments and clasts, as well as some foraminifera. Occasional rock outcrops reflect pillow basalts and potentially tuffites, both likely of relatively old age. Scattered bacterial mats as well as widespread Eh- and temperature anomalies

in the area are indicative of diffuse fluid seepage from the seabed, but focused outflow could not be localized.

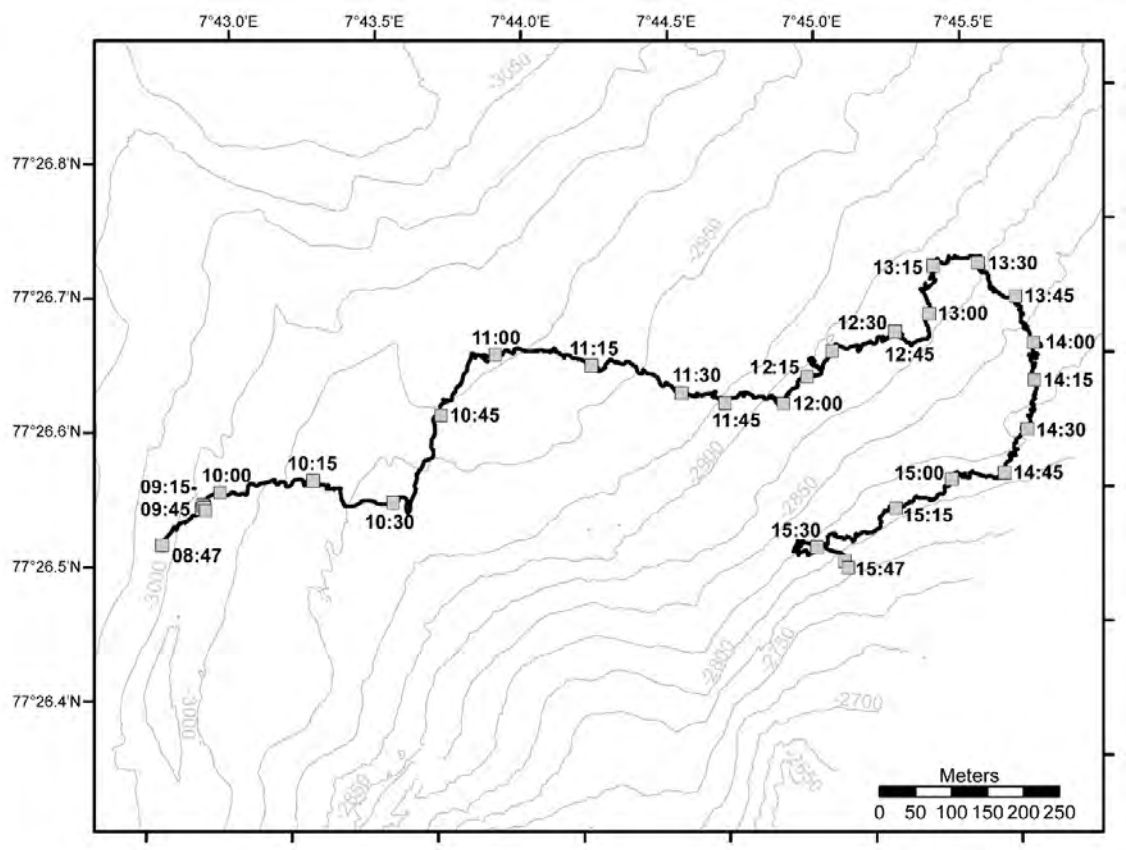

Fig. 5.8.22 Map of ROV Dive track 460 and the investigated terrain.

Table 5.8.6 Samples recovered during ROV dive 460

GeoB No	Instrument	UTC Start	Latitude Longitude	Depth m	Comment
25023-2	KIPS A	09:41	77°26.539' N 7°42.778' E	3012 m	Water sample at the bacterial mat

Dive Description

ROV QUEST dive 460 was intended to investigate a bathymetric plain as part of a slide complex along the eastern flank of the Knipovich graben. Numerous CTD deployments, as well as an AUV dive had revealed several Eh- and temperature anomalies in the area, and the hope was that dive 460 would uncover the source of these anomalies. The dive started at a water depth of 3,024m and moved in a general eastward direction across the plain and then up the flank of the slide complex (Fig. 5.8.22). For the majority of the time the seafloor was composed of mud with variable amounts of rock fragments and foraminifera. In several areas the seafloor seemed relatively homogeneous, flat and smooth, with only rare clasts and rock fragments. On occasion, pillow basalts appeared on the seafloor, where they manifested as mounds and pillar-like structures, often in association with some white staining (Fig. 5.8.23). A white color at the base of individual pillow structures was, in fact, quite common, with the intensity of the staining diminishing towards the top of the rocks, thought to indicate fluid seepage from the seafloor. Individual rocks were completely white and inhabited by limpets (Fig. 5.8.23) and possibly reflect precipitates of gypsum or anhydrite.

Occasional areas reminiscent of bacterial mats also seemed to indicate widespread diffuse seepage from the seabed, which was further confirmed by methane concentrations as high as 360 nmol measured in a KIPS sample taken from one of these bacterial mats. Nevertheless, more focused outflow of hydrothermal fluids in the form of shimmering water and/or chimney structures could not be localised.

Peculiarities observed throughout the dive were on one hand a large number of sponges settling on much of the harder substrate, and on the other hand some "outcrops" and pillars of a breccia-like rock (Fig. 5.8.23). Although the origin of these rocks could not be determined, it is possible that they reflect tuffs or tuffites related to the magmatic activity at the slow-spreading Knipovich ridge.

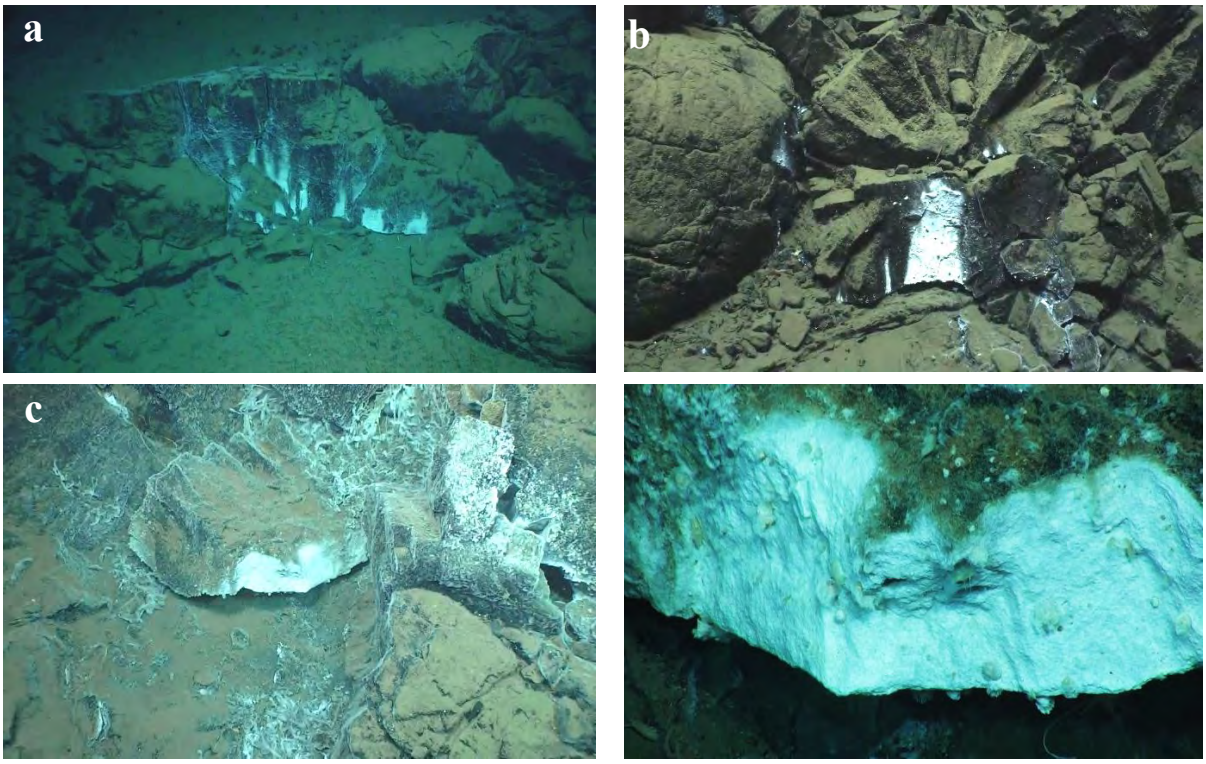

Fig. 5.8.23 Examples of observations made during ROV QUEST dive 460. A), B) White staining at the base and center of pillow basalts. C), D) example of white rocks observed in some areas of the slide complex, which could represent precipitates of gypsum or anhydrite.

ROV Dive 461 (GeoB25024-1; Station MSM109/24-1)

Area: Jøtul hydrothermal field
Date: Saturday, July 23, 2022
Start bottom (UTC): 09:21
End bottom (UTC): 15:50
Bottom Time: 06:09
Start bottom (Lat/Long/Depth): 77°26.453'N / 7°42.504'E / 3022 m
End bottom (Lat/Long/Depth): 77°26.380'N / 7°42.291'E / 3034 m
Responsible scientist: Gerhard Bohrmann

Key Results

The dive was planned following ROV QUEST dives 458 and 460 at the lower slope of the eastern end where a shimmering water vent site of 8°C and other indications of diffusive venting of the Jøtul hydrothermal field were explored (Fig. 5.8.24).

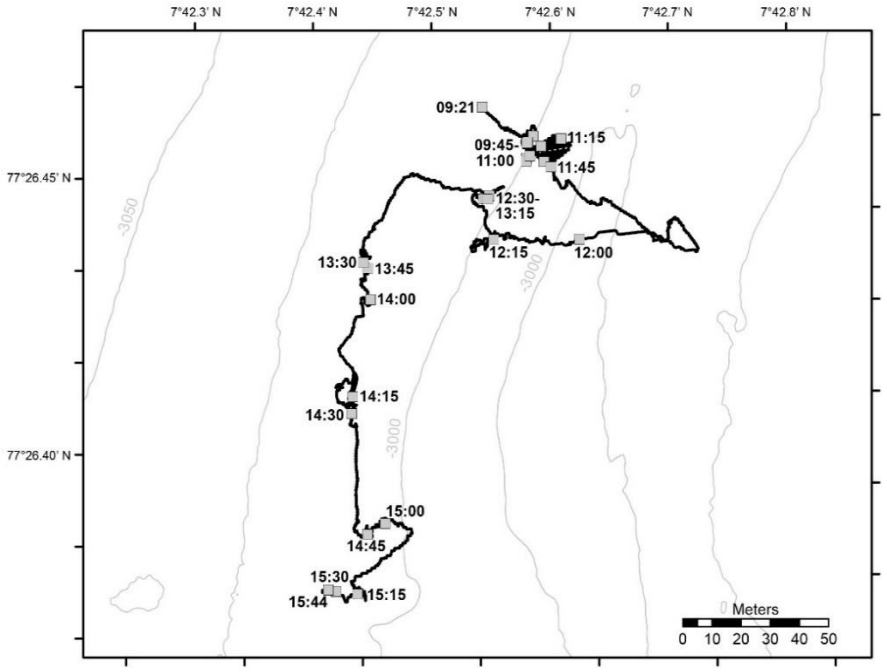

Fig. 5.8.24 Area of ROV Dive 461 at the southern tip of Axial volcanic ridge north and track of the seafloor observation.

Table 5.8.7 Samples during ROV dive 461

GeoB No	Instrument	UTC Start	Latitude Longitude	Depth m	Comment
25024-2	KIPS	09:45	77°26.444'N 07°42.537'E	3016	Bottle A
25024-3	MAN	10:30	77°26.444'N 07°42.537'E	3016	Hot vent rock
25024-4	MAN	10:46	77°26.446'N 07°42.534'E	3015	Hot vent rock
25024-5	KIPS	12:31	77°26.447'N 07°42.538'E	3017	Bottle B
25024-6	NET green	12:55	77°26.447'N 07°42.539'E	3018	Dark spot material
25024-7	NET blue	13:11	77°26.448'N 07°42.545'E	3017	Feeder material
25024-8	MAN	13:48	77°26.442'N 07°42.437'E	3033	Yellow small rock
25024-9	MAN	13:52	77°26.442'N 07°42.436'E	3033	Rock sample
25024-10	MAN	14:13	77°26.410'N 07°42.378'E	3034	Precipitates
25024-11	MAN	14:57	77°26.392'N 07°42.346'E	3031	Precipitates
25024-12	MAN	15:25	77°26.379'N 07°42.316'E	3030	Chimney wall
25024-13	KIPS	15:39	77°26.380'N 07°42.291'E	3034	Bottle C

Dive Description

The dive started on 9:21 UTC at the seafloor, and it was planned to investigate the distribution of hydrothermal venting of the Jøtul hydrothermal field. On the way to the Southeast, diffusive venting appeared at 11:22 when a patch of Siboglinid tubeworms appeared which are accompanied by bacterial filaments. During exploring this venting area, we saw that a larger vent field with pillow basalts followed in eastwards direction. In a fracture of the rocks which are completely stained by white material (Figures. 5.8.25 and 5.8.26) we recognized shimmering water and took KIPS samples A and B and rock samples (Table 5.8.7). Camera focusing of the rocks showed many small gastropods flocculate bacterial mass in the open fracture. The whole area was scanned by 8 tracks 10 m long for producing a detailed photo mosaic.

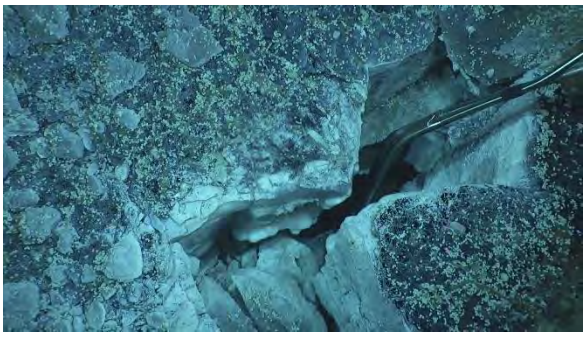

Fig. 5.8.25 Shimmering water outflow of 8°C, sampled by the KIPS A and B bottle

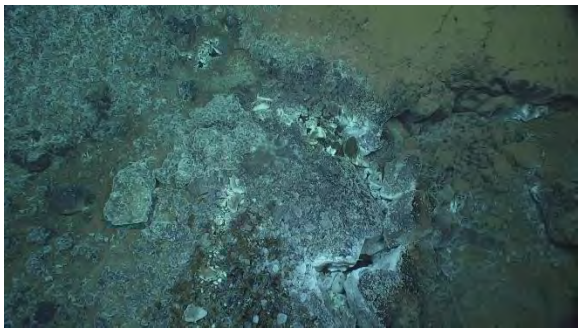

Fig. 5.8.26 Overview look of the shimmering water outflow.

We then moved further to the east (Fig. map) and realized that pillow lavas appeared and we reached a fracture several meter deep, with talus at the bottom of the fracture. We changed again the direction and moved to the West where white patches of bacterial mats were seen between the rocks and later on above the sediment surface. At 12:20 UTC we reached a dark spot surrounded by Siboglinid tubeworms and bacterial filaments and took a temperature probe and two net samples, one from the dark spot with a lot of elongate fecal material and from the white area in the surroundings.

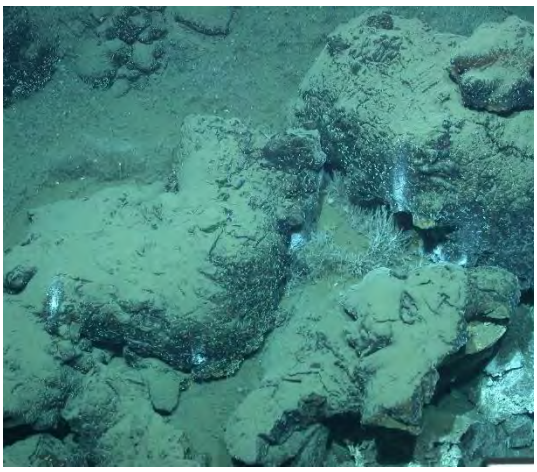

Fig. 5.8.27 Rocks of pillow basalt with tubeworms and white patches of bacterial mats.

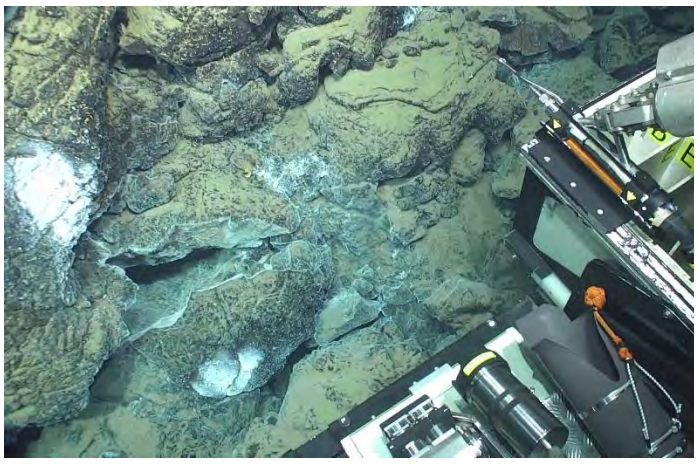

Fig. 5.8.28 Preparation for a temperature measurement at a vent location.

During take the sampling from the dark spot a lot of very dark (H_2S-rich) anoxic sediment material was suspended. On the way to the South we again reached pillow basalts west of a steep slope, which showed white patches of bacterial filaments (Figures. 35.8.27 and 5.8.28). In one open fracture, we measured a small increase of temperature of about 1°C, and we took a rock sample at 13:48.

On the way south, other precipitates were sampled at 14:13 and 14:57 in an area where many indications for diffusive venting occurs. At 15:11 a single extinct chimney was found and sampled, which broke down in several pieces during the sampling. The pieces showed two empty tubes surrounded by white precipitate which is most likely anhydrate or gypsum. Close by we found an opening in an area of unknown precipitates and took a temperature probe and a KIPS sample at 15:39. The dive ended after 6 hours and 9 minutes at 15:50.

Fig. 5.8.29 Single chimney from an extinct hydrothermal vent.

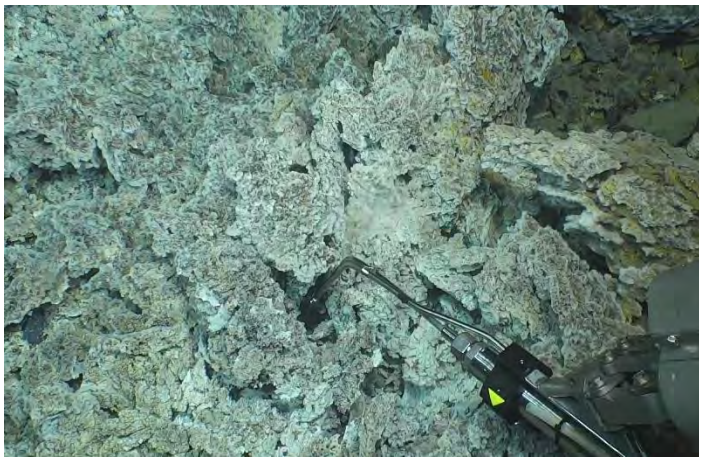

Fig. 5.8.30 Temperature measurement at an unknown precipitate.

ROV Dive 462 (GeoB25026-1; Station MSM109/26-1)
Area: Jøtul hydrothermal field
Date: Sunday, 24 July 2022
Start bottom (UTC): 10:51
End bottom (UTC): 15:46
Bottom Time: 04:55
Start bottom (Lat/Long/Depth): 77°26.368 N / 7°42.326 E / 3023m
End bottom (Lat/Long/Depth): 77°26.135 N / 7°43.312 E / 2739m
Responsible scientist: Stig-Morten Knutsen

Key Results

The dive investigated the flank of the central graben of the Knipovich Ridge (Fig. 5.8.31). The location is to the East of an axial volcanic ridge (AVR) and in an area with several observations of increased Eh and methane readings from CTD measurements. In orientation it covered an area of approximately 200 meters in a NW direction before shifting to an overall S/SE direction for approximately 500 meters. In depths it ranged from about 3,023m to 2,739m, becoming steeper

the more E we got. The occurrence of staining might appear to be a bit less, the further south and southeast the dive / observations moved. However, a large scar-like feature at seabed, and assumed rocks related to mass-movements just below what could be a vent hole for hydrothermal activity (at about 2,835m) might indicate that pressurized (high temperature) water could escape to the seabed also in the area covered by this dive.

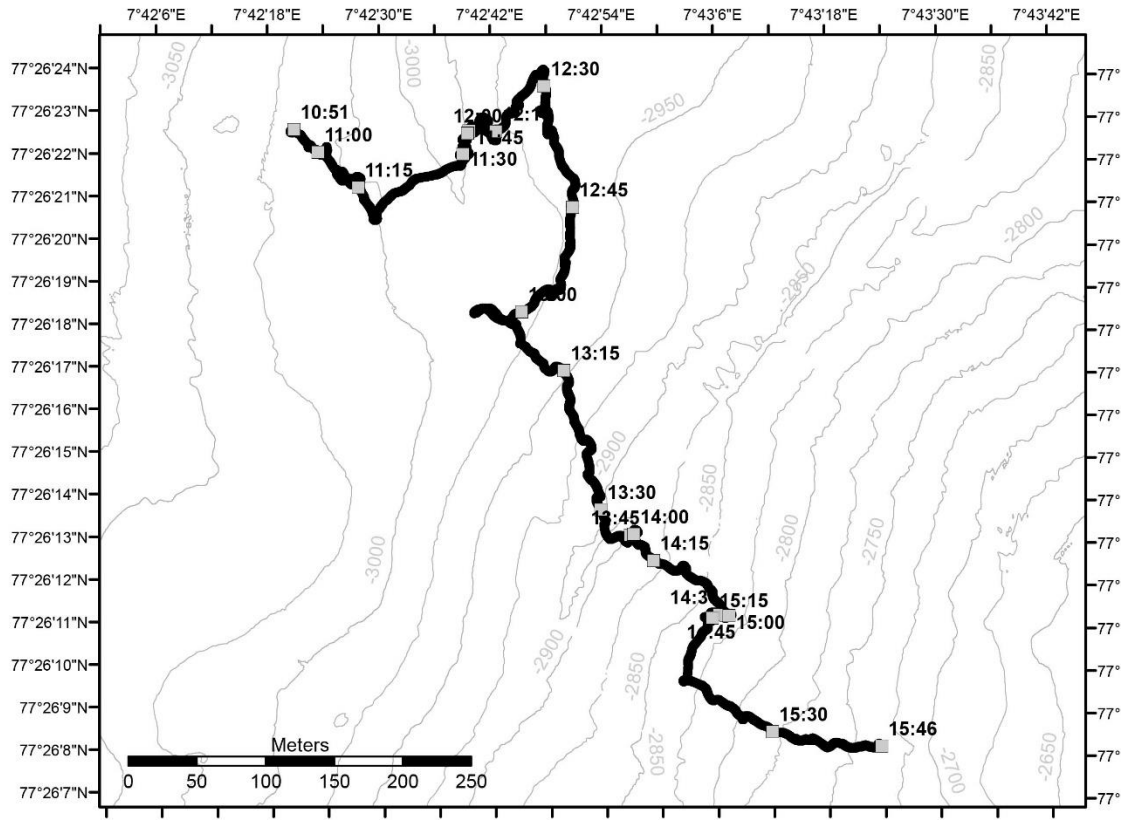

Fig. 5.8.31 Area of ROV Dive 462.

Table 5.8.8 Samples during ROV dive 462 No

GeoB No	Instrument	UTC Start	Latitude Longitude	Depth m	Comment
25026-2	ORION manipulator	13:38	77°26.199 N 7°42.850 E	2907	Rock – brittle/ porous(?) grey with yellow and white staining
25026-3	ORION manipulator	13:51	77°26.200 N 7°42.869 E	2899	Rock – solid (basalt?) with yellow and white staining
25026-4	ORION manipulator	14:07	77°26.000 N 7°42.866 E	2899	Rock- black with glassy surface on one side – yellow staining
25026-5	ORION manipulator	14:39	77°26.169 N 7°43.003 E	2846	Rock – brittle with yellow (brown) and white staining
25026-6	Scoop	14:55	77°26.171 N 7°43.026 E	2839	Sediment – black (clay?) strong sulfur odor
25026-7	Net	15:08	77°26.172 N 7°43.029 E	2837	As above – but slightly less sulfur odor
25026-8	ORION manipulator	15:44	77°26.135 N 7°43.312 E	2739	Large black rock, massive (basalt?) with biological growth

Dive Description

Sea-bottom was smooth and dominated by fine-grained pelagic (hemipelagic) material and local black clasts. Observed white patches of assumed foraminifera and bacterial activity. Moved towards the SE slightly shallowing. More clast turning into areas of rubble (mass deposits), combined with pillow lavas. Moving up a hill or mound approximately 10 meters high, larger boulders on top. Moving further to the SE, seabed becoming smoother with more sediments.
At 11:22 UTC changing direction towards NE. At 11:30 UTC observing large black, assumed basalt rock with clear white staining, limpets, and adjacent bacterial mat / matter on the seabed. Tried to measure temperature, which showed possible slight increase from surroundings of -0.6 and measuring 0.95ºC. (Fig. 5.8.32a and b).

Fig. 5.832a Black assumed basalt rock / lava flow with white staining coming from the base. Occurrences of lighter areas on seafloor in front assumed to represent bacterial mat / matter.

Fig. 5.8.32b Pillow lava with pronounced white colorations / staining. Also note possible “holes” in the lower front part of the lava.

Continued moving to the NE, observing more large, well-defined pillow outcrops with widespread white colorations / staining (Fig.3). Moving further NE to shallower water-depths, the pillow-lava continues, but less white staining is observed.

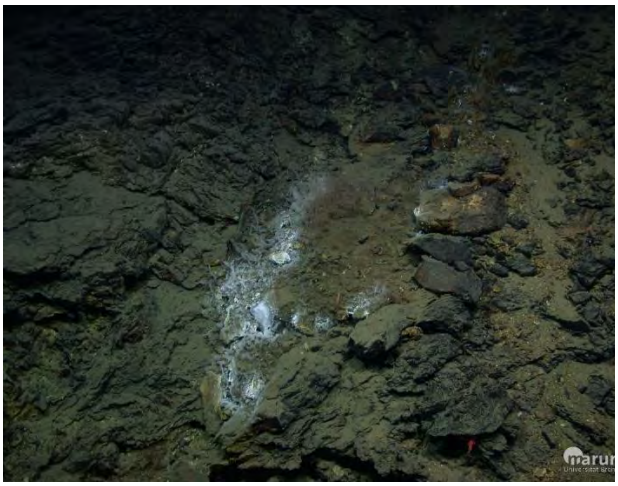

Fig. 5.8.33 Broken-up or fragmented mainly black to gray rocks with white staining patches of yellow color.

Fig. 5.8.34 Rock field covered with fine-grained sediments. Note possible bone in the center of picture, to the left of rock with clear white staining.

At 12:32 UTC change direction and start moving towards the S. Seabed covered with fine grained sediments and very few rocks. Continued moving in same direction, with same seabed conditions. At about 13:03 UTC shifted direction to more SE and "climbing" more upwards steeper gradient of the seafloor. At about 2925m depth more rocks and pillow-lavas emerge along the dipping seabed. Areas of white bacterial (?) mats on seafloor and more frequent occurrences of white staining on the otherwise black rocks.
Continuing S/SE, observing more black rock outcrops – fragmented and broken up. Areas of white precipitation and with white / yellow staining (Fig. 5.8.33). Decided to take sample 25026-2 to investigate type and mineralogy.

The fragmented field changes slightly into more solid rocks and what appears to be lava. At 13:47 UTC stop to collect sample and also observe what looks like a bone laying at seabed (Fig. 5.8.34). Manage to collect a piece of the bone with the ORION manipulator arm, but as it appears to be very light it disappears during the decent and never gets back to the ship. Makes two rock samples (25026-3 and -4).

Following slope further upwards. Seabed morphology and sediments changing between rock debris, occasional pillows and areas of more fine-grained sediments. At about 2,875m a gradual increase of sponges (mainly white color but also yellow) is seen.
At a depth of approximately 2,835m, we observed the top of what appeared to be a large scar from mass-movements. At the top an opening, possible venting hole with clear and significant white coloring is present below what looks like harder crust above and softer sediments below (deeper) (Fig. 5.8.35).

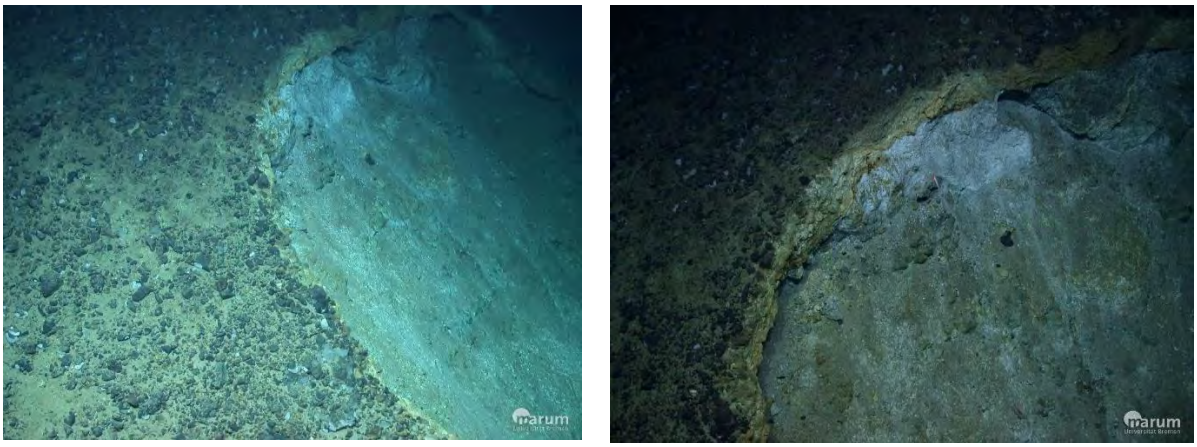

Fig. 5.8.35 (right) Possible scar of mass-moments falling to the left of the picture. Note crust like seabed with looser material below, and hole with associated white staining at top of the scar. Dimensions of feature are more than ten meters long / deep, and about four to five meters wide.

The scar in the steep topography is more than ten meters long / deep, and about four – five meters wide. Dive some meters into the scar and acquire sample / rock which quite clearly has fallen from the brittle crust-like units along the fringe of the scar (sample 25026-5). Take two samples – one with scoop (25026-6) and one with net (25026-7) – of the looser material / sediments just below the top of the scar (hole).

Continuing SW at about 2,830m. Seabed mainly covered with pieces of black rocks with slight cover of fine / pelagic sediments. The steeper parts to the east of the ROV track occasionally changes to more blocky areas with clear stacks of pillow lavas – frequent white sponges and indications of white staining.
Changing direction at 15:24 UTC – now heading E and climbing upwards. For the next 100 meters upwards, i.e. towards the end of the dive, at approximately 2,725m, the seabed is dominated by larger boulders and black rocks with many white sponges and various types of biological growth (Fig. 5.8.36). At UTC 15:44 stopped to sample (25026-8) the dominant black rock to investigate if this is (still (pillow)) lava or if the composition has changed. Dive ended at 15:46 UTC.

Fig. 5.8.36 Large black rocks / boulders with strong biological overgrowth.

ROV Dive 463 (GeoB25028-1; Station MSM109/28-1)
Area: Jøtul hydrothermal field
Date: Monday, 25 July 2022
Start bottom (UTC): 10:14
End bottom (UTC): 15:58
Bottom Time: 06:12
Start bottom (Lat/Long/Depth): 77°26.162'N / 7°40.196'E / 3044 m
End bottom (Lat/Long/Depth): 77°26.488'N / 7°42.834'E / 3002 m
Responsible scientist: Gerhard Bohrmann

Key Results

A Black Smoker with high fluid outflow rates was found and sampled. Temperature measurement failed because of technical problems. Parts of the Jøtul hydrothermal field was explored to the north. Further patches of diffusive venting were found.

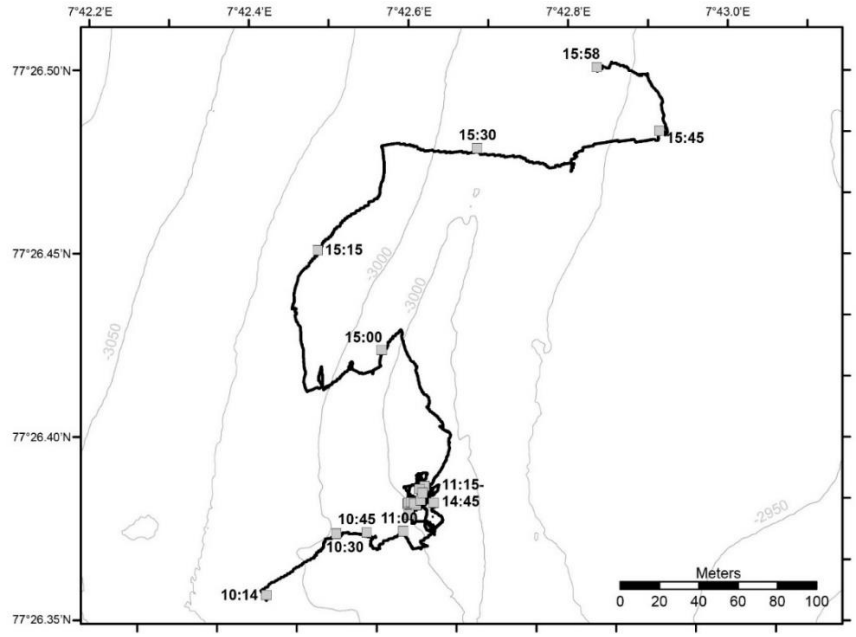

Fig. 5.8.37 ROV Dive 463 track within the Jøtul hydrothermal field.

Table 5.8.8 Samples during ROV dive 463

GeoB No	Instrument	UTC Start	Latitude Longitude	Depth m	Comment
25028-2	ORION manipulator	10:45	77°26.176 07°40.297	3031	Unknown precipitate
25028-3	Net	11:25	77°26.380 07°42.562	3013	White chimney, broken pieces
25028-4	KIPS A	12:12	77°26.376 07°42.535	3010	Fluid center
25028-5	KIPS B	12:29	77°26.376 07°42.533	3010	Fluid rim
25028-6	KIPS C	12:51	77°26.376 07°42.535	3010	Fluid 50 cm outside
25028-7	Net	13:52	77°26.377 07°42.557	3011	Three metallic smoker pieces
25028-8	ORION manipulator	14:09	77°26.372 07°42.579	3013	Old Smoker piece at the base
25028-9	ORION manipulator	14:37	77°26.378 07°42.545	3009	Old precipitate, top nearby smoker

Dive Description

Dive 463 started around 10:45 (UTC) at the seafloor, which was covered by soft sediments. We steamed in northwestern direction where we found first bacterial mats with Siboglinid tubeworms (Fig. 5.8.39) at 10:20. Further exploration showed that unknown precipitates are close by, and at 10:45 we sampled a piece from these precipitates (Fig. 5.8.40; Table 5.8.8) with the ORION arm.

Further exploration to the East showed many isolated rock pieces of different sizes distributed on the sea floor, and around 11:18 we reached a mound with big blocks of sediment and bacterial filaments in the surroundings.

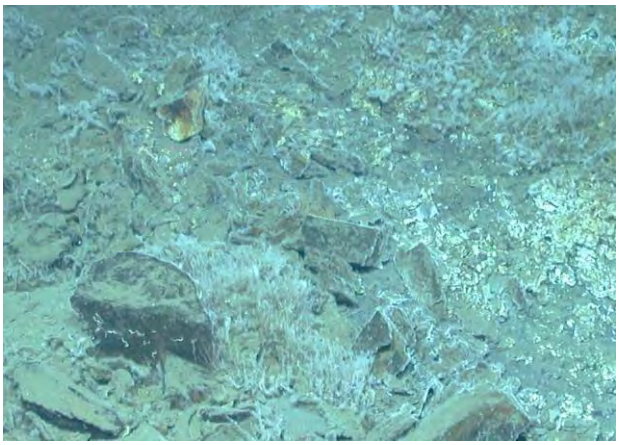

Fig. 5.8.39 Probably diffusive venting area with white bacterial filaments and Siboglinid tubeworms.

Fig. 5.8.40 Probably hydrothermal precipitate at an extinct venting area.

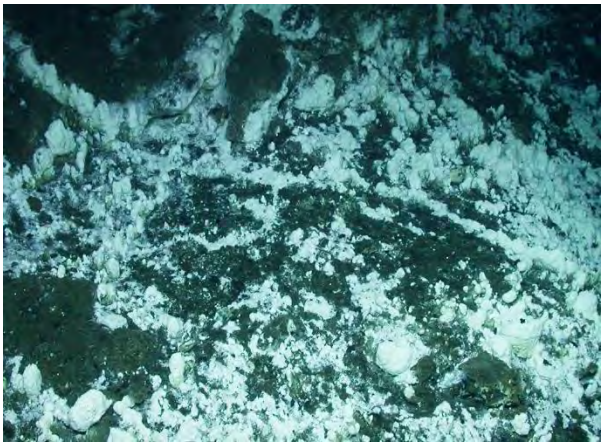

Fig. 5.8.41 Small white chimneys, often in line and covered by bacterial mats.

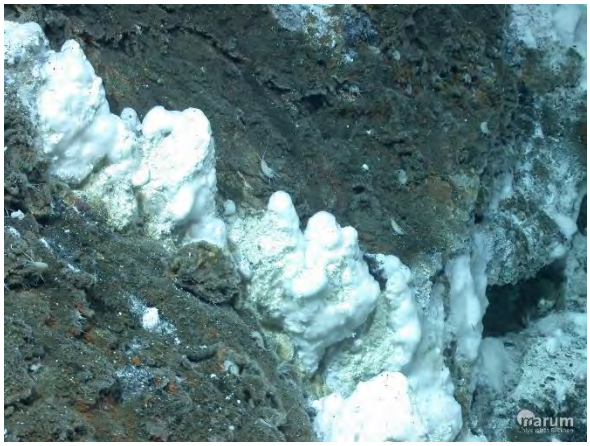

Fig. 5.8.42 Detail of Fig. 3, white precipitate covered by bacterial mats.

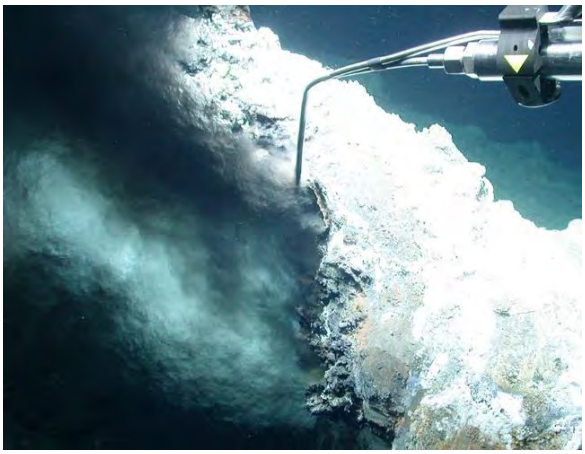

Fig. 5.8.43 Temperature probe measurement and fluid sampling at the Black Smoker

Fig. 5.8.44 Chaotic terrain close to the Black Smoker, mainly composed of brownish precipitates; coverage of white bacteria.

At one side of the mound an area of intensive light bacterial mats are concentrated, very often with small white chimneys of unknown material (Fig. 5.8.41 and 5.8.42). Since this material was very fragile, we took a net sample which crumbled during the sampling procedure (Table 5.8.8). After

we did more pictures of this area, at 11:42 we saw a black smoke in the water at the corner and found a black smoker. Since the opening was not directed upwards but to the side and the chimney area sat relatively short on a mound of older hydrothermal deposits, it was a great challenge for the ROV pilots to carry out the necessary sampling on the smoker. In addition to the fluid samples at three different points (Table 5.8.8) of the outflow (Fig. 5.8.43), a piece of the sulfide precipitates could also be obtained from the edge of the smoker taken with a net at 13:52. The methane levels, which are in the range of mmol/L, surprised us, but explain why we measured quite high levels of methane in the water of our CTD- casts and profiles. After the sampling of the smoker was finished, we sampled a piece of a precipitate at 14:09 deeper at the base of the smoker (Table 5.8.8)

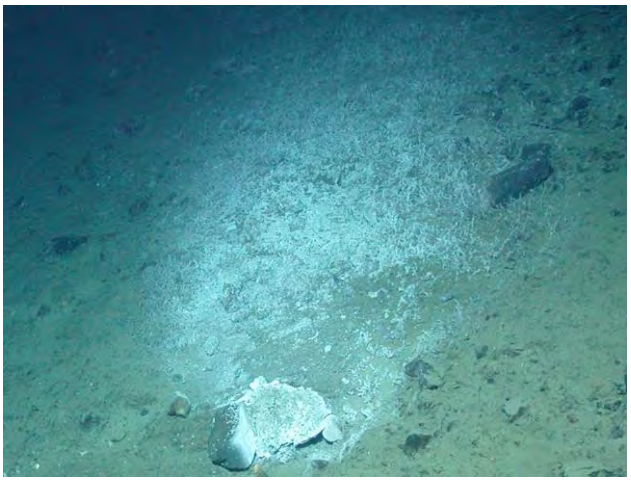

Fig. 5.8.45 Diffusive venting through sediments indicated by white bacterial filaments and Siboglinid tubeworms.

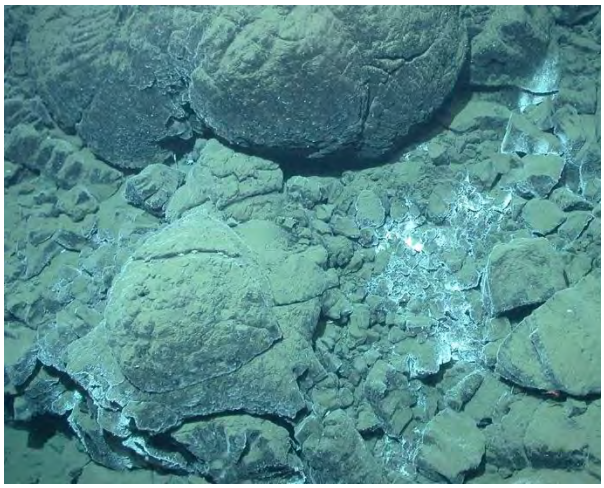

Fig. 5.8.46 Diffusive venting associated to pillow basalts by white staining from bacterial filaments.

After that, the surrounding area of the smoker was explored and we came again to the chaotic area with big blocks higher up of the black smoker (Fig. 5.8.44) and took another sample of probably older precipitates from past hydrothermal activity. Diffuse venting was recognized still in this region by a thin coverage of bacterial filaments. The ROV moved to the north where we saw further bacterial mats on the seafloor. At 15:02 we reached tubular pillow lava first imbedded in sediments and later on flown over sediments.

Also at some rims of the pillow basalt bacterial filaments very obvious because of their white color staining (Fig. 8). Following the track to the north (Fig. 5.8.37) and then to the East, where pillow lava again was met. Diffuse vent fields were seen at the end of the dive close to 16:00 (Figs. 5.8.45 and 5.8.46).

ROV Dive 464 (GeoB25031-1; Station MSM109/31-1)
Area: Jøtul hydrothermal field
Date: Tuesday, 26 July, 2022
Start bottom (UTC): 08:45
End bottom (UTC): 13:12
Bottom Time: 04:27

Start bottom (Lat/Long/Depth): 77°26.379’ N ,7°42.549’ E
End bottom (Lat/Long/Depth): 77°26.602’ N, 7°43.135
Responsible scientist: Katharina Streuff

Key Results

Hydrothermal fluids exit an active smoker vent at a temperature of 316.9° C. The site is surrounded by several dormant and/or collapsed smokers, which the presence of smoker debris, including pipes and mineralized rock fragments attest to. North of the smoker the seafloor is covered with smooth sediments with only rare scattered clasts. A crater towards the end of the dive yielded shimmering water and bacterial mats, indicating diffuse outflow of 2°-warm fluids from beneath the seabed.

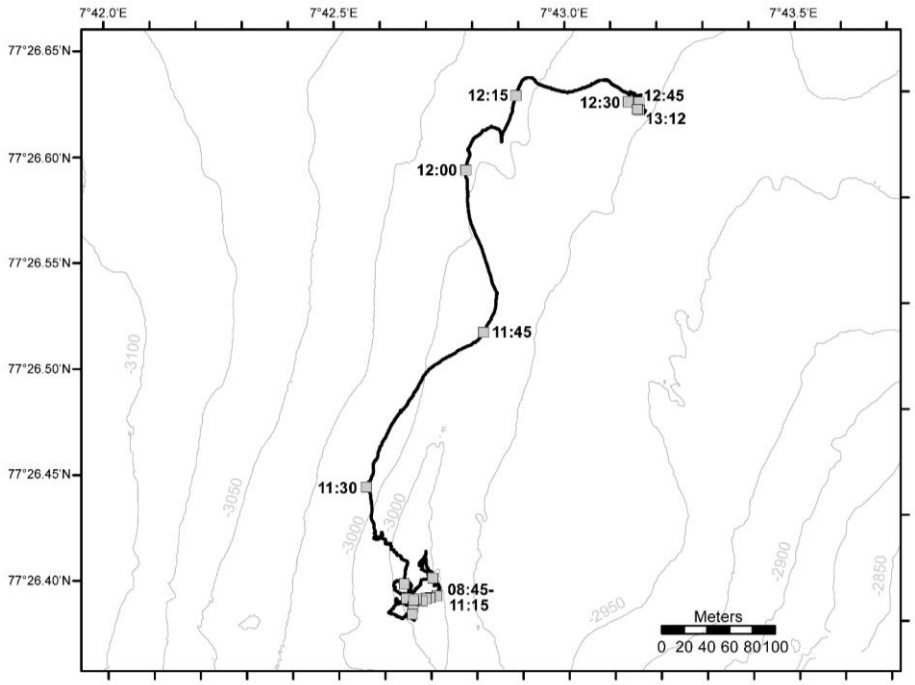

Fig. 5.8.47 Track of ROV Dive 464

Dive Description

Starting at the site where the active black smoker had been discovered during ROV dive 463, dive 464 (Fig. 5.8.47) intended to further investigate the smoker and see whether any more sites of active hydrothermal activity could be detected north of the smoker. Due to problems with the accuracy of the ranger, it took a while to find the smoker again, but when the ROV reached it after ~45 minutes, we were able to measure the temperature and acquire three samples with the KIPS instrument (Fig. 2a). These were taken at different distances from the exit (Table 5.8.9) to investigate the lateral changes in fluid composition. The temperature probe showed that fluids exit the vent at 316.9° C, and the site is therefore an ideal example of hydrothermal activity at the slow-spreading Knipovich Ridge. A large area just north of the smoker showed further signs of past hydrothermal activity in the form of precipitates and old chimney structures, of which two were sampled using the ORION manipulator arm attached to the ROV (Fig. 5.8.48; Table 5.8.9).

Table 5.8.9 Samples taken during ROV dive 464

GeoB No	Instrument	UTC Start	Latitude Longitude	Depth m	Comment
25031-2	KIPS A	09:46	77°26.383 7°42.586	3011 m	Sample from immediate vent exit, measured to be 316.65° C
25031-3	KIPS B	10:12	77°26.382 7°42.575	3011 m	Sample from 30 cm above vent
25031-4	KIPS C	10:22	77°26.382 7°42.573	3011 m	Sample from 1 m above vent
25031-5	MAN	10:46	77°26.383 7°42.564	3014 m	Old smoker pipe
25031-6	Net, blue	11:02	77°26.383 7°42.565	3014 m	Old smoker pipe
25031-7	MAN	13:12	77°26.591 7°42.989	3005 m	Black rock with shrinking cracks from crater

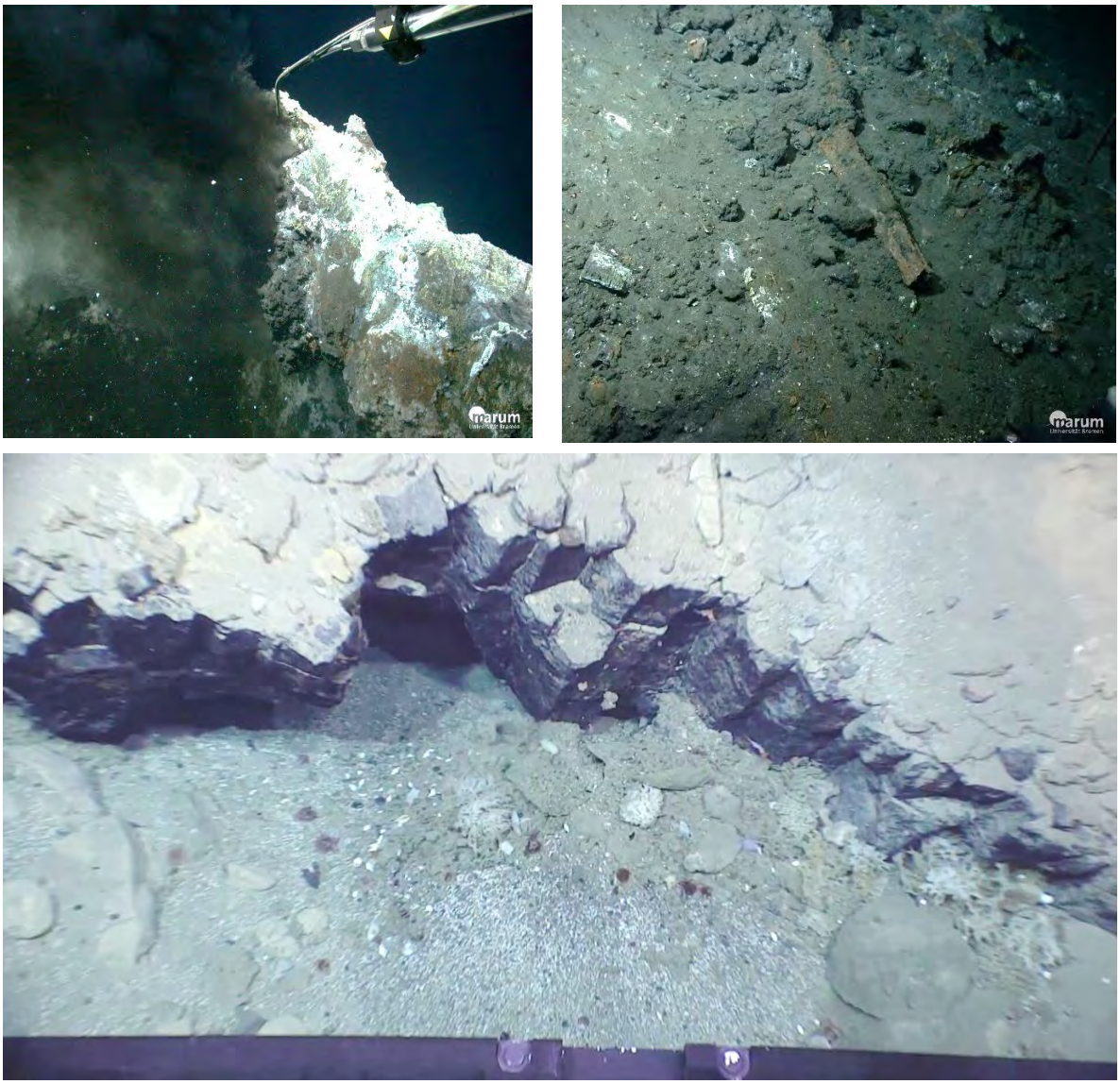

Fig. 5.8.48 Examples of the observations made during ROV dive 464. Top left) Measuring the temperature and taking KIPS samples with the temperature probe at the site of the black smoker. Top right) Old chimney structures indicating earlier intense hydrothermal activity. Bottom) Dark rocks with shrinking fractures in a crater-like depression on the seafloor at the end of the dive. Note the whitish bacterial mats in front, which occurred together with some shimmering H_2O.

After leaving the hydrothermal field behind, the dive progressed in a generally northwards direction, at first following a large ridge structure composed of pillow basalts. North of approximately 77°26.41'N, the seafloor consisted of smooth sediment with only few scattered clasts, a composition which characterized the seabed during the majority of the remaining dive. Several walls made of pillow basalts were encountered, that reached reliefs of up to 20 m. Just before ascending, the ROV discovered an approximately 1 m-deep crater of ~17m in diameter, where mass flow activity and associated collapse uncovered very dark rocks with characteristic shrinking faults (Fig. 5.8.48). White bacterial mats and the observation of shimmering water indicated a site of diffuse fluid flow, which was confirmed with a temperature probe measurement. With 2°C the fluids exiting the site are likely either associated with cold seepage or, alternatively, too weak and diffuse flow to maintain high temperatures.

ROV Dive 465 (GeoB25034-1; Station MSM109/34-1)
Area: Jøtul hydrothermal field
Date: Wednesday, 27 July, 2022
Start bottom (UTC): 08:37
End bottom (UTC): 16:09
Bottom Time: 07:46
Start bottom (Lat/Long/Depth): 77°26.337'N / 07°42.715'E / 3010 m
End bottom (Lat/Long/Depth): 77°26.177'N / 07°42.398 / 2989 m
Responsible scientist: Gerhard Bohrmann

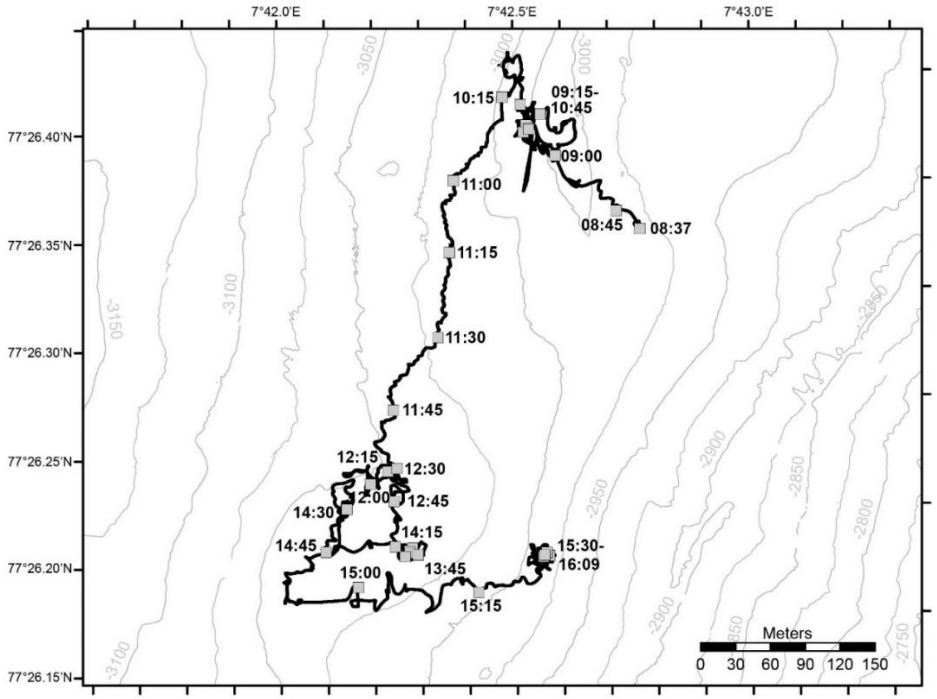

Fig. 5.8.49 Area of ROV Dive 465 at the southern extension of the Jøtul hydrothermal field

Table 5.8.10 Samples during ROV dive 465

GeoB No	Instrument	UTC Start	Latitude Longitude	Depth m	Comment
25034-2	ORION manipulator	12:34	77°26.114'N 07°41.056'E	3051	Precipitate
25034-3	KIPS A	13:15	77°26.196'N 07°42.182'E	3031	Shimmering water
25034-4	ORION manipulator	13:26	77°26.196'N 07°42.184'E	3031	Chimney fragment
25034-5	ORION manipulator	13:45	77°26.193'N 07°42.190'E	3030	Chimney fragment
25034-6	ORION manipulator	14:10	77°26.195'N 07°42.167'E	3028	Chimney fragment
25034-7	ORION manipulator	14:36	77°26.220'N 07°42.082'E	3054	Rock
25034-8	KIPS B	15:40	77°26.176'N 07°42.405'E	2989	Shimmering water
25034-9	ORION manipulator	16:00	77°26.176'N 07°42.400'E	2989	Chimney fragment

Key Results

The exploration of the area south of the known hydrothermal activity showed that the venting area extends to the South. Fluid temperature of the Black Smoker found during dive 464 was 303°C. Further indications for fluid venting were found, and chimneys were sampled. A multi-flanged chimney complex was discovered and a temperature measurement at a vent revealed 272°C. The structure was named Yggdrasil venting complex.

Fig. 5.8.50 Nidhogg venting site with several chimneys formed by dense vent precipitates.

Fig. 5.8.51 Sampling a fluid outflow with KIPS sampler at Nidhogg vent site.

Dive Description

The dive started at 08:37 in 3,010m water depth at a position about 120m southeast of the Black Smoker found during Dive 463. On the way to the smoker mainly sediment-covered seabed was found. Occasionally, pillows were observed, and intermittent patches of white bacterial mats with worms surrounded them, likely representing evidence of diffuse venting. Due to difficulties with the USBL positioning, it was initially difficult to find the Black Smoker again. The temperature measurement from the previous day was repeated there, and revealed a fluid temperature in the outlet channel of 303°C. Due to strong currents from southwest to northeast, the ROV had

difficulties to steam to the South. Between 10:36 and 12:09 the ROV was about 200m above the seafloor and moved around 350m to the South (Fig. 5.8.49). Steaming in the water column was faster than at the seafloor.

At 12:21 , ROV QUEST was back on the seabed at a water depth of 3,050m. The flat seabed here was covered with a fine crust and partially showed white bacterial growth. A sample of the precipitated seafloor was taken with the ORION manipulator arm (Table 5.8.10). Heading south, a block field of precipitates was first encountered at around 12:50, and numerous chimney structures were seen at the top while climbing a hill (Fig. 5.8.50). Circumnavigating the structure, a fluid outflow through shimmering water was found on one side. The temperature measurement showed values up to a maximum of 33.6°C, and a fluid sample was taken with the KIPS sampler (Table 5.8.10 and Fig. 5.8.51). Furthermore, a piece of the edge of the exit point was sampled with the ROV QUEST arm (Table 5.8.10). Based on the impressive construction of the edifice, we named this cluster of coalescing chimneys Nidhogg vent site.

Fig. 5.8.52 Bacterial mat at an active part, at the base of the vent structure.

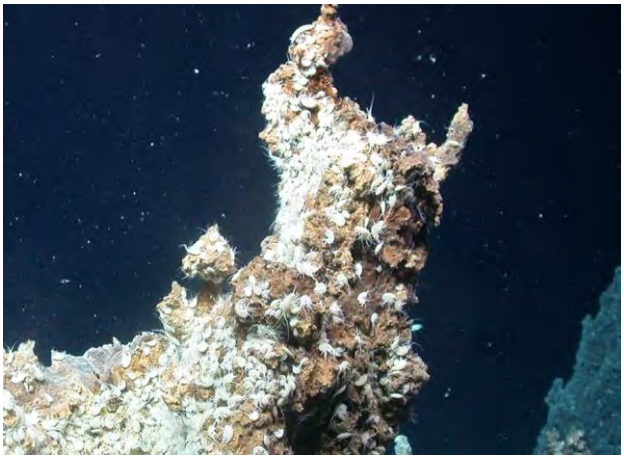

Fig. 5.8.53 Chimney with dense population of amphipodes.

During the examination of the overall structure, it was shown that many fragments of rearranged precipitates build up the structure, but individual areas are colonized by leaking fluids with dense bacterial material (Fig. 5.8.52). A chimney was observed at the top of the complex venting structure, which was very densely populated with amphipods (Fig. 5.8.53). A sample of the chimney was taken at 14:10 (Table 5.8.10).

After this survey, the trail first headed west and briefly north and back to examine isolated structures on the dive map. White mats of bacteria were often found on rock edges and in cracks in sedimentary rocks. In many cases, the seabed was broken up by blocks, some of which were large, and appeared to have been relocated. Since the rock blocks showed neither stratification nor clearly magmatic structure, a sample was taken at 14:34 with the ORION arm (Table 5.8.10). Later inspection of the rock revealed that it is a black schist. From 15:00 we decided to fly the ROV east to examine a crater structure on the map about 150m away at the end of the dive.

ROV Dive 466 (GeoB25035-1; Station MSM109/35-1)

Area: Young volcanic area (high backscatter area) north of Logachev Seamount
Date: Thursday, 28 July, 2022
Start bottom (UTC): 08:51
End bottom (UTC): 13:24
Bottom Time: 04:33
Start bottom (Lat/Long/Depth): 76°49.650’ N, 7°19.987’ E, 3255 m
End bottom (Lat/Long/Depth): 76°49.940’ N, 7°19.928’ E, 3286 m
Responsible scientist: Katharina Streuff

Key Results

The volcanic mound close to the Logachev axial volcanic ridge (AVR) is associated with a rugged terrain of generally young pillow basalts and other magmatic rocks that are covered by little sediment. Only in depressions and specific locations is the sediment cover thicker, giving the seafloor a smooth appearance. Orange-colored sediments, the expulsion of ~2°-warm fluids as well as sampled metallic rocks are indicators of low-grade, potentially dormant, hydrothermal activity.

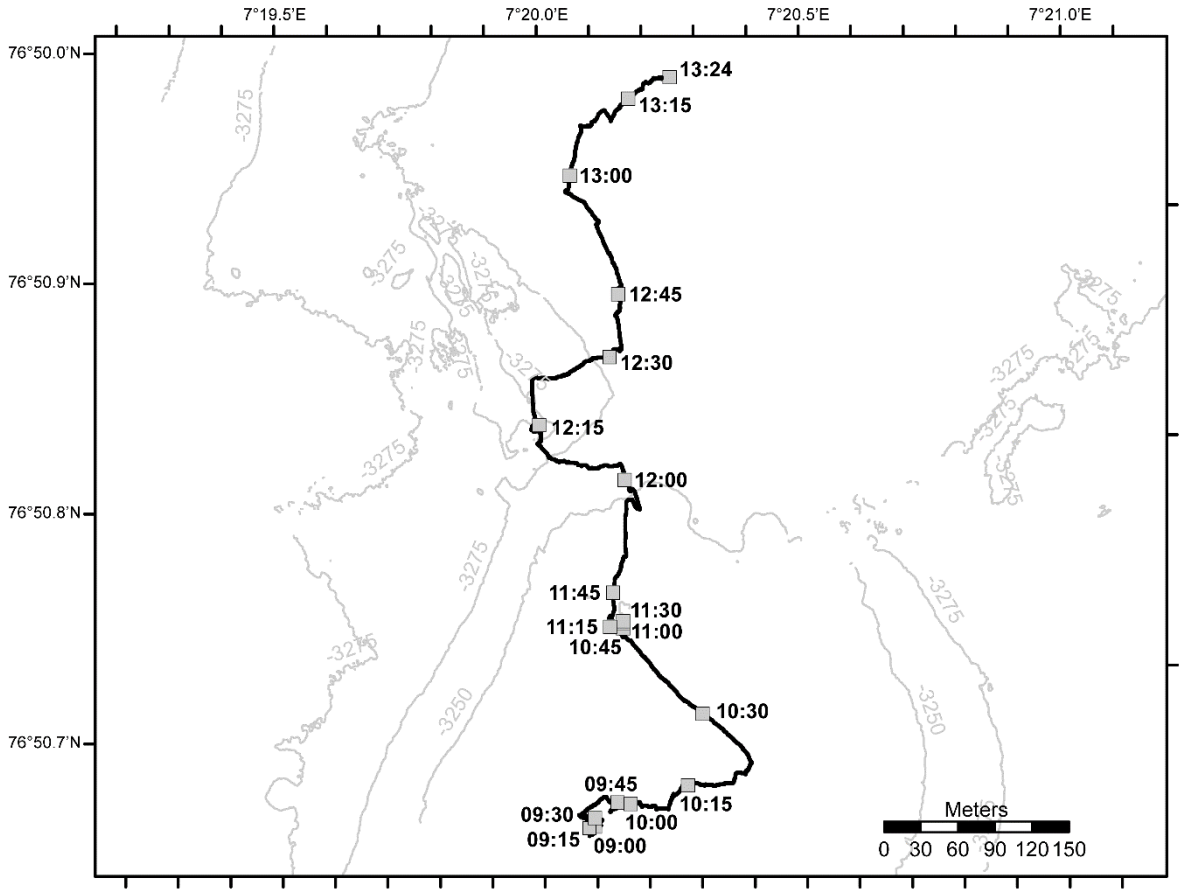

Fig. 5.8.54 Track of ROV Dive 466 across a large volcanic mound located in the vicinity of the Logachev AVR. ROV QUEST started its dive in the center of the mound and worked its way up north.

Table 5.8.11 Samples taken during ROV dive 466

GeoB No	Instrument	UTC Start	Latitude Longitude	Depth m	Comment
25035-2	scoop	11:04	76°49.724' N 7°19.999' E	3256 m	Hydrothermal sediment
25035-3	ORION manipulator	11:10	76°49.724' N 7°19.999' E	3256 m	Dark precipitate

Dive Description

ROV dive 466 (Fig. 5.8.54) was intended to further investigate a large volcanic mound of approximately 500 m in diameter and a height of ~50 m, which is located close to the Logachev axial volcanic ridge and is associated with a high backscatter signal. The dive started in a water depth of 3,255m at the location where dive 457 had discovered a field of fossil smokers, including one large one and several miniature sulfide chimneys scattered on a generally smooth and sediment-covered seafloor. However, the terrain in the area is very rough and undulating, with large pillars and walls of lava and pillow basalts interspersed with numerous trenches and cracks (Fig. 5.8.55). These frequent changes in elevation and water depth not only made ROV navigation very challenging, but also made it difficult to keep track of where the ROV was. This was further exacerbated by uncertainty with the Ranger position. Furthermore, because the ROV often was too large to navigate through the small valleys, bottom view could not always be kept, thus unfortunately making it impossible to find the hydrothermal field again.

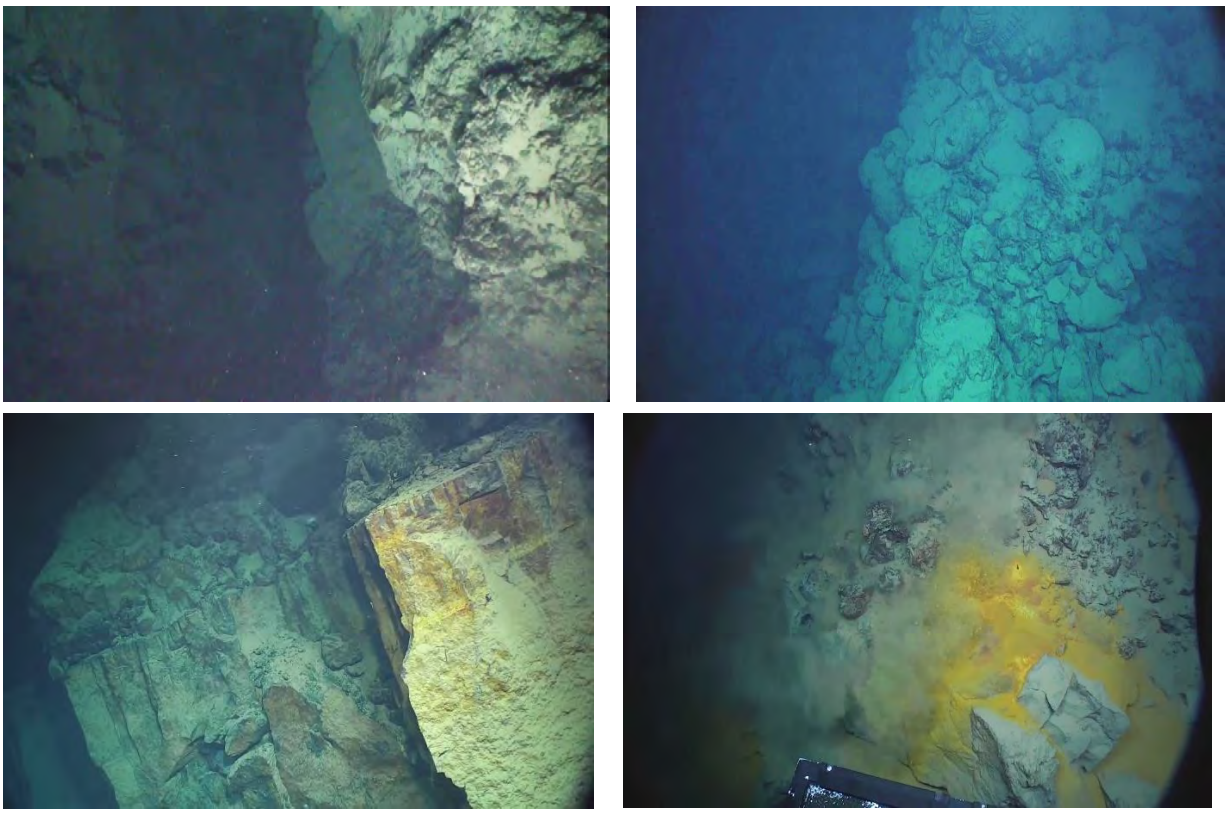

Fig. 5.8.55 Overview of some of the observations made during ROV Quest dive 466. Left above) Uneven terrain with large rock columns, walls and deep fissures making for difficult navigation. Right above) Large rock columns from pillow basalts. Left below) Light magmatic rocks associated with pillow basalts. Right below) Yellow to orange sediments associated with magmatic rocks.

After about an hour of searching, the dive was therefore continued into a generally northward direction to further explore the area and investigate the composition of the seafloor along the large volcanic mound.

The seafloor continued to be characterized by frequent pillow basalts and lava outflows that often build large walls and pillar structures (Fig. 5.8.55). Generally, the pillows appear relatively young and are covered by comparably little sediment, indicating that they only formed recently. Several areas showed occurrences of massive, often weathered-looking rocks, building large columns or walls with pillow basalts on their top (Fig. 5.8.55). Although it was difficult to ascertain the origin of these rocks, we expect them to be also of magmatic origin, albeit of a likely felsic composition. At one site the ROV discovered a patch of brightly yellow to orange sediments, draped around pillows and dark, glittering rocks in the area (Fig. 5.8.55). Indeed, yellow to orange coloring of the seafloor in several areas indicated low-grade hydrothermal activity during dive 466, possibly related to a dormant hydrothermal field. A scoop sample from the brightly orange sediments was taken to investigate the chemical composition after the cruise. The sediments showed a small circular opening at the seafloor, in which the temperature probe attached to the ROV Quest measured fluids exiting at a temperature of 1.8°C. The adjacent dark and glittering rocks were sampled using the ORION manipulator and revealed magmatic rock with a metallic composition.

ROV Dive 467 (GeoB25037-1; Station MSM109/37-1)

Area: Young volcanic area (high backscatter area) north of Logachev Seamount
Date: Friday, 29 July, 2022
Start bottom (UTC): 08:39
End bottom (UTC): 12:29
Bottom Time: 03:50
Start bottom (Lat/Long/Depth): 76°49.616’ N, 7°24.450’ E, 3263 m
End bottom (Lat/Long/Depth): 76°49.612’ N, 7°24.861’ E, 3263 m
Responsible scientist: Daniel Smrzka

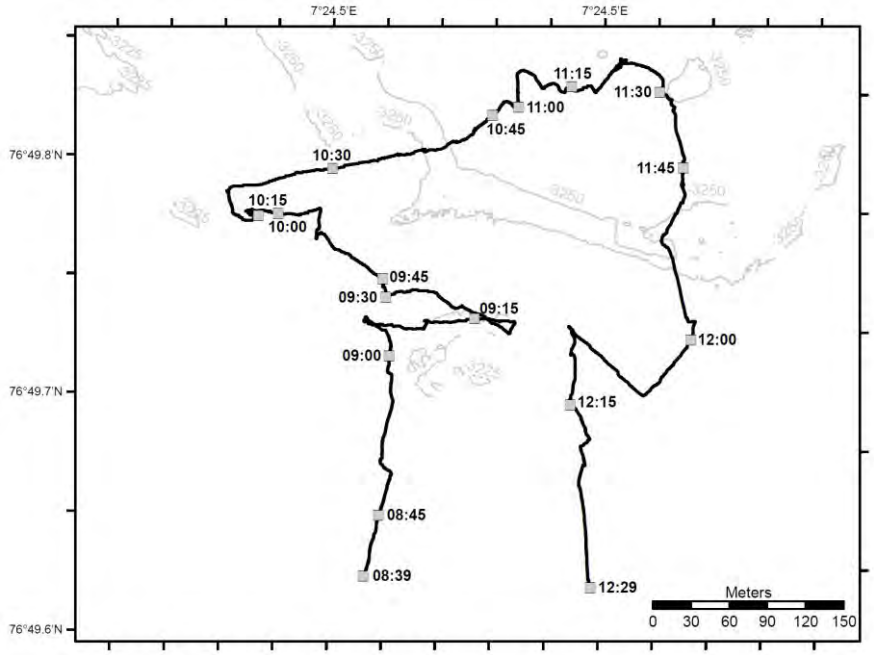

Fig. 5.8.56 Area of ROV Dive 467 Young volcanic area (high backscatter area) north of Logachev Seamount and track of the seafloor observation.

Key Results

The seafloor north of the Logachev Seamount is characterized by a terrain of basalts of various morphologies including large pillows, extensive areas of shardy and ropy basalts, as well as areas covered with soft sediments. Among the pillow basalts large blocks and boulders of volcanic rock are present which was sampled. The areas covered by sediments often feature larger and smaller cracks, as well as networks of smaller cracks of various depth. Almost all of the exposed rocks on the seafloor are covered by various amounts of sediment. Areas of pillows, ropy and shardy basalt often feature large fissures and crevasses that measure up to several meters in width and up to 7 meters in depth. This area further shows a low density of animals compared to other areas, with some individual white anemones attached to the basalts.

Table 5.8.12 Samples during ROV dive 467

GeoB No	Instrument	UTC Start	Latitude Longitude	Depth m	Comment
25037-2	ORION manipulator	09:38	76°49.722'N 7°24.457'E	3260	2 pieces from pillow lava
25037-3	ORION manipulator	10:11	76°49.750'N 7°24.290'E	3252	Massive lava fragment
25037-4	ORION manipulator	11:01	76°49.808'N 7°24.827'E	3260	Piece of ropy lava

Dive Description

ROV dive 467 (Fig. 5.8.56) explored the young volcanic area of high backscatter north of Logachev Seamount. This area is generally characterized by three different terrain types: The first one is marine sediment with cracks of various types (Fig. 5.8.57A), the second is characterized by shardy to ropy lava flows with a large variety of small distinct morphologies (Fig. 2B), and the third type is pillow basalt, typical for the area (Fig. 5.8.57C). The dive started in a water depth of 3,263m on a seafloor featuring pillow basalts covered in fine-grained sediments. The dive started northward towards waypoint 3 flying over various types of basalts including pillow lava, shardy, ropy lava, as well as a seafloor covered in sediments. Many of the areas devoid of rocks are characterized by cracks in the seafloor (Fig. 5.8.57A). These cracks exhibit various depths and are sometimes present as networks of smaller, thinner cracks. A large fissure was encountered shortly after, possibly with a depth of up to 10 meters with beautifully exposed pillow basalts along its walls. The dive continued upslope climbing a topographic high that appears without much surface morphology on the bathymetric map. Although much exposed basalt was encountered going upslope, the top of this feature was only covered with sediments and was devoid of any rocks. After reaching the top, we continued toward waypoint 3, and a sample was taken among collapsed pillows covered in sediments. A rock sample of putative volcanic glass was taken and stored. The dive then pursued towards a NNE-SSW-feature on the bathymetric map, which possibly represents a fault or fracture among stacked pillow basalts. A second sample was taken from a large wall of various types of basalts featuring fractured flows and ropy lava (Fig. 5.8.57D).

After having obtained the second sample, the heading was changed towards waypoint 5 in a northeastern direction, proceeding into deeper terrain covered by alternating sediments, and various types of basalt morphologies covered by sediments. We then flew over a valley-like feature on the bathymetry at an altitude of 9.5 meters to cover more ground, and then encountered an area of extensive and large piles of ropy lava where one large piece was sampled. We then decided to

move toward waypoint 4 in a northwestern direction, passing over an area featuring sediment with open, elongated cracks, as well as various areas of lava shards and ropy lava.

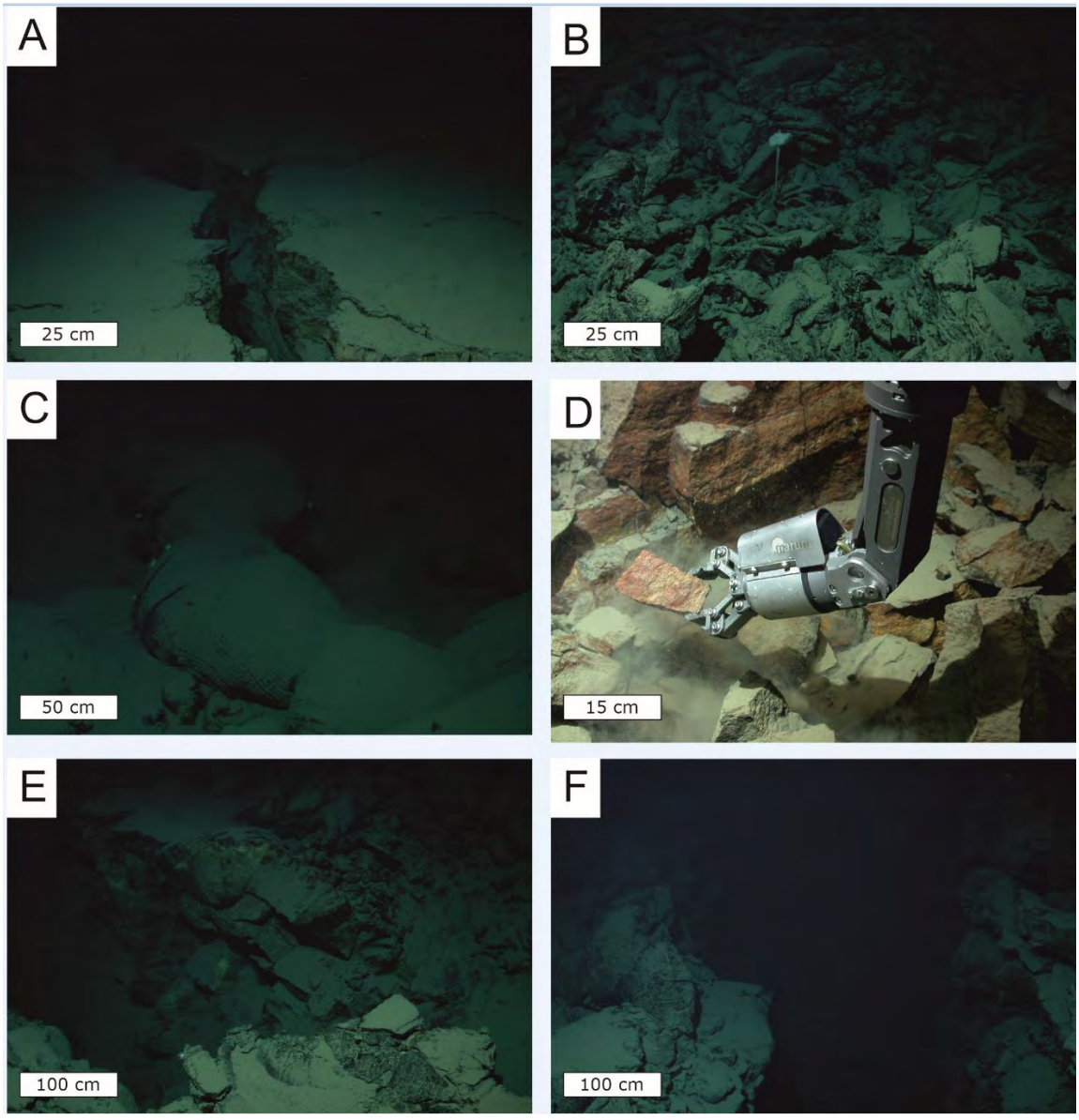

Fig. 5.8.57 Photographs of seafloor features captured with the Scorpio camera of ROV QUEST. A: Sediment-covered seafloor with cracks. B: Shardy and ropy basalt morphology. C: Typical elongated pillow basalt covered with sediments. D: Basalt sample GeoB 25037-3 grabbed with ORION manipulator arm. E: Fissure within various types of basalts. F: Large, deeper fissure within the basalt.

We then changed our heading towards 100° to head towards a chain of small depressions on the bathymetric map, which appeared to be more patches and small fields of basalt, including ropy and shardy lava. The last heading change was then decided to be headed towards the south, passing over various rugged and more smooth features on the bathymetry. During this part of the dive, journeying south, we passed over several large fissures of various width and depth, some were over 2 meters wide and up to 7 meters deep (Fig. 5.8.57E and F). Interestingly, none of the fissures in this area were clearly identifiable in the bathymetric map. The fissures are essentially located within fields of various basalt morphologies. After passing over several fissures, we decided to

change our heading slightly towards the NW towards a crescent-shaped feature on the bathymetric map, which did not appear to be much different from the terrain we had covered up to that point. The rest of the dive was characterized by a seafloor with alternating rock outcrops of basalt, and areas covered by sediments with cracks. After a dive time of 3 hours and 50 minutes the dive was aborted and the ROV ascent began.

5.8.3 Fluid Sampling

(Jan Kleint)

ROV-based sampling of vents and seeps in e.g. hydrothermal systems is essential to constrain physical, chemical, and biological processes in the deep sea. However, sampling of hydrothermal systems is challenging due to mostly extreme temperatures (up to 400°C), high pressure, potentially enormous gas contents and/or highly corrosive fluid properties. For the analyses of particularly rare trace elements and their isotopic systematics, samples were taken by the Kiel Pumping System (KIPS) (Garbe-Schönberg et al., 2006) which had proven ideally suited for varied types of trace element work including hydrothermal fluid and plume studies (e.g., Kleint et al., 2019; Schmidt et al., 2017; Koschinsky et al., 2008). The KIPS is an inert, temperature-resistant, modular, and remotely controlled fluid sampling system for the storage of 4 samples with up to 750 ml volume (Fig. 5.8.58).

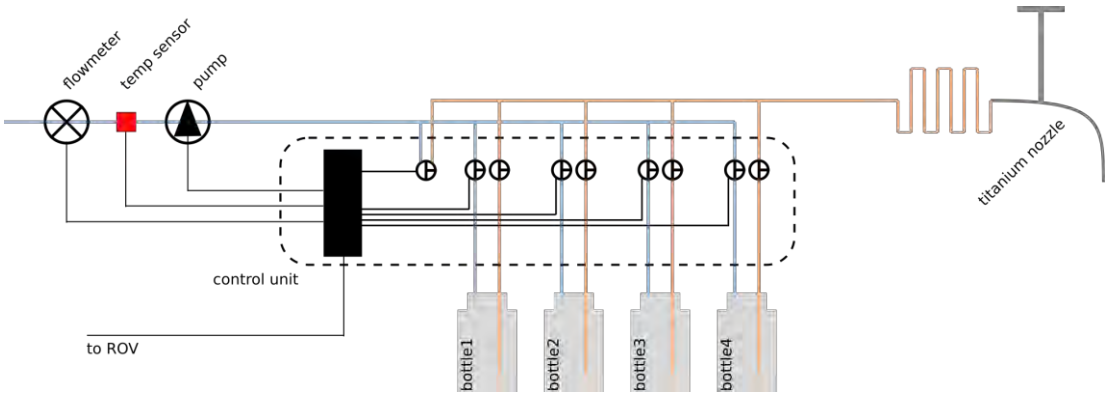

Fig. 5.8.58 The setup of the Kiel Pumping System (KIPS).

During ROV-based sampling, fluids enter the KIPS via a titanium tube, that is guided by the ROV's manipulator to the point of sampling. Sampled fluids are pumped through coiled PFA tubing (3/8" O.D., 6 m length) to the remotely controlled valve pack with 4 sample lines and one purge line. The sample lines could be used for different configurations such as filling either (i) individual sampling flasks of 750 mL and/or (ii) *in situ* filtration units for molecular microbiology. During MSM109, sampling flasks were filled, only. The KIPS gear pump (0-1 L/min) is mounted downstream and an in-line flow meter delivers real-time data for flow rate and total fluid volume. In general, sample flasks are pre-filled with ambient bottom water and sampled fluids are slowly pumped over 5 min, giving a >5-fold exchange of the flask's volume. Immediately after recovery of the ROV on deck, all KIPS sample flasks are transferred to the ship's laboratory for sub-sampling following the standardized protocols.

During MSM109 the KIPS was deployed starboard on ROV QUEST (Fig. 5.8.59), and the *in situ*-MS was connected downstream the KIPS pump.

Fig. 5.8.59 The fluid sampling system KIPS deployed from MARUM ROV QUEST during MSM109.

In total 12 samples were taken with the KIPS for the onboard methane analyses and laboratory analyses following the cruise (Table 5.8.13). All samples were taken in the Jøtul hydrothermal field.

Table 5.8.13 Overview of samples taken with the KIPS during MSM109

Sample No.	ROV dive	Date & Time	Latitude	Longitude	Feature	Depth [m]	Bottle	T [°C]
25023-2	460	22.07.22 09:41	77° 26.520	7° 42.650	fracture with bacterial mat	3012	A	no data
25024-2	461	23.07.22 09:45	77° 26.444	7° 42.537	fracture with bacterial mat	3016	A	8.0
25024-5	461	23.07.22 12:31	77° 26.447	7° 42.538	bacterial mat	3017	B	0.6 (ambient)
25024-13	461	23.07.22 15:39	77° 26.380	7° 42.291	fracture with bacterial mat	3034	C	0.6 (ambient)
25028-4	463	25.07.22 12:12	77° 26.376	7° 42.535	black smoker (vent center)	3010	A	no data
25028-5	463	25.07.22 12:29	77° 26.376	7° 42.533	black smoker (vent rim)	3010	B	no data
25028-6	463	25.07.22 12:51	77° 26.376	7° 42.535	black smoker (50cm above)	3010	C	no data
25031-2	464	26.07.22 09:46	77° 26.383	7° 42.586	black smoker (vent center)	3011	A	316.6
25031-3	464	26.07.22 10:12	77° 26.382	7° 42.575	black smoker (30cm above)	3011	B	92.2
25031-4	464	26.07.22 10:22	77° 26.382	7° 42.573	black smoker (1m above)	3011	C	42.0
25034-3	465	207.07.22 13:15	77° 26.196	7° 42.182	shimmering water	3031	A	32.8
25034-8	465	207.07.22 15:43	77° 26.176	7° 42.405	shimmering water	2989	B	272.0

5.8.4 Rocks and Precipitates Sampled During ROV Dives

(Daniel Smrzka, Henri Renzelmann)

During MSM109, a total of 43 rock and sediment samples were collected during 10 ROV dives.

Table 5.8.14 All precipitates collected during MSM109

GeoB Number	Rov Dive	Area	Description
GeoB 25004-2	455	Southern tip of Brøgger AVR	Rock Sample
GeoB 25004-3			Rock Sample
GeoB 25009-2	457	North of Logachev AVR	Ropy Lava
GeoB 25009-3			Layered Rock
GeoB 25009-4			A'a Lava
GeoB 25009-5			Sulfide Chimney
GeoB 25016-2	458	Jøtul hydrothermal field	Rock and whitish precipitate
GeoB 25016-3			Whitish precipitate
GeoB 25024-3	461	Jøtul hydrothermal field	Hot Vent Rock
GeoB 25024-4			Hot Vent Rock
GeoB 25024-6			Dark Spot Material
GeoB 25024-7			Feeder Material
GeoB 25024-8			Yellow small Rock
GeoB 25024-9			Rock Sample
GeoB 25024-10			Precipitates
GeoB 25024-11			Precipitates
GeoB 25024-12			Chimney Wall
GeoB 25026-2	462	Jøtul hydrothermal field	Brittle gray rock with yellow staining
GeoB 25026-3			Rock with yellow and white staining
GeoB 25026-4			Black rock with glassy surface and yellow staining
GeoB 25026-5			Rock with yellow and white staining
GeoB 25026-6			Black sediments
GeoB 25026-7			Black sediments
GeoB 25026-8			Large black rock
GeoB 25028-2	463	Jøtul hydrothermal field	Unknown precipitate
GeoB 25028-3			White chimney
GeoB 25028-7			Metallic smoker pieces
GeoB 25028-8			Old smoker piece
GeoB 25028-9			Old precipitate near the smoker
GeoB 25031-5	464	Jøtul hydrothermal field	Old smoker pipe
GeoB 25031-6			Old smoker pipe
GeoB 25031-7			Black rock with shrinking cracks from crater
GeoB 25034-2	465	Jøtul hydrothermal field	Precipitate
GeoB 25034-4			Chimney fragment
GeoB 25034-5			Chimney fragment
GeoB 25034-6			Chimney fragment
GeoB 25034-7			Rock

GeoB 25034-9			Chimney fragment
GeoB 25035-2	466	North of Logachev seamount	Hydrothermal Sediment
GeoB 25035-3			Dark precipitate
GeoB 25037-2	467	North of Logachev seamount	2 pillow lavas
GeoB 25037-3			Massive lava fragment
GeoB 25037-4			Ropy Lava

The majority of these samples were volcanic rocks, combined with numerous samples collected from extinct putative black smoker chimneys, from the actively venting black smokers, as well as from the active Yggdrasil and Nidhogg emitting shimmering water. Samples were collected from the Brøgger Axial Volcanic Ridge (AVR), the Jøtul hydrothermal field, and from areas around the Logachev Seamount. A complete list of all precipitates collected (rocks and sediments) is given in Table 5.8.14.

Fig. 5.8.60 Dark fine-grained lava (GeoB 25004-2) from the southern tip of Brøgger AVR.

Fig. 5.8.61 Pillow lava collected north of Logachev Seamount.

Fig. 5.8.62 Sample GeoB 25024-4 collected from Jøtul hydrothermal field.

Pillow and Ropy Lavas

In the majority of the ROV dives various types of volcanic rocks were encountered, specifically different forms of black, fine-grained lava including pillow lavas, A'a lavas, as well as ropy- and shardy lava. The first samples that had been collected during ROV dive 455 are two examples of

these volcanic rocks, which are very dark, fine-grained, and often feature dark orange to reddish staining on the surface (Fig. 5.8.60). Some of these basalts were covered in whitish precipitates, which were also sampled. Some of the pillow lavas show signs of rapid cooling during their expulsion and exposition to seawater, as well as thin black crusts surrounding the often tube- and rope-shaped lava flows (Fig. 5.8.61).

Fig. 5.8.63
Sample GeoB 25037-2 collected from the vicinity of Logachev Seamount.

Other lava samples showed a glassy, fragmented surface of black volcanic glass, as well as orange to red staining that are presumably iron or manganese oxides (Fig. 5.8.62).

Chimney and Smoker Precipitates

Most of the collected samples were obtained from either extinct venting structures and edifices, or from active black smokers and venting sites. These precipitates exhibit various morphologies and appearances, yet they share some common attributes.

Fig. 5.8.64 Sample GeoB 25024-11 collected from Jøtul hydrothermal field.

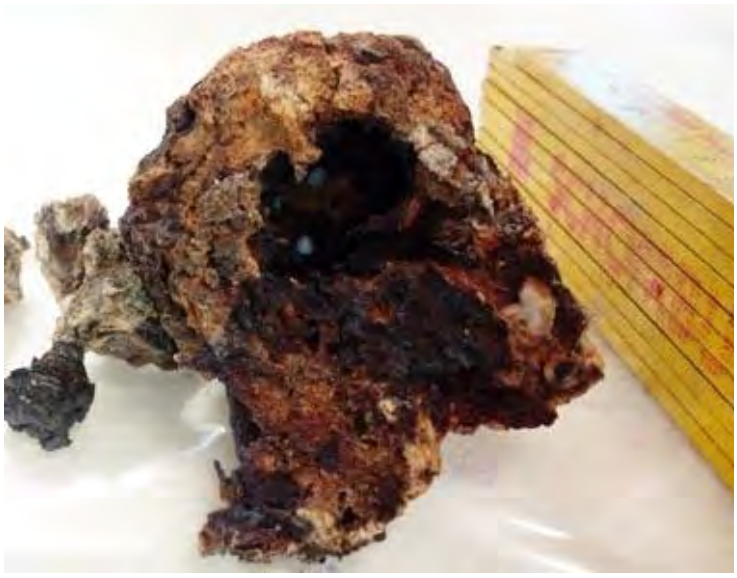

Fig. 5.8.65 Looking inside the chimney (GeoB 25034-2) with small amphipods nesting inside.

Rocks collected from extinct venting structures are often highly brittle and fragile, crumbling into pieces during sampling with the ORION manipulator arm. For this reason, some of these samples were collected using the net instead. The coloration of these precipitates is usually a mixture of light orange to brown, to dark brown, orange, red, and black. In some rarer cases, precipitates from extinct vent structures are more solid, rather porous yet with high density, and covered by

amphipods (Fig. 5.8.64). These amphipods were often seen, nesting in dense communities within void spaces of these inactive venting structures. It is yet unclear if the dark brownish to black precipitates were formed during venting of hydrothermal fluids, or during oxidation of reduced iron and manganese minerals during exposition to seawater. In some cases, these precipitates retained the morphology of fluid channels and resemble small chimneys, which are an indication that hydrothermal fluids may have passed through these chimneys (Figs. 5.8.65). As mentioned above, most of the material collected from inactive venting structures was brittle and soft and was often collected as fragments or as smaller pieces within net samples.

During ROV dive 461 a whitish chimney was discovered next to a larger inactive venting structure. This chimney was smaller in size, and no fluid emission could be detected. During sampling the fragile chimney broke into pieces, which were afterwards recovered using the ORION manipulator arm. The fragmented sample is composed of several smaller chimney and fluid escape structures (Figs. 5.8.66, 67, 68), which are themselves coated by very fine layers of whitish minerals, possibly carbonate or barite, although the mineralogy is not known at this point. These layers form a foamy texture, possibly representing small gas pockets and pathways for fluid and gas venting (Fig. 5.8.67).

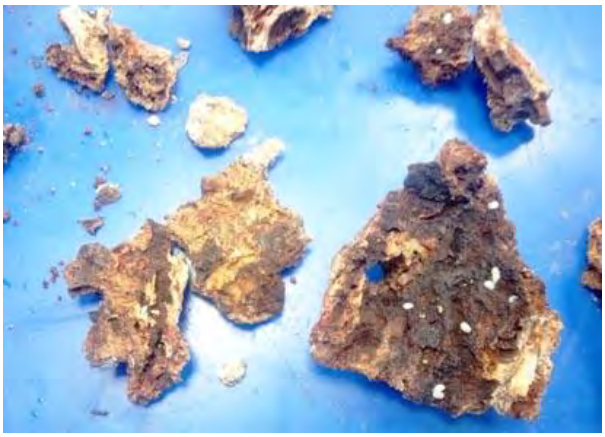

Fig. 5.8.66 Rock fragments from a vent structure at Jøtul hydrothermal field (GeoB 25034-2)

Fig. 5.8.67 Chimney sample from Jøtul hydrothermal field (GeoB 25024-12)

Fig. 5.8.68 Chimney sample from Jøtul hydrothermal field (GeoB 25024-12)

Fig. 5.8.69 Chimney sample from the north of Logachev Seamount (GeoB 25009-5

Some other precipitates collected from inactive chimneys were composed of heavy, black material, possibly metal sulfides, and exhibited twisted morphologies (Fig. 5.8.69). These types of samples

were rare, and only one of these was collected north of the Logachev Axial Volcanic Ridge. A variety of rock samples were collected from the active black smoker emitting a vigorous flow of hot hydrothermal fluid during ROV dive 463. These samples were collected with the net using the ORION manipulator arm, and contained darkish, black sediments with larger pieces of rock. These rocks were dense and heavy pieces, possibly with a high content of metallic ore (Fig. 5.8.70). Further net- and ORION samples yielded whitish sediments, as well as rock material similar to that collected previously from inactive smokers.

During the next dive to the active black smoker (ROV dive 464), old smoker material was recovered using the net and the ORION manipulator arm. These samples were highly fragile and porous, and could hardly be handled without collapsing. These samples were carefully retrieved from the vehicle and placed into a dry oven at 40°C for 48 hours to extract moisture. These samples consist of black to brownish host sediments at the base of the smoker, as well as large tubular pipes of 25 to 30 cm in length featuring brownish and whitish surface precipitates (Figs. 5.8.71 and 72).

Fig. 5.8.70 Net sample from the base of the active black smoker at Jøtul hydrothermal field (GeoB 25028-7).

Fig. 5.8.71 ORION arm pipe sample (GeoB 25031-5) from the base of the active black smoker at Jøtul hydrothermal field.

A further sample collected from the north of Logachev Seamount was different from any other precipitate sampled during MSM109. It is a very dark sample of possibly volcanic origin, featuring abundant highly reflecting minerals, possibly pyrite or other metal sulfides (Figs. 5.8.72 and 73).

Fig. 5.8.72 Black rock sample (GeoB 25035-3) from north of Logachev Seamount containing abundant glittering minerals, possibly sulfides.

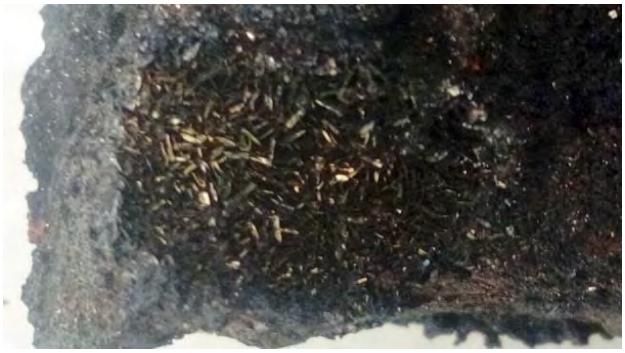

Fig. 5.8.73 Needly minerals from the black rock sample (GeoB 25035-3) collected from north of Logachev Seamount.

6. Station List MSM109

Date	St.	Instrument	GeoB	Location	Time (UTC)				Begin / on seafloor			End / off seafloor			Remarks
						on	off		Latitude	Longitude	Water	Latitude	Longitude	Water	
2022	MSM109/		Number		Begin	seafloor	seafloor	End	N	E	depth (m)	N	E	depth (m)	
07.07.2022	001-1	CTD-01	25001-1	Knipovich R. South	22:26	23:34		00:36	74° 43.093	8° 24.419	3121				sensors stop at 1700m
08.07.2022	002-1	CTD-02	25002-1	Knipovich R. South	19:46	20:53		21:52	74° 43.112	8° 24.470	3310				
09.07.2022	003-1	CTD-03	25003-1	Brøgger AVR	21:54	22:59	04:34	05:47	77° 25.295	7° 16.632	3244	77° 24.030	7° 27.258	3438	Tow-Yo CTD
10.07.2022	004-1	ROV-455	25004-1	Brøgger AVR	06:20	10:24	12:27	14:32	77° 24.824	7° 20.742	3076	77° 24.780	7° 20.460	3073	
10.07.2022	004-2	MAN	25004-2			11:05			77° 24.799	7° 20.757	3125				Rock sample
10.07.2022	004-3	MAN	25004-3			11:07			77° 24.799	7° 20.757	3125				Rock sample
11.07.2022	005-1	CTD-04	25005-1	Brøgger AVR	11:02	12:05		13:00	77° 24.809	7° 20.664	3078				
11.07.2022	006-1	CTD-05	25006-1	Jøtul field	13:56	14:46		15:52	77° 26.7256	7° 44.155	2981				
12.07.2022	007-1	ROV-456	25007-1	Brøgger AVR	06:13	08:55	13:58	16:28	77° 24.816	7° 20.592	3136	77° 24.967	7° 20.407	3138	
12.07.2022	007-2	SCO	25007-2			12:55			77° 24.974	7° 19.841	3108				Soft sediment
12.07.2022	008-1	AUV-102	25008-1	Brøgger AVR	17:48	18:33	01:45	02:15	77° 25.284	7° 46.728	2170	77° 25.956	7° 43.632	2400	
13.07.2022	009-1	ROV-457	25009-1	N of Logachev AVR	07:30	10:00	16:49	19:10	76° 49.243	7° 17.991	3126	76° 49.399	7° 19.854	3315	
13.07.2022	009-2	MAN	25009-2			10:42			76° 49.242	7° 17.977	3303				Lava sample
13.07.2022	009-3	MAN	25009-3			11:34			76° 49.277	7° 17.901	3304				Sheeted rock
13.07.2022	009-4	MAN	25009-4			13:24			76° 49.166	7° 17.279	3252				
13.07.2022	009-5	NET	25009-5			14:32			76° 49.649	7° 19.977	3261				Dead smoker
14.07.2022	010-1	CTD-06	25010-1	Jøtul field	09:53	10:55	15:21	16:26	77° 24.994	7° 40.964	3044	77° 26.989	7° 44.484	3030	Tow-Yo CTD
14.07.2022	011-1	AUV-103	25011-1	Jøtul field	17:17	19:09	03:07	04:14	77° 27.399	7° 45.356	2920	77° 25.985	7° 34.198	3070	
15.07.2022	012-1	CTD-07	25012-1	Jøtul field	06:07	07:05		07:59	77° 26.614	7° 43.865	2954				
15.07.2022	013-1	CTD-08	25013-1	Jøtul field	10:05	11:09	15:15	16:04	77° 26.404	7° 41.159	3142	77° 27.125	7° 49.692	2611	Tow-Yo CTD
16.07.2022	014-1	CTD-09	25014-1	Jøtul field	11:10	12:14	16:10	16:57	77° 26.988	7° 38.914	3230	77° 26.064	7° 46.323	2379	Tow-Yo CTD
17.07.2022	015-1	CTD-10	25015-1	Jøtul field	05:57	06:54		07:50	77° 26.549	7° 43.052	2969				
17.07.2022	016-1	ROV-458	25016-1	Jøtul field	08:19	10:59	15:59	18:04	77° 26.449	7° 42.434	3053	77° 26.424	7° 43.386	2952	
17.07.2022	016-2	MAN	25016-2			11:29			77° 26.450	7° 42.484	3046				Rock plus precipitate
17.07.2022	016-3	MAN	25016-3			11:45			77° 26.450	7° 42.484	3047				Whitish precipitate
17.07.2022	017-1	AUV-104	25017-1	Jøtul field	19:01	20:25	02:50	03:42	77° 23.550	7° 16.752	3250	77° 23.790	7° 26.638	3400	
18.07.2022	018-1	CTD-11	25018-1	Jøtul field	06:29	07:22		08:14	77° 26.745	7° 45.536	2872				
20.07.2022	019-1	CTD-12	25019-1	Molløy Ridge	12:03	13:02	16:54	17:48	79° 29.877	3° 32.578	2972	79° 26.944	3° 25.550	2410	Tow-Yo CTD
20.07.2022	020-1	AUV-105	25020-1	Molløy Ridge	19:00	21:38	03:38	04:30	79° 26.907	3° 38.010	2900	79° 26.997	3° 33.553	2800	
21.07.2022	021-1	CTD-13	25021-1	Molløy Ridge	05:10	06:06		07:01	79° 24.461	3° 25.372	3022				
21.07.2022	022-1	ROV-459	25022-1	Molløy Ridge	07:54	10:25	13:58	16:27	79° 24.630	3° 22.205	2891	79° 25.084	3° 24.694	2842	
22.07.2022	023-1	ROV-460	25023-1	Jøtul field	06:10	08:48	15:48	18:04	77° 26.498	7° 42.600	3024	77° 26.657	7° 45.306	2762	
22.07.2022	023-2	KIPS A	25023-2			09:41			77° 26.520	7° 42.650	3012				at bacterial mat
23.07.2022	024-1	ROV-461	25024-1	Jøtul field	06:41	09:21	15:50	18:12	77° 26.453	7° 42.504	3022	77° 26.380	7° 42.291	3034	
23.07.2022	024-2	KIPS A	25024-2			09:45			77° 26.444	7° 42.537	3016				
23.07.2022	024-3	MAN	25024-3			10:30			77° 26.444	7° 42.534	3016				Hot vent rock

					Time (UTC)				Begin / on seafloor			End / off seafloor			
Date	St.	Instrument	GeoB	Location		on	off		Latitude	Longitude	Water	Latitude	Longitude	Water	Remarks
2022	MSM109/		Number		Begin	seafloor	seafloor	End	N	E	depth (m)	N	E	depth (m)	
23.07.2022	024-4	MAN	25024-4			10:46			77° 26.446	7° 42.534	3015				Hot vent rock
23.07.2022	024-5	KIPS B	25024-5			12:31			77° 26.447	7° 42.538	3017				
23.07.2022	024-6	NET green	25024-6			12:55			77° 26.447	7° 42.539	3018				Dark spot material
23.07.2022	024-7	NET blue	25024-7			13:11			77° 26.448	7° 42.545	3017				Feeder material
23.07.2022	024-8	MAN	25024-8			13:48			77° 26.442	7° 42.437	3033				Yellow small rock
23.07.2022	024-9	MAN	25024-9			13:52			77° 26.442	7° 42.436	3033				Rock sample
23.07.2022	024-10	MAN	25024-10			14:13			77° 26.410	7° 42.378	3034				Precipitates
23.07.2022	024-11	MAN	25024-11			14:57			77° 26.392	7° 42.346	3031				Precipitates
23.07.2022	024-12	MAN	25024-12			15:25			77° 26.379	7° 42.316	3030				Chimney wall
23.07.2022	024-13	KIPS C	25024-13			15:39			77° 26.380	7° 42.291	3034				
23.07.2022	025-1	AUV-106	25025-1	Brøgger AVR	19:02	20:20	05:27	06:53	77° 32.496	7° 40.699	2920	77° 34.343	7° 41.459	3110	
24.07.2022	026-1	ROV-462	25026-1	Jøtul field	08:18	10:51	15:46	18:00	77° 26.368	7° 42.326	3043	77° 26.135	7° 43.312	2739	
24.07.2022	026-2	MAN	25026-2			13:38			77° 26.199	7° 42.850	2907				Rock sample
24.07.2022	026-3	MAN	25026-3			13:51			77° 26.200	7° 42.869	2899				Rock sample
24.07.2022	026-4	MAN	25026-4			14:07			77° 26.000	7° 42.866	2899				Rock sample
24.07.2022	026-5	MAN	25026-5			14:39			77° 26.169	7° 43.003	2864				Rock sample
24.07.2022	026-6	SCO	25026-6			14:55			77° 26.171	7° 43.026	2839				Sediment sample
24.07.2022	026-7	NET	25026-7			15:08			77° 26.172	7° 43.029	2837				Sediment sample
24.07.2022	026-8	MAN	25026-8			15:44			77° 26.135	7° 43.312	2739				Rock sample
24.07.2022	027-1	AUV-107	25027-1	Jøtul field	19:08	20:03	06:03	06:54	77° 25.409	7° 51.921	1957	77° 24.396	7° 47.808	2157	
25.07.2022	028-1	ROV-463	25028-1	Jøtul field	07:44	10:14	15:58	18:04	77° 26.162	7° 40.196	3044	77° 26.488	7° 42.834	3002	
25.07.2022	028-2	MAN	25028-2			10:45			77° 26.176	7° 40.297	3031				Unknown precipitate
25.07.2022	028-3	NET	25028-3			11:25			77° 26.380	7° 42.562	3013				White chimney
25.07.2022	028-4	KIPS A	25028-4			12:12			77° 26.376	7° 42.535	3010				Fluid center
25.07.2022	028-5	KIPS B	25028-5			12:29			77° 26.376	7° 42.533	3010				Fluid rim
25.07.2022	028-6	KIPS C	25028-6			12:51			77° 26.376	7° 42.535	3010				Fluid 50 cm outside
25.07.2022	028-7	NET	25028-7			13:52			77° 26.377	7° 42.557	3011				3 metallic smoker pieces
25.07.2022	028-8	MAN	25028-8			14:09			77° 26.372	7° 42.579	3013				Piece at the base
25.07.2022	028-9	MAN	25028-9			14:37			77° 26.378	7° 42.545	3009				Precipitate
25.07.2022	029-1	CTD-14	25029-1	Jøtul field	18:20	19:15	19:58	20:56	77° 26.375	7° 42.516	2984				
25.07.2022	030-1	CTD-15	25030-1	Jøtul field	21:22	22:22	03:16	04:18	77° 26.261	7° 42.110	3034	77° 27.522	7° 45.377	3033	Tow-Yo CTD Black smoker
26.07.2022	031-1	ROV-464	25031-1	Jøtul field	06:11	08:45	13:12	15:24	77° 26.379	7° 42.549	3023	77° 26.602	7° 43.135	3005	
26.07.2022	031-2	KIPS A	25031-2			09:46			77° 26.383	7° 42.586	3011				Sample vent exit
26.07.2022	031-3	KIPS B	25031-3			10:12			77° 26.382	7° 42.575	3011				Sample 30 cm above vent
26.07.2022	031-4	KIPS C	25031-4			10:22			77° 26.382	7° 42.573	3011				Sample 1m above vent
26.07.2022	031-5	MAN	25031-5			10:46			77° 26.383	7° 42.564	3014				Old smoker pipe

					Time (UTC)				Begin / on seafloor			End / off seafloor			
Date	St.	Instrument	GeoB	Location		on	off		Latitude	Longitude	Water	Latitude	Longitude	Water	Remarks
2022	MSM109/		Number		Begin	seafloor	seafloor	End	N	E	depth (m)	N	E	depth (m)	
26.07.2022	031-6	NET	25031-6			11:02			77° 26.383	7° 42.565	3014				Old smoker pipe
26.07.2022	031-7	MAN	25031-7			13:12			77° 26.591	7° 42.989	3005				Black rock from crater
26.07.2022	032-1	AUV-108	25032-1	Jøtul field	16:20	17:47	00:29	01:33	77° 27.291	7° 45.440	2870	77° 26.389	7° 41.014	3090	
27.07.2022	033-1	CTD-16	25033-1	Jøtul field	04:00	04:56		05:49	77° 26.548	7° 43.342	2942				
27.07.2022	034-1	ROV-465	25034-1	Jøtul field	06:10	08:37	16:09	18:23	77° 26.337	7° 42.715	3010	77° 26.177	7° 42.398	2989	
27.07.2022	034-2	MAN	25034-2			12:34			77° 26.114	7° 41.056	3051				Precipitate
27.07.2022	034-3	KIPS A	25034-3			13:15			77° 26.196	7° 42.182	3031				Shimmering water
27.07.2022	034-4	MAN	25034-4			13:26			77° 26.196	7° 42.184	3031				Chimney fragment
27.07.2022	034-5	MAN	25034-5			13:45			77° 26.193	7° 42.190	3030				Chimney fragment
27.07.2022	034-6	MAN	25034-6			14:10			77° 26.195	7° 42.167	3028				Chimney fragment
27.07.2022	034-7	MAN	25034-7			14:36			77° 26.220	7° 42.082	3054				Rock sample
27.07.2022	034-8	KIPS B	25034-8			15:43			77° 26.176	7° 42.405	2989				Shimmering water
27.07.2022	034-9	MAN	25034-9			16:00			77° 26.176	7° 42.400	2989				Chimney fragment
28.07.2022	035-1	ROV-466	25035-1	N of Logachev AVR	06:07	08:51	13:24	16:34	76° 49.650	7° 19.987	3255	76° 49.940	7° 19.928	3286	
28.07.2022	035-2	SCO	25035-2			11:04			76° 49.724	7° 19.999	3256				Hydrothermal sediment
28.07.2022	035-3	MAN	25035-3			11:10			76° 49.724	7° 19.999	3256				Dark precipitate
28.07.2022	036-1	AUV-109	25036-1	N of Logachev AVR	17:18	18:46	19:37	20:38	76° 49.584	7° 20.893	3150	76° 49.776	7° 18.592	3170	
29.07.2022	037-1	ROV-467	25037-1	N of Logachev AVR	06:05	08:39	12:29	14:54	76° 49.616	7° 24.450	3263	76° 49.612	7° 24.861	3263	
29.07.2022	037-2	MAN	25037-2			09:38			76° 49.722	7° 24.457	3260				2 pieces from pillow lava
29.07.2022	037-3	MAN	25037-3			10:11			76° 49.750	7° 24.290	3252				Massive lava fragment
29.07.2022	037-4	MAN	25037-4			11:01			76° 49.808	7° 24.827	3260				Piece of ropy lava

AUV SEAL 5000:	AUV
CTD + Rosette:	CTD
ROV QUEST:	ROV
ORION manipulator:	MAN
Net sample:	NET
Scoop:	SCO
Fluid sampler:	KIPS

7 Data and Sample Storage and Availability

Metadata of the cruise, as well as the station list, were submitted to Pangaea data bank (https://www.pangaea.de/). Samples collected during the ROV dives were divided into 2 halves. One sample set was transferred to the repository of the Norwegian Petroleum Directorate in Stavanger. The second sample set is under investigation at the Department of Geosciences, University of Bremen (gbohrmann@marum.de). Non-cruise participants can request samples after the moratorium of three years. In addition, data (raw and processed) will be submitted to Pangaea along with the scientific publication.

Table 7.1 Overview of data availability.

Type	Database	Available	Free Access	Contact
Sediment echosounder (Parasound P70)	PANGAEA	https://doi.pangaea.de/10.1594/PANGAEA.959613	August 2025	gbohrmann@marum.de
Water column data, (Kongsberg EM122)	PANGAEA	https://doi.pangaea.de/10.1594/PANGAEA.959613	August 2025	gbohrmann@marum.de
Multibeam bathymetry data (Kongsberg EM122)	PANGAEA	https://doi.org/10.1594/PANGAEA.955507	August 2025	gbohrmann@marum.de
CTD data	PANGAEA	December 2024	August 2025	gbohrmann@marum.de

8 Acknowledgements

We scientists are very happy about the goals achieved and return on land with great results. We also owe the success of the scientific work to the excellent and friendly support from the ship's crew in all areas (nautical, WTD, deck crew, engine and service area, etc.) of the shipping company and the employees of the control center in Hamburg and at MARUM. A special thanks to the Norwegian Petroleum Directorate in Stavanger for supporting the planning of the cruise. We would especially like to thank Captain Björn Maass and his entire crew, who supported us in all matters. At the same time we thank both teams of ROV and AUV - without their achievements we would not have reached our scientific goals. The ship time of R/V MARIA S. MERIAN was provided by Deutsche Forschungsgemeinschaft, and additional funding came from the Bremen Cluster of Excellence “The Ocean Floor – Earth’s Uncharted Interface”.

9 References

Batsi, E., Tsang-Hin-Sun, E., Klingelhoefer, F., Bayrakci, G., Chang, E. T. Y., et al. (2019), Nonseismic Signals in the Ocean: Indicators of Deep Sea and Seafloor Processes on Ocean-Bottom Seismometer Data, Geochem. Geophys. Geosyst., 20(8), 3882-3900, doi:10.1029/2019gc008349

Baumberger, T., Früh-Green, G. L., Thorseth, I. H., Lilley, M. D., Hamelin, C., et al. (2016), Fluid composition of the sediment-influenced Loki’s Castle vent field at the ultra-slow spreading Arctic Mid-Ocean Ridge, Geochim. Cosmochim. Acta, 187, 156-178, doi:10.1016/j.gca.2016.05.017

Bell, R. J., R. T. Short, F. H. W. Van Amerom, and R. H. Byrne. 2007. Calibration of an in situ

membrane inlet mass spectrometer for measurements of dissolved gases and volatile organics in seawater. Environ. Sci. Technol. **41**: 8123–8128. doi:10.1021/es070905d

Botz, R., Winckler, G., Bayer, R., Schmitt, M., Schmidt, M., et al. (1999), Origin of trace gases in submarine hydrothermal vents of the Kolbeinsey Ridge, north Iceland, Earth. Planet. Sci. Lett., 171(1), 83-93, doi:10.1016/S0012-821X(99)00128-4

Boulart, C., D. P. Connelly, and M. C. Mowlem. 2010. Sensors and technologies for in situ dissolved methane measurements and their evaluation using Technology Readiness Levels. TrAC - Trends Anal. Chem. **29**: 186–195. doi:10.1016/j.trac.2009.12.001

Carbotte, S. M., Smith, D. K., Cannat, M., and Klein, E. M. (2016), Tectonic and magmatic segmentation of the Global Ocean Ridge System: a synthesis of observations, Geological Society, London, Special Publications, 420(1), 249-295, doi:10.1144/sp420.5

Caress, D. W., and D. N. Chayes. "New software for processing sidescan data from sidescan-capable multibeam sonars." 'Challenges of Our Changing Global Environment'. Conference Proceedings. OCEANS'95 MTS/IEEE. Vol. 2. IEEE, 1995

Chamov, N. P., Sokolov, S. Y., Kostyleva, V. V., Efimov, V. N., Peive, A. A., et al. (2010), Structure and composition of the sedimentary cover in the Knipovich Rift valley and Molloy Deep (Norwegian-Greenland basin), Lithol. Mineral Resour., 45(6), 532-554, doi:10.1134/S0024490210060039

Connelly, D. P., German, C. R., Asada, M., Okino, K., Egorov, A., et al. (2007), Hydrothermal activity on the ultra-slow spreading southern Knipovich Ridge, Geochem. Geophys. Geosyst., 8(8), doi:10.1029/2007gc001652

Crane, K., and Solheim, A. (1995), Seafloor atlas of the northern Norwegian-Greenland Sea, Norsk Polarinstitutt, Oslo

Crane, K., Eldholm, O., Myhre, A. M., and Sundvor, E. (1982), Thermal implications for the evolution of the Spitsbergen Transform Fault, Tectonophys., 89(1), 1-32, doi:10.1016/0040-1951(82)90032-4

Curewitz, D., Okino, K., Asada, M., Baranov, B., Gusev, E., et al. (2010), Structural analysis of fault populations along the oblique, ultra-slow spreading Knipovich Ridge, North Atlantic Ocean, 74°30′N-77°50′N, JSG, 32(6), 727-740, doi:10.1016/j.jsg.2009.08.011

Dubinin, E. P., Kokhan, A. V., and Sushchevskaya, N. M. (2013), Tectonics and magmatism of ultraslow spreading ridges, Geotectonics, 47(3), 131-155, doi: 10.1134/S0016852113030023

Edmonds, H. N., Michael, P. J., Baker, E. T., Connelly, D. P., Snow, J. E., et al. (2003), Discovery of abundant hydrothermal venting on the ultraslow-spreading Gakkel ridge in the Arctic Ocean, Nature, 421(6920), 252-256, doi:10.1038/nature01351

Eickmann, B., Thorseth, I. H., Peters, M., Strauss, H., Bröcker, M., et al. (2014), Barite in hydrothermal environments as a recorder of subseafloor processes: a multiple-isotope study from the Loki's Castle vent field, Geobiology, 12(4), 308-321, doi:10.1111/gbi.12086

Etiope, G., Sherwood Lollar, B., 2013. Abiotic methane on earth. Reviews of Geophysics 51, 276-299, doi: 10.1002/rog.20011

Franek, P., Plaza-Faverola, A., Mienert, J., Buenz, S., Ferré, B., et al. (2017), Microseismicity Linked to Gas Migration and Leakage on the Western Svalbard Shelf, Geochem. Geophys. Geosyst., 18(12), 4623-4645, doi:10.1002/2017gc007107

Frank, K.L., Rogers, D.R., Olins, H.C., Vidoudez, C., Girguis, P.R., 2013. Characterizing the distribution and rates of microbial sulfate reduction at Middle Valley hydrothermal vents. Isme Journal 7 (7), 1391-1401. 10.1038/ismej.2013.17

Garbe-Schönberg D., Koschinsky A., Ratmeyer V., Jähmlich H., Westernströer U. 2006.KIPS—a new multiport valve-based all-Teflon fluid sampling system for ROVs. Geophys. Res. Abstr., 8, p. 07032

Gentz, T., and M. Schlüter. 2012. Underwater cryotrap-membrane inlet system (CT-MIS) for improved in situ analysis of gases. Limnol. Oceanogr. Methods **10**: 317–328. doi:10.4319/lom.2012.10.317

Gentz, T., E. Damm, J. Schneider von Deimling, S. Mau, D. F. McGinnis, and M. Schlüter. 2014. A water column study of methane around gas flares located at the West Spitsbergen continental margin. Cont. Shelf Res. **72**: 107–118. doi:10.1016/j.csr.2013.07.013

Hannington, M.D., Herzig, P., Stoffers, P., Scholten, J., Garbe-Schonberg, D., Jonasson, I.R., Roest, W., and Shipboard Scientific Party, 2001, First high-temperature submarine hydrothermal vents and massive anhydrite deposits off the north coast of Iceland: Marine Geology, v. 177, p. 199–220

Jokat, W., Kollofrath, J., Geissler, W. H., and Jensen, L. (2012), Crustal thickness and earthquake distribution south of the Logachev Seamount, Knipovich Ridge, Geophys. Res. Lett., 39(8), doi: 10.1029/2012gl051199

Kleint C, Bach W, Diehl A, Fröhberg N, Garbe-Schönberg D, Hartmann JF, de Ronde CEJ, Sander SG, Strauss H, Stucker V, Thal J, Zitoun R, Koschinsky A (2019): Geochemical characterization of highly diverse hydrothermal fluids from volcanic vent systems of the Kermadec intraoceanic arc. Chemical Geology **528**, doi: 10.1016/j.chemgeo.2019.119289

Klenke, M., and Schenke, H. W. (2002), A new bathymetric model for the central Fram Strait, MarGR, 23(4), 367-378, doi:10.1023/A:1025764206736

Koschinsky A., Garbe-Schönberg D., Sander S., Schmidt K., Gennerich H.H., Strauss H. 2008. Hydrothermal venting at pressure-temperature conditions above the critical point of seawater, 5°S on the Mid-Atlantic Ridge. *Geology*; 36 (8): 615–618. https://doi.org/10.1130/G24726A.1

Kowalik, Z., Marchenko, A., Brashnikov, D., Marchenko, N. 2015. Tidal currents in the western Svalbard Fjords, Oceanologia, 57, 318-327

Mau, S., Tu, T.-H., Becker, M., dos Santos Ferreira, C., Chen, J.-N., Lin, L.-H., Wang, P.-L., Lin, S., Bohrmann, G., 2020. Methane seeps and independent methane plumes in the South China Sea offshore Taiwan. Frontiers in Marine Science 7. doi: 10.3389/fmars.2020.00543

Okino, K., Curewitz, D., Asada, M., Tamaki, K., Vogt, P., et al. (2002), Preliminary analysis of the Knipovich Ridge segmentation: influence of focused magmatism and ridge obliquity on an ultraslow spreading system, *Earth. Planet. Sci. Lett.*, *202*(2), 275-288, doi: 10.1016/S0012-821X(02)00790-2

Olins, H.C., Rogers, D.R., Frank, K.L., Vidoudez, C., Girguis, P.R., 2013. Assessing the influence of physical, geochemical and biological factors on anaerobic microbial primary productivity within hydrothermal vent chimneys. Geobiology 11 (3), 279-293. 10.1111/gbi.12034

Pedersen, R. B., Thorseth, I. H., Nygård, T. E., Lilley, M. D., and Kelley, D. S. (2010a), Hydrothermal activity at the Arctic Mid-Ocean Ridges, *Geophysical Monographs Series*, *188*, 67-89, doi:10.1029/2008gm000783

Pedersen, R. B., Rapp, H. T., Thorseth, I. H., Lilley, M. D., Barriga, F. J. A. S., et al. (2010b), Discovery of a black smoker vent field and vent fauna at the Arctic Mid-Ocean Ridge, *Nat. Commun.*, *1*(1), 126, doi:10.1038/ncomms1124

Perner, M., Gonnella, G., Hourdez, S., Bohnke, S., Kurtz, S., Girguis, P., 2013. In situ chemistry and microbial community compositions in five deep-sea hydrothermal fluid samples from Irina II in the Logatchev field. Environmental Microbiology 15 (5), 1551-1560. 10.1111/1462-2920.12038

Petersen, J.M., Zielinski, F., Pape, T., Seifert, R., Moraru, C., Amann, R., Hourdez, S., Girguis, P.R., Wankel, S.D., Barbe, V., Pelletier, E., Fink, D., Borowski, C., Bach, W., Dubilier, N., 2011. Hydrogen is an energy source for hydrothermal vent symbioses. Nature 476 (11 August 2011), 176-180. doi:10.1038/nature10325

Schlindwein, V., Demuth, A., Geissler, W. H., & Jokat, W. (2013). Seismic gap beneath Logachev seamount: Indicator for melt focusing at an ultraslow mid-ocean ridge? Geophysical Research Letters, 40(9), 1703–1707. https://doi.org/10.1002/grl.50329

Schlindwein, V., Krüger, F., Schmid, F., Schmidt-Aursch, M., Brune, R., et al. (2017), KNIPAS - Knipovich Ridge Passive Seismic Experiment, Cruise No. MSM68, October 6 - October 18, 2017, Svalbard (Norway) - Emden (Germany), MARIA S. MERIAN Reports. doi: 10.2312/cr_msm68

Schlüter, M., and T. Gentz. 2008. Application of Membrane Inlet Mass Spectrometry for Online and In Situ Analysis of Methane in Aquatic Environments. J. Am. Soc. Mass Spectrom. 19: 1395–1402. doi:10.1016/j.jasms.2008.07.021

Schmid, F., Schlindwein, V., Koulakov, I., Plötz, A., and Scholz, J.-R. (2017), Magma plumbing system and seismicity of an active mid-ocean ridge volcano, Scientific Reports, 7(1), 42949, doi:10.1038/srep42949

Schmidt, K., Garbe-Schönberg D., Hannington M.D., Anderson M.O., Bühring B., Haase K., Haruel C., Lupton J., Koschinsky A. 2017. Boiling vapour-type fluids from the Nifonea vent field (New Hebrides Back-Arc, Vanuatu, SW Pacific): Geochemistry of an early-stage, post-eruptive hydrothermal system, Geochimica et Cosmochimica Acta, Volume 207, Pages 185-209, ISSN 0016-7037, https://doi.org/10.1016/j.gca.2017.03.016

Short, R. T., S. K. Toler, G. P. G. Kibelka, D. T. Rueda Roa, R. J. Bell, and R. H. Byrne. 2006. Detection and quantification of chemical plumes using a portable underwater membrane introduction mass spectrometer. TrAC - Trends Anal. Chem. 25: 637–646. doi:10.1016/j.trac.2006.05.002

Snow, J., Hellebrand, E., Jokat, W., and Mühe, R. (2001), Magmatic and hydrothermal activity in Lena Trough, Arctic Ocean, Eos, Transactions American Geophysical Union, 82(17), 193-198, doi:10.1029/01eo00101

Spang, A., Saw, J. H., Jorgensen, S. L., Zaremba-Niedzwiedzka, K., Martijn, J., et al. (2015), Complex archaea that bridge the gap between prokaryotes and eukaryotes, Nature, 521(7551), 173-179, doi:10.1038/nature14447

Thiede, J., Pfirman, S., Schenke, H.-W., and Reil, W. (1990), Bathymetry of Molloy Deep: Fram Strait between Svalbard and Greenland, MarGR, 12(3), 197-214, doi: 10.1007/BF02266713

Vogt, P. R. (1986), Geophysical and geochemical signatures and plate tectonics, in The Nordic Seas, edited by B. G. Hurdle, pp. 413-664, Springer New York, New York, NY, doi:10.1007/978-1-4615-8035-5_11

Wankel, S.D., Chen, Y., Kendall, C., Post, A.F., Paytan, A., 2010a. Sources of aerosol nitrate to the Gulf of Aqaba: Evidence from δ15N and δ18O of nitrate and trace metal chemistry. Marine Chemistry 120 (1-4), 90-99. 10.1016/j.marchem.2009.01.013

Wankel, S.D., Joye, S.B., Samarkin, V.A., Shah, S.R., Friederich, G., Melas-Kyriazi, J., Girguis, P.R., 2010b. New constraints on methane fluxes and rates of anaerobic methane oxidation in a Gulf of Mexico brine pool via in situ mass spectrometry. Deep-Sea Research Part Ii-Topical Studies in Oceanography 57 (21-23), 2022-2029. 10.1016/j.dsr2.2010.05.009

Wankel, S.D., Germanovich, L.N., Lilley, M.D., Genc, G., DiPerna, C.J., Bradley, A.S., Olson, E.J., Girguis, P.R., 2011. Influence of subsurface biosphere on geochemical fluxes from diffuse hydrothermal fluids. Nature Geoscience 4 (7), 461-468. 10.1038/ngeo1183

Wankel, S.D., Adams, M.M., Johnston, D.T., Hansel, C.M., Joye, S.B., Girguis, P.R., 2012. Anaerobic methane oxidation in metalliferous hydrothermal sediments: influence on carbon flux and decoupling from sulfate reduction. Environmental Microbiology 14 (10), 2726-2740. 10.1111/j.1462-2920.2012.02825.x

Wenner, P. G., R. J. Bell, F. H. W. Van Amerom, and others. 2004. Environmental chemical mapping using an underwater mass spectrometer. TrAC - Trends Anal. Chem. **23**: 288–295. doi:10.1016/S0165-9936(04)00404-2

Zarayskaya, Y. A. (2017), Segmentation and seismicity of the ultraslow Knipovich and Gakkel mid-ocean ridges, Geotectonics, 51(2), 163-175, doi:10.1134/S0016852117010095